



Norwegian University of  
Science and Technology

# Master's degree thesis

IP501909 MSc thesis, discipline oriented master

Modeling, Simulation and Control of Motion

Compensated Gangway in Offshore Operations

10009/Feilong Yu

Number of pages including this page: 136

Aalesund, 06/06/2017

## Mandatory statement

Each student is responsible for complying with rules and regulations that relate to examinations and to academic work in general. The purpose of the mandatory statement is to make students aware of their responsibility and the consequences of cheating. **Failure to complete the statement does not excuse students from their responsibility.**

<p>Please complete the mandatory statement by placing a mark <u>in each box</u> for statements 1-6 below.</p>		
1.	I/we hereby declare that my/our paper/assignment is my/our own work, and that I/we have not used other sources or received other help than is mentioned in the paper/assignment.	<input type="checkbox"/>
2.	<p>I/we hereby declare that this paper</p> <ol style="list-style-type: none"> <li>1. Has not been used in any other exam at another department/university/university college</li> <li>2. Is not referring to the work of others without acknowledgement</li> <li>3. Is not referring to my/our previous work without acknowledgement</li> <li>4. Has acknowledged all sources of literature in the text and in the list of references</li> <li>5. Is not a copy, duplicate or transcript of other work</li> </ol>	<p>Mark each box:</p> <ol style="list-style-type: none"> <li>1. <input type="checkbox"/></li> <li>2. <input type="checkbox"/></li> <li>3. <input type="checkbox"/></li> <li>4. <input type="checkbox"/></li> <li>5. <input type="checkbox"/></li> </ol>
3.	I am/we are aware that any breach of the above will be considered as cheating, and may result in annulment of the examination and exclusion from all universities and university colleges in Norway for up to one year, according to the <a href="#">Act relating to Norwegian Universities and University Colleges, section 4-7 and 4-8</a> and Examination regulations .	<input type="checkbox"/>
4.	I am/we are aware that all papers/assignments may be checked for plagiarism by a software assisted plagiarism check	<input type="checkbox"/>
5.	I am/we are aware that NTNU will handle all cases of suspected cheating according to prevailing guidelines.	<input type="checkbox"/>

6.	I/we are aware of the NTNU's rules and regulation for using sources.	<input type="checkbox"/>
----	--	--------------------------

# Publication agreement

ECTS credits: 30

Supervisor: Houxiang Zhang, Vilmar Æsøy

## Agreement on electronic publication of master thesis

Author(s) have copyright to the thesis, including the exclusive right to publish the document (The Copyright Act §2).

All theses fulfilling the requirements will be registered and published in Brage, with the approval of the author(s).

Theses with a confidentiality agreement will not be published.

**I/we hereby give NTNU the right to, free of charge, make the thesis available for electronic publication:** yes no

**Is there an [agreement of confidentiality](#)?** yes no

(A supplementary confidentiality agreement must be filled in and included in this document)

- If yes: **Can the thesis be online published when the period of confidentiality is expired?** yes no

This master's thesis has been completed and approved as part of a master's degree programme at NTNU Ålesund. The thesis is the student's own independent work according to section 6 of Regulations concerning requirements for master's degrees of December 1st, 2005.

**Date: 06/06/2017**

## Preface

This master's thesis is submitted to the Norwegian University of Science and Technology (NTNU) in fulfilment of the requirements for the degree Master of Science in Product and System Design. This study introduces a parallel force/position control algorithm for the control of the contact force between the gangway tip and the platform during motion compensated operations. The dynamic systems including the hydraulic power systems and the multi-body dynamics of gangway were modelled with bond-graph approach. One paper is written based on this thesis and can be found in the Appendix D of this thesis.

The thesis has been conducted at the department of Ocean Operations and Civil Engineering from January 2017 to May 2017 under supervision of Professor Houxiang Zhang and Vilmar Æsøy. First, I offer my sincerest gratitude to them, who has given me a lot of good advice and guidance during the thesis project. In addition, I would like to thank PhD candidate Yingguang Chu and Senior Principle Engineer Øyvind Bunes who gave me very inspiring and helpful instructions on solving different problems of the thesis work.

Finally, I would like to thank my families for supporting my study in Norway.

Feilong Yu

Ålesund, Norway

Tuesday 6th June, 2017



## **Abstract**

This thesis is based on the idea to develop the integrated model of offshore gangway model including multi-body dynamics model and hydraulic system model with bond-graph method in 20-sim. And based on that model, active motion compensation control approach will be developed in order to compensate the ship motion during gangway operation and further more a parallel position and force control method will be proposed to make the gangway tip maintain constant contact force with windmill platform as well as compensate ship motion during transferring process.

In order to get reasonable data for modeling, simulation and control of gangway operation, an offshore gangway was designed first based on the relative rules and existing products from Uptime Company. Then multi-body dynamic model is developed with IC-field based on the Lagrangian Hamiltonian equation of gangway. After that, the hydraulic system for gangway was designed and verified with simulation. Based on this developed model, the control algorithm for active motion control and parallel position and force control were proposed. The active heave compensation control is based on the kinematics solving method to mapping the gangway tip trajectory to actuator trajectory and then control the actuator by position and velocity feedback with velocity feedforward controller. And the parallel position and force control was based on the inner position loop outer force control and the idea is to adjust the desired gangway tip trajectory by the force modulator to achieve the desired contact force.





# Table of Contents

Preface .....	i
Abstract .....	iii
Table of Contents .....	v
List of Figures .....	ix
List of Tables .....	xiii
Acronyms .....	xv
1 Introduction .....	1
1.1 Background .....	1
1.2 Motivation .....	2
1.3 Problems and Challenges .....	3
1.4 Objective .....	4
1.5 Scope of the thesis .....	4
1.6 Related Work .....	5
1.7 Structure of the Thesis .....	6
2 Background Theories .....	9
2.1 Bond Graph Modeling .....	9
2.1.1 Bond Graph Basics .....	9
2.1.2 Multiport Fields .....	14
2.2 Kinematics .....	15
2.2.1 Rigid Body Motion .....	15
2.2.2 Manipulator Kinematics .....	17
2.2.3 Jacobians .....	20
2.3 Manipulator Dynamics .....	22
2.3.1 Euler-Lagrange Equation .....	22
2.3.2 Kinetic and Potential Energy of an N-Link Manipulator .....	23
2.3.3 Bond Graph Modeling of Manipulator Motion Dynamics .....	25

3	Gangway Design.....	27
3.1	Design requirements .....	27
3.2	Conceptual Design.....	27
4	Mechanical Model of Gangway.....	29
4.1	Simplifications .....	29
4.2	Kinematics of the Gangway .....	29
4.2.1	Forward Kinematics and Jacobian Transformation .....	29
4.2.2	Inverse Kinematics.....	32
4.2.3	Joint-Space to Actuator-Space kinematics .....	33
4.3	Dynamics of the Gangway .....	34
4.3.1	Jacobian Derivation.....	35
4.3.2	Kinetic Energy of the Gangway .....	36
4.3.3	Hamiltonian-Lagrange Equation and Bond Graph Implementation .....	38
5	Modeling and Design of Hydraulic Systems of Gangway .....	41
5.1	Description of Hydraulic System of Gangway .....	41
5.2	Specification of Parameters of Hydraulic Components .....	43
5.2.1	Slewing Motor .....	43
5.2.2	Luffing Cylinder and Telescopic Cylinder .....	45
5.2.3	Hydraulic Pump.....	48
5.2.4	Relative Valves and Pipes .....	49
5.3	Bond Graph Modeling of Hydraulic System Components .....	49
5.3.1	HPU.....	50
5.3.2	Pipe.....	51
5.3.3	Valves .....	52
5.3.4	Hydraulic Motor .....	57
5.3.5	Hydraulic Cylinder.....	58
5.3.6	Tank.....	60

5.4	Simulation and Verification of Complete Hydraulic Systems .....	60
5.4.1	Shared Pump and Pipe Parameters.....	62
5.4.2	Hydraulic System for Slewing King .....	62
5.4.3	Hydraulic System for Luffing Boom .....	64
5.4.4	Hydraulic System for Telescopic Boom.....	66
6	Control of Gangway .....	69
6.1	Control Task.....	69
6.2	Active Motion Compensation Control and Simulation .....	70
6.2.1	Control algorithm of active motion compensation.....	70
6.2.2	Design of Actuator Controller .....	72
6.2.3	Performance of Gangway under Active Heave Compensation Control .....	73
6.3	Parallel Position and Force Control and Simulation.....	77
6.3.1	Principle of Parallel Position and Force Control Algorithm .....	77
6.3.2	Parallel Position and Force Controller Design .....	78
6.3.3	Performance of Gangway under Parallel Position and Force Control .....	80
6.4	Summary .....	84
7	Conclusions and Future Work .....	85
7.1	Conclusions .....	85
7.2	Future Work .....	86
8	Bibliography.....	87
9	Appendix .....	89
	Appendix A Strength Analysis of Designed Gangway .....	89
	Appendix B Parameters of Gangway for Kinematic and Dynamic Calculation.....	99
	Appendix C Technical Sheets for Selected Hydraulic Components .....	101
	Appendix D Thesis based Paper .....	107



# List of Figures

Fig. 1.1: Example of existing offshore ship-based motion compensation gangways..... 2

Fig. 2.1: Sign convention on power and signal bonds ..... 9

Fig. 2.2: Example of power transmitted between subsystem A and B with power bond..... 10

Fig. 2.3: Illustration of description the orientation of body-attached coordinate system..... 16

Fig. 2.4: Illustration of D-H parameters and link-attached frames ..... 18

Fig. 2.5 Illustration of modeling manipulator dynamics with bond-graph..... 26

Fig. 3.1 3D model of designed gangway ..... 28

Fig. 4.1 The D-H sketch of simplified gangway system ..... 30

Fig. 4.2 The geometry relation of luffing joint ..... 34

Fig. 4.3 Bond graph implementation of gangway dynamics with IC-field ..... 39

Fig. 5.1 Overall Hydraulic circuit of gangway system..... 42

Fig. 5.2 Inverse kinematics model of gangway ..... 47

Fig. 5.3 Required luffing and telescopic velocity ..... 47

Fig. 5.4 Bond graph model of HPU ..... 51

Fig. 5.5 Bond graph model of hydraulic pipe..... 51

Fig. 5.6 Bond graph model of pressure compensator valve ..... 53

Fig. 5.7 Bond graph model of DCV ..... 54

Fig. 5.8 Bond graph model of counter balance valve ..... 55

Fig. 5.9 Bond graph model of relief valve..... 56

Fig. 5.10 Bond graph model of hydraulic motor..... 57

Fig. 5.11 Bond graph model of hydraulic cylinder ..... 58

Fig. 5.12 Complete hydraulic system model integrated with gangway dynamics..... 61

Fig. 5.13 Rotation speed of slewing king ..... 63

Fig. 5.14 Pressure of both sides of motor ..... 63

Fig. 5.15 Luffing cylinder rod speed and position ..... 65

Fig. 5.16 Working pressure of luffing sub hydraulic system ..... 65

Fig. 5.17 Telescopic cylinder rod speed and position.....	67
Fig. 5.18 Working pressure of telescopic sub hydraulic system .....	67
Fig. 6.1 Relation between gangway base frame and world frame .....	70
Fig. 6.2 Structure of AMC control algorithm.....	71
Fig. 6.3 Complete model of gangway system under active motion compensation control .....	74
Fig. 6.4 Gangway tip position in X-axis under AMC control in two load cases .....	75
Fig. 6.5 Gangway tip position in Z-axis under AMC control in two load cases.....	75
Fig. 6.6 Luffing cylinder pressure under AMC control in two load cases .....	76
Fig. 6.7 Telescopic cylinder pressure under AMC control in two load cases .....	76
Fig. 6.8 Schematic for illustrating the concept for force control .....	77
Fig. 6.9 Force servo with inner position loop.....	78
Fig. 6.10 Structure of parallel position and force control algorithm for gangway system .....	79
Fig. 6.11 Complete model of gangway system under parallel position and force control .....	80
Fig. 6.12 Gangway tip position Vs ship motion in X-axis under two control algorithms.....	81
Fig. 6.13 Gangway tip position Vs ship motion in Z-axis under two control algorithms .....	82
Fig.6.14 Contact force under two control algorithms in X-axis.....	82
Fig. 6.15 Luffing cylinder pressure under two control methods .....	83
Fig. 6.16 Telescopic cylinder pressure under two control methods .....	83
Fig. 9.1 Mesh model of gangway structure .....	91
Fig. 9.2 Constraints and load set up for load case NO-PT-C .....	92
Fig. 9.3 Stress of overall structure of gangway under load case NO-PT-C .....	92
Fig. 9.4 Stress for aluminum parts of gangway under load case NO-PT-C .....	93
Fig. 9.5 Deflection of gangway under load case NO-PT-C .....	93
Fig. 9.6 Constraints and load set up for load case NO-PT-I.....	94
Fig. 9.7 Stress of overall structure of gangway under load case NO-PT-I.....	94
Fig. 9.8 Stress of aluminum parts of gangway under load case NO-PT-I.....	95
Fig. 9.9 Deflection of gangway under load case NO-PT-I.....	95

Fig. 9.10 Constraints and load set up for load case EO .....	96
Fig. 9.11 Stress of overall structure of gangway under load case EO .....	96
Fig. 9.12 Stress of aluminum parts of gangway under load case EO .....	97
Fig. 9.13 Deflection of gangway under load case EO .....	97





# List of Tables

Table 2.1 Variables of some different energy-domain systems in bond graph..... 11

Table 2.2 Basic bond graph elements ..... 12

Table 2.3 Definition of C-field and I-field ..... 14

Table 2.4 Illustration of IC-field and the constitutive relation..... 15

Table 3.1 Materials used for each part of gangway ..... 28

Table 4.1 The operational range of joint variables ..... 30

Table 4.2 D-H parameters of redefined gangway sketch ..... 31

Table 5.1 Operating cycles of slewing king ..... 43

Table 5.2 Data for calculating motor size..... 44

Table 5.3 Desired gangway tip velocity ..... 47

Table 5.4 Calculated inner diameter of pressure pipe and return pipe ..... 49

Table 5.5 Data of selected pressure pipe and return pipe ..... 49

Table 5.6 Pump and Pipe parameters..... 62

Table 5.7 Parameters of main components of slewing sub hydraulic system ..... 62

Table 5.8 Parameters for luffing hydraulic system ..... 64

Table 5.9 Parameters for telescopic hydraulic system..... 66

Table 9.1 Load cases for gangway design ..... 89

Table 9.2 Permissible Stress for materials used in gangway design..... 90

Table 9.3 Allowed deflection of designed gangway ..... 90



## Acronyms

3D	Three Dimensional
CBV	Counter Balance Valve
COG	Center of Gravity
D-H	Denavit-Hartenberg
DOF	Degree of Freedom
DCV	Directional Control Valve
EO	Emergency Operation
FEA	Finite Element Analysis
HPU	Hydraulic Power Unit
NO-PT-C	Normal Operation for People for Transferring in Cantilever Positon
NO-PT-I	Normal Operation for People for Transferring in Inclined Positon
O&M	Operation and Maintenance
PD	Proportional Derivative
PCV	Pressure Compensate Valve
RPM	Revolution per Minute



# 1 Introduction

This chapter presents a brief introduction and general description of this thesis, containing the background, motivations, as well as problems and challenges; it also covers the main objectives of this thesis. And the structure of this thesis is given at the end of this chapter.

## 1.1 Background

Wind energy has been used by people in transport, industry and agriculture for thousands of years. And the use of wind turbine to produce electricity began at 1891 in Scotland in a limited scale but the modern wind power industry did not start until the late 1970s when the great development of technology took place. And from that point, wind power continues to expand worldwide, reaching 456 GW by the end of June 2016 according to World Wind Energy Association. However, the majority of installed capacity is on land and onshore wind power has often been complained due to the generated noise, virtual intrusion and threats for ecological system. So more and more effort has been paid to the offshore wind power due to the higher and more stable winds.

At present, the major offshore wind farms in Europe are built in UK, Germany and Denmark. Most of the existing offshore wind farms are located in the shallow water within average 25 km offshore where the average wave height is 1.5 meter. And for the deep-water wind farms, which are located more than 50 km offshore and the wave height can reach to 3 meters or even higher(WindEUROPE 2017). These harsh weather conditions impose great challenge on the access to the offshore wind turbines for operation and maintenance (O&M) activities. And downtime of wind turbines due to waiting for weather windows is one of the major factors causing the loss of production and profit. Thus, there is a great potential to enlarge the weather window and increase profit through an economical and robust access system to offshore wind turbines for O&M activities.

Motion compensated gangway is believed to be one of the most economical and effective access solutions to increase the weather window for operations comparing to the traditional approach of transferring crew to or from offshore wind turbines by helicopter and climbing the ladder from the vessel directly. This ship-based motion compensation gangway is much more economical, safe and robust. Today, there are many companies making this type of gangway. But in working principle of motion compensation, it can be classified into three types of ship-based motion compensated gangways as shown in the following Fig. 1.1.

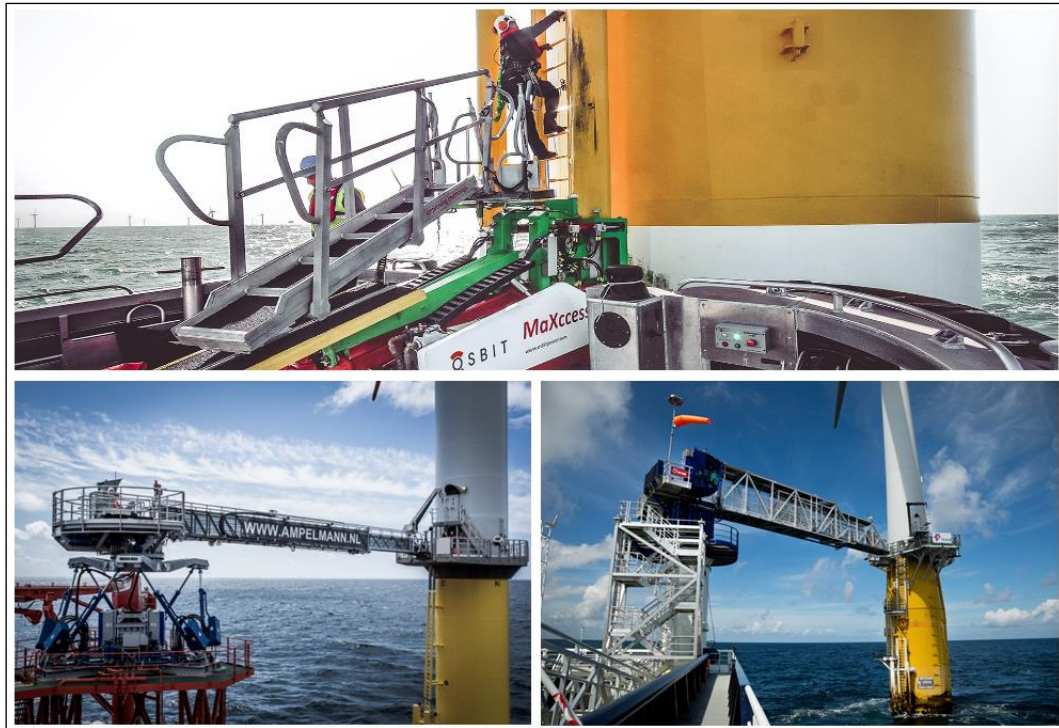


Fig. 1.1: Example of existing offshore ship-based motion compensation gangways

Top is Maxcess solution, bottom left is Ampelmann solution and bottom right is Uptime solution

The Maxcess solution compensates the motion by allowing relative motion between gangway and vessel when the end of gangway mechanically connected to the wind turbines. The Ampelmann solution compensates six degrees freedom (DOF) of motions with the use of the hydraulic hexapod and gangway is connected to the top of hexapod mechanically. For Uptime solution, it allows for full position compensation through slewing, luffing and telescopic motion of the gangway. These solutions are very popular in the offshore industry in the recent years but there are also many problems during the operation of gangway.

## 1.2 Motivation

The shortage of Maxcess solution is the limit ability of heave compensation. For Ampelmann solution, it is the only product, which allows full motion compensation, and obviously, it is the most complex solution. Also Cerda Salzman (2010) did a thorough research from modeling and simulation to field test on that system. But for Uptime solution, there is no research to investigate the dynamics of gangway during operation, which have great influence on the performance of the system. During the transferring operation, the gangway passageway connecting the ship and the wind turbine is pushed against to wind turbine platform via bumpers or similar clamping mechanisms considering the limited space and weight of wind turbine

platforms. But inaccuracy of either the measured motions of the ship from sensors or the compensating motions of the gangway causes residual motions that hampers safe positioning of the operation. And the contact force between gangway tip and the wind turbine platform is hard to control with pure active motion compensation (AMC). Consequently, the uncontrollable contact force may damage the wind turbine and the gangway, and affect the dynamic positioning of the small weight-class vessels. As a result, a proper control algorithm for controlling the contact force as well as compensating ship motion is necessary.

Hence, the reasons forming the motivations for the author to write this thesis are presented in the following:

- 1) The system of gangway need to be modeled in details and accurate way. Because the correct modeling of hydraulic system and multi-body dynamics is the key to simulate and predict the performance of gangway in the real operation.
- 2) The proper modeling and simulation of gangway operation system on vessel plays an important role to investigate the dynamics during gangway operation. This also can help to find an optimal control method.
- 3) A proper control approach for controlling the contact force as well as compensating the vessel motion should be developed and verified.

### **1.3 Problems and Challenges**

In order to investigate the gangway dynamics during operation and develop the control algorithm for the specified operation. The first problem comes to have a reasonable mechanical design for model development. And due to the lack of resources of such gangway model, an offshore gangway should be designed based on relative rules and existing products.

And the second problem to tackle is the development of mathematical framework in 20-sim for modeling the basic multi-body dynamics, described by Lagrangian equations of motion and dynamics of hydraulic system with bond graph language. We know that a good mathematical framework is important to achieve good simulation results and accurate control. Hence, the model should be developed in with proper complexity and details to capture the necessary dynamics for gangway operation.

The third problem is to develop a control algorithm for active motion compensation and contact force control. For AMC gangway, currently, the contact force between gangway tip and wind turbine platform is passively controlled by adjusting the pressure of the relief valve in the hydraulic circuits(Salen 2016). Depending on the performance of the hydraulic systems, this

control method is more efficient in principle since the pressure relieve valve directly responds to the controlled force. However, the effectiveness of such controller is unknown when both position and force control are active. So a parallel position and force control theory for robotic systems can be investigated and applied to gangway system to maintain the desired contact force between gangway and windmill platform as well as compensate ship motion.

#### **1.4 Objective**

The focus of this thesis is to develop proper position and force control algorithm for offshore AMC gangway during transferring operation. In order to develop and verify such controller, the model of gangway including hydraulic system model and multi-body dynamic model should be properly derived. Thus, the objective of thesis can be given as below:

- 1) To design the offshore gangway based on relative rules and the existing product of Uptime company and verify the structure with finite element analysis
- 2) To develop an approach to implement the multi-body dynamics of gangway into the gangway model with bond graph method.
- 3) To design the hydraulic system of gangway based on operational requirements and develop hydraulic system model of the gangway systems with bond graph method.
- 4) To derive proper control algorithm for active motion compensation.
- 5) To derive proper parallel position and force control algorithm for maintaining the gangway tip contact with windmill platform with desired level force (4000 N suggested by supervisors) as well as compensating the ship motion during transferring process.

#### **1.5 Scope of the thesis**

- a) Literature review on:
  - Application and operation of offshore motion compensated gangway systems
  - Modeling approach of hydraulic systems
  - Modeling approach of the kinematics and dynamics of rigid linked body systems
  - Active motion compensation control approach in marine operations
  - Combination of position and force control approach for manipulators
- b) Model development:
  - 3D model development of AMC gangway based on relative rules and finite element analysis
  - Multi-body dynamics model development of gangway with bond graph approach



- Hydraulic systems model development of the designed gangway using bond graph approach
  - Active motion compensation control algorithm development for AMC gangway system based on inverse kinematics calculation.
  - Combination of position and force control algorithm development for AMC gangway system based on parallel position and force control strategy in robotics.
- c) Perform simulation
- Perform simulation under designed active motion compensation controller and discuss results
  - Perform simulation under designed parallel position and force control controller and discuss results
  - Document each step in progress

## 1.6 Related Work

In this section, we present the most important references used in this thesis.

The mechanical design of offshore gangway is mainly based on the rules of DNVGL-ST-0358 (2015) and the existing product from Uptime company (UPTIME-Brochure). And some knowledge for design of gangway and finite element analysis is come from Cerda Salzman (2010) and Subramanian (2016).

Modeling and simulation of the dynamics of gangway system is mainly based on Lagrangian mechanics and bond-graph method. The main references for derivation the motion of equations and kinematics calculation of gangway are Spong (2006), Craig (2005) and Zhang (2015). These references provide the comprehensive knowledge and basic principles on manipulator kinematics and dynamics modeling.

References for bond-graph method used in this thesis are Karnopp, Margolis et al. (2012) and Pedersen and Engja (2014). These references provide the basic concept and framework for modeling dynamic systems of different energy domains. Also modeling method with IC-field for rigid-body motions and dynamics are provided. The master thesis Rokseth (2014) and Zhang (2015) helps me on implementation of the multi-body dynamics model of gangway into 20-sim with IC-field.

Bak and Hansen (2013) helps me on design and specify the relative parameters of hydraulic system of gangway. Pedersen and Engja (2014) and Karnopp, Margolis et al. (2012) provide

the basic principles regarding modeling of hydraulic components of hydraulic system. Chu, Æsøy et al. (2014) helps me on how implement the hydraulic system model into 20-sim with bond-graph methods.

In the controller design of gangway system, a variety of references has been used. Bak and Hansen (2013) and Kontz (2007) proposed position feedback and velocity feedforward controller for controlling directional control valve for a hydraulic manipulator. The master thesis of Sanders (2016) used inverse kinematics to map desired crane position and velocity to actuator space and then control the actuator with position and velocity feedback with velocity feedforward controller to compensate the ship motion. These references provides the general idea for the active motion compensation controller design for gangway system.

The main references for parallel position and force control are Su, Choi et al. (1990), Kesner and Howe (2011) and Fatemi, Majd et al. (2012). These references provide the method to implement the inner position loop force control approach for robotic where the position trajectory is adjusted to achieve a desired force on the target. Related to marine applications, Skaare and Egeland (2006) proposed a parallel position and force controller for the control of the load through the wave zone in offshore crane operation in order to reduce the wire oscillations. Wijnheijmer (2009) proposed a combination of position and force control algorithm for active tension control for heave compensation systems where position controller is used to compensate the ship motion and force controller is used to adjust the trajectory to achieve the desired riser tension. These references gives me a lot hint about the development of parallel position and force controller of gangway system.

## **1.7 Structure of the Thesis**

The structure of this thesis is present below by summarizing the main content of the following chapters.

**Chapter 2** provides an introduction to the background theories that will be used in this thesis. The bond graph modeling method for different energy domain system and IC field for modeling complex systems are introduced first. Then kinematics knowledge for manipulator is introduced. Finally, the approach for derivation of the equations of motion of manipulator using Lagrangian-Hamilton method and implementation the dynamics equation in bond graph language (IC-field) are given.

**Chapter 3** gives the concept design of offshore gangway based on the relative rules and existing product from Uptime company. And then the gangway structure is verified with finite element analysis.

**Chapter 4** presents the mathematical model of gangway dynamics and kinematics. It includes the simplification that made in order to simplify the overall model of gangway system, the kinematic model of gangway and dynamic model of gangway based on that simplification.

**Chapter 5** presents the basic hydraulic system of off shore heave compensated gangway and the system model based on bond graph method. First, the hydraulic system description regarding the basic components of hydraulic system for slewing king, luffing boom and telescopic boom will introduced. Then a design process regarding how to select proper hydraulic motor, hydraulic cylinders and pump and relative valves will be given. At last, the bond graph modeling of each components and overall system will be presented.

**Chapter 6** introduces the control algorithm for the gangway operation. It includes the definition of control task, control algorithm for active heave compensation and parallel position and force control algorithm for controlling the contact force as well as compensating ship motion during transferring operation.

**Chapter 7** concludes the work in this thesis and the recommendation for the future work on this subject.



## 2 Background Theories

In this chapter, the basic theories, which are used in the developing of gangway model in this thesis, will be presented. It will covers the theory of bond graph modeling, Lagrange approach for modeling linked rigid bodies and the method of implementation of the multi-body dynamics in 20-sim with bond graph theory.

### 2.1 Bond Graph Modeling

This section mainly introduce some of the basic elements and method for modeling for modeling system dynamics with bond graphs. A more detailed and thorough description of this approach is given by Karnopp, Margolis et al. (2012) and Pedersen and Engja (2014).

#### 2.1.1 Bond Graph Basics

Bond graph is a graphical representation of a system based on identifying the energetic properties of the system. The behavior of dynamic systems is governed by the flow, storage and interchange of various forms of energy between subsystems or elements. Therefore, a system can be divided into such group of elements, which are used for energy supply, energy storage, energy dissipation and energy transduction. And the bond graph approach naturally provides such basic elements for energy interaction between subsystems for modeling and simulation of a dynamic system. Each element in bond graph language has one or more ports used for energy flow between each other. And the power is transferred by the bonds between these ports. In this way, the model of a dynamic system can be built by these elements graphically.

In the bond graph language, the power  $P(t)$  transmitted through the port is determined by two variables, namely effort  $e(t)$  and flow  $f(t)$ , given by the relation

$$P(t) = e(t)f(t) \quad (2.1)$$

The direction of power flow can be indicated by a half-arrow on one end of the bond and a full arrow on a bond is called signal bond, which indicates a signal flow at very low power. The notation of these two bonds is shown Fig. 2.1 in below



Fig. 2.1: Sign convention on power and signal bonds

The power flowing direction is interpreted as the direction of the half-arrow whenever the power is positive. And the power variables  $e$  and  $f$  can be indicated on each side of a bond. By

convention, the effort variable  $e$  is written above a bond and flow variable  $f$  is written below a bond. Besides these, the casual stroke indicated by a vertical line between a bond and a subsystem is used to specify the causality. The following Fig. 2.2 shows the power transmitted from subsystem A to subsystem B. Based on convention, for subsystem A, the flow is input and effort is output; for subsystem B, the effort is the input to and flow is output. We can find that the effort is the input for a subsystem where the casual stroke end.

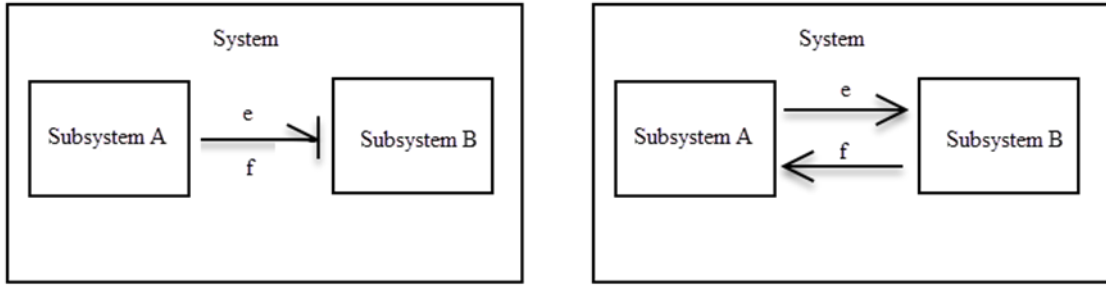


Fig. 2.2: Example of power transmitted between subsystem A and B with power bond

Besides the two power variables, there are still two other variables which are important to describe the energetic relation of systems. One is the generalized momentum  $p(t)$  and another is generalized displacement  $q(t)$  as defined below

$$p(t) = \int_0^t e(t)dt + p(0) \quad (2.2)$$

$$q(t) = \int_0^t f(t)dt + q(0) \quad (2.3)$$

As the effort and flow are defined as power variables, the momentum and displacement are called energy variable because stored energy  $E(t)$  can be expressed in terms of these variables as shown below.

$$E(t) = \int_0^t P(t)dt = \int_0^t e(t)f(t)dt \quad (2.4)$$

And from Eq. 2.2 and Eq. 2.3 we can obtain

$$edt = dp \quad \text{and} \quad fdt = dq \quad (2.5)$$

So the expression for stored energy can be rewritten in the terms of momentum function  $f(q)$  and displacement function  $e(q)$  as below

$$E(p) = \int_0^p f(p)dp \quad (2.6)$$

$$E(q) = \int_0^q e(q) dq \quad (2.7)$$

We know that in mechanics  $E(p)$  is called kinematic energy and  $E(q)$  is called potential energy. And until now we have four variables  $e(t), f(t), p(t)$  and  $q(t)$  to define the dynamic behavior of a multi-domain system.

The key to build the model of a multi-energy domain system is to identifying these variables in different energy domain. The following Table 2.1 shows a list of variables in some energy domains used for developing of gangway model in this thesis. For comprehensive study of these variables in different energy-domain systems, the reader is advised to consult Pedersen and Engja (2014).

Table 2.1 Variables of some different energy-domain systems in bond graph

Energy domain	Effort	Flow	Momentum	Displacement
Electrical	Voltage [V]	Current [A]	Flux linkage [Vs]	Charge [As] or [C]
Mechanical translation	Force [N]	Velocity [m/s]	Linear Momentum [kgm/s]	Distance [m]
Mechanical rotation	Torque [Nm]	Angular velocity [rad/s]	Angular momentum [Nms]	Angle [rad]
Hydraulic	Pressure [Pa]	Volume flow rate [m <sup>3</sup> /s]	Pressure momentum N/m <sup>2</sup> s]	Volume [m <sup>3</sup> ]

In order to develop the system model with bond graphs, a set of basic elements describing the energetic properties of the system need to be defined. As we mentioned previously, these elements function as energy supply, energy storage, energy dissipation, and energy conversion.

In addition to these elements, in order to link these elements together to represent the properties of a real physical system, two types of junction element are defined in the formalism of bond graphs. One is 0-junction and another is 1-junction. They neither store nor dissipate energy, but merely transmit it. Table 2.2 conclude the most common used basic elements in the bond graph modeling and the constitutive relations for these elements (Pedersen and Engja 2014). symbol

Table 2.2 Basic bond graph elements

Name	Bond-graph Symbol	Constitutive relation
Effort source	$S_e \longrightarrow$	$e(t) = \text{given}$
Flow source	$S_f \longleftarrow$	$f(t) = \text{given}$
Resistance	$\longleftarrow R$	$e = \Phi_R(f)$
	$\longrightarrow R$	$f = \Phi_R^{-1}(e)$
Capacitance	$\longleftarrow C$	$e = \Phi_C^{-1}(\int f dt)$
	$\longrightarrow C$	$f = \frac{d}{dt}[\Phi_C(e)]$
Inertia	$\longrightarrow I$	$f = \Phi_I^{-1}(\int e dt)$
	$\longleftarrow I$	$e = \frac{d}{dt}[\Phi_I(f)]$
Transformer	$\xrightarrow{1} \text{TF} \xrightarrow{2}$	$e_1 = m e_2, \quad f_2 = m f_1$
	$\xleftarrow{1} \text{TF} \xleftarrow{2}$	$e_2 = \frac{e_1}{m}, \quad f_1 = \frac{f_2}{m}$
Gyrator	$\xrightarrow{1} \text{GY} \xrightarrow{2}$	$e_1 = r f_2, \quad e_2 = r f_1$
	$\xleftarrow{1} \text{GY} \xleftarrow{2}$	$f_1 = \frac{e_2}{r}, \quad f_2 = \frac{e_1}{r}$
0-junction	$\xrightarrow{1} 0 \xleftarrow{2}$ $\uparrow 3$	$e_1 = e_2 = e_3$ $f_1 + f_2 + f_3 = 0$
1-junction	$\xrightarrow{1} 1 \xleftarrow{2}$ $\uparrow 3$	$f_1 = f_2 = f_3$ $e_1 + e_2 + e_3 = 0$

Based on the constitutive relations given in Table 2.2, we can see that the  $S_e$ -element gives a prescribed effort to a system regardless of the flow. And for the  $S_f$ -element, it inputs a given



flow to a system regardless of the effort. Both of these two source elements can be modified to take input signals and act as modified source elements denoted by  $MS_e$  and  $MS_f$  respectively.

The R-element takes away energy from the system. It can be used to model all kinds of energy dissipation such as mechanical and hydraulic friction and electrical resistance. The C-element and I-element are such kind of elements used to store energy. The difference between them are that C-element stores kinematic energy and I-element stores potential energy. C-elements are usually used to model physical components such as springs, capacitors and liquid storage tanks. For the I-element, it is often used to model physical objects such as a mass, inductance in electrical system and inertia effects in hydraulic systems.

The TF-element and GY-element are used to transduce the energy between two components. TF-elements transforms an effort of one port to an effort of the other port with a magnitude depending on the transformer modulus. In contrast to the TF-element, GY-element transforms an effort on one bond into flow of the other bond with a magnitude depending on the gyrator modulus. Also, these two elements can take input signals and act as modified transformer element and gyrator element denoted by MTF and MGY respectively.

The last two elements in the Table 2.2 are called junction elements as mentioned before and both of them are multi-ports elements. All the power bonds connected to 0-junction have the same effort and the algebraic sum of all flow is zero. As opposed to 0-junction, all the elements connected to 1-junction share the same flow and the algebraic sum of all effort is zero.

Apart from these basic bond-graph elements, proper causality assignment is the key to model a system correctly. From the description previously, we know that the causality for source element is quite straightforward. And based on that, the causality of other elements can be easily derived. For C element, it has two possible causalities according to the constitutive relation. If the flow is the input, then the causality is called integral causality otherwise it is called derivative causality. And for I element, it also has two possible causalities. If the effort is input, then the causality is integral causality otherwise, it is derivative causality. But integral causality is the preferable choice for these two elements based on the physical properties of real systems. But sometimes, the causality for I element and C element will be mathematically forced to be derivative.

According to the constitutive relation of 0-junction and 1-junction, we can see that there should only one effort can be an independent variables and all of the rest are dependent variables. It means that only one stroke is placed on junction side of bond. In contrast, for 1-junction, all the

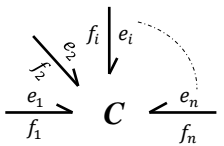
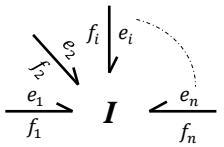
casual stroke of bonds except one should be placed on the junction side. For the rest of basic elements, both integral and derivative causality can be assigned and usually they should be determined by the other element causalities assignment when creating a bond-graph model for a system. However, for modeling in 20-sim, the causalities of elements will be assigned automatically based above conventions.

### 2.1.2 Multiport Fields

Although we have such basic bond-graph elements described above, we will find that it has difficulties when modeling complex system with many power and energy variables. So it is convenient to represent these system properties using vector relations rather than scalar bond-graph elements. To address this problem, fields, which are multiport generalization of R, C and I elements, are introduced. Similar to the basic bond graph elements, to hook these fields together, junction structures will be utilized which include 0-junction, 1-junction, multiport transformer and multiport gyrator. In this part, we focus on I-fields; C-fields and IC-fields applications because IC-field will be utilized when implement the Hamiltonian-Lagrangian equation of gangway dynamics with bond graphs in 20-sim software in the later chapter.

Because IC fields is a combination of I-fields and C-fields in some way. So I-fields and C-fields will be studied before look into IC-fields. We should notice that the physical properties for I-element and C-element still hold true for I-fields and C-fields. The following Table 2.3 shows the symbol for C-field, I-field, and the constitutive relations.

Table 2.3 Definition of C-field and I-field

Fields name	Bond-graph symbol	Constitutive relation	Variables
N-port <b>C</b> -field		$e = \Phi_C^{-1}(q)$ $q = \Phi_C(e)$	$e = [e_1, e_2, \dots, e_n]^T$ $q = [q_1, q_2, \dots, q_n]^T$
N-port <b>I</b> -field		$f = \Phi_I^{-1}(p)$ $p = \Phi_I(f)$	$f = [f_1, f_2, \dots, f_n]^T$ $p = [p_1, p_2, \dots, p_n]^T$

Based on the constitutive relations of C-field and I-field shown in Table 2.3, we can easily see that both of C-field and I-field can have complete integral causality and derivative causality. In addition, C-field and I-field can be assigned mixed causality, i.e. it has mixed integral-

differential causality. For a more comprehensive study of the causality assignment of C-field and I-field, the reader is advised to consult Karnopp, Margolis et al. (2012).

However, sometimes when dealing with modeling of single component of the system involved both kinematic and potential energy or even more energy domains, we can find advantageous by combining I-field and C-field together to model that system. This kind of field combining I-field and C-field into one field called IC-field. It accumulates both the kinematic and potential energy. It is often used to model transducers, rigid body motion or fluid flow. The general symbol for IC-field and its constitutive relation are shown in Table 2.4 below.

Table 2.4 Illustration of IC-field and the constitutive relation

Field name	Bond-graph symbol	Constitutive relation	Variables
IC-field		$f = \Phi_i(p, q)$ $e = \tilde{\Phi}_j(p, q)$	$f = [f_1, f_2, \dots, f_I]$
			$e = [\tilde{e}_1, \tilde{e}_2, \dots, \tilde{e}_C]$
			$p = [p_1, p_2, \dots, p_I]$
			$q = [q_1, q_2, \dots, q_C]$
			$i = [1, 2, \dots, I]$
			$j = [1, 2, \dots, C]$

Up to now, we have went through the necessary knowledge of bond-graph theory for this thesis. And the application of bond-graph approach in thesis in deriving gangway motion dynamics and modeling and simulation for the whole system will be presented in the later chapters.

## 2.2 Kinematics

In this section, we will introduce the basic theory regarding the kinematics of robot manipulator and this will be used to derive the kinematics of gangway system in this thesis. It will cover the basic rigid body motion theory, forward manipulator kinematics, inverse manipulator kinematics robotic manipulator and Jacobians. Most of the following theories in this section are coming from Zhang (2015), Craig (2005) and Spong (2006).

### 2.2.1 Rigid Body Motion

To describe the motion of rigid body means to specify the orientation and position of the rigid body to some specified reference frame. In order to describe the orientation of a body, we will attach a coordinate system to the body and then give a description of this coordinate system to

the reference system. To illustrate this principle, we will demonstrate how to describe body-attach coordinate system with origin of P on the rigid body in the reference coordinate system as below.

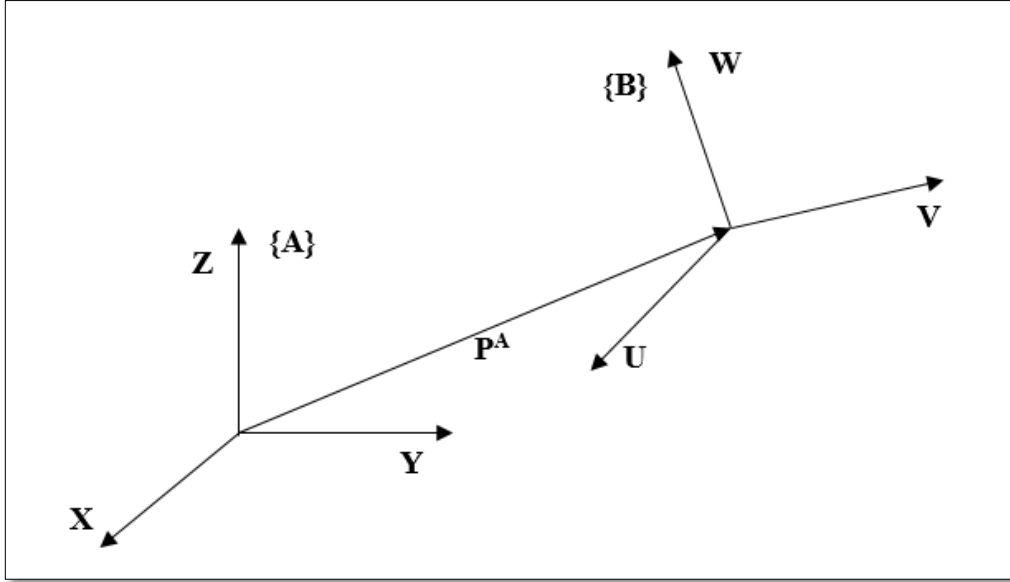


Fig. 2.3: Illustration of description the orientation of body-attached coordinate system

We can see that the position of P can be specified by the vector  $P^A$  and the orientation of this rigid body can be described by the description of body-attached coordinate system {B} to coordinate system {A}. One way to describe the {B} relative to {A} is to express the unit vector of its three principal axes in terms of the coordinate system {A}. The unit vectors of {B} axes are denoted as  $i_u, j_v$  and  $k_w$ . When expressed these axes in terms of unit vectors of {A}, i.e.  $i_x, j_y$  and  $k_z$ , they are called  $U^A, V^A$  and  $W^A$ . So the rotation matrix from {B} to {A} can be given below

$$R_B^A = [U^A, V^A, W^A] = \begin{bmatrix} i_x \cdot i_u & i_x \cdot j_v & i_x \cdot k_w \\ j_y \cdot i_u & j_y \cdot j_v & j_y \cdot k_w \\ k_z \cdot i_u & k_z \cdot j_v & k_z \cdot k_w \end{bmatrix} \quad (2.8)$$

We can easily find that this rotation matrix is orthogonal matrix. Then we have following

$$R^T R = I \quad (2.9)$$

Where R is rotation matrix and I is three by three identity matrix

So we have

$$R^T = R^{-1} \quad (2.10)$$

When these two coordinates have both relative rotational and translational motion, then any point P in coordinate system {B} can be expressed in coordinate system {A} as following

$$P^A = R_B^A P^B + P_{BORG}^A \quad (2.11)$$

Where  $P^B$  is  $3 \times 1$ -position vector of point P expressed in {B} and  $P_{BORG}^A$  is the  $3 \times 1$ -position vector of the origin of coordinate system {B} expressed in coordinate system {A}.

Based on Equation 2.11, we have the following

$$r^A = \begin{bmatrix} R_B^A & P_{BORG}^A \\ 0 & 1 \end{bmatrix} r^B \quad (2.12)$$

Where  $r^A$  is  $[P^A, 1]^T$  and  $r^B$  is  $[P^B, 1]^T$

Then the homogenous transformation matrix between to relative frames are given as

$$T_B^A = \begin{bmatrix} R_B^A & P_{BORG}^A \\ 0 & 1 \end{bmatrix} \quad (2.13)$$

So until now we have the rotation and transformation matrix between two relative coordinate systems. With these, we can express any point in coordinate system {B} in the coordinate system {A} and this is quite useful in solving the kinematics problem of linked rigid bodies in spatial motion.

## 2.2.2 Manipulator Kinematics

Kinematics is the science of motion that treats the subject without considering forces or torques that cause it. It can be divided into forward kinematics and inverse kinematics. Forward kinematics is such method used to compute the position and orientation of end-effector relative to the base frame of the manipulator in terms joint variables. In contrast, inverse kinematics is to calculate the joint variables for a given position and orientation of end-effector.

A manipulator can be described as a set of links connected in a chain by joints. Most of the manipulator has simple joints such as revolute and prismatic joints. In the rare case, if there is a mechanical joint with  $n$  degrees of freedom, it still can be modelled as  $n$  joints of one degree of freedom connected with  $n - 1$  links with zero length. So the joints of manipulator will be considered only has one degree of freedom.

The links are numbered from the immobile base of the manipulator, which is called link 0 and the first moving body is link 1, and so on, out to the end-effector, which is called link  $n$ . By convention, the axis of joint  $i$  is defined by a vector in the space, about which link  $i$  rotates relative to link  $i - 1$  as shown in Fig. 2.4. And the joint variable for the  $i_{th}$  joint is defined as below

$$q_i = \begin{cases} \theta_i & \text{if joint } i \text{ is revolute} \\ d_i & \text{if joint } i \text{ is prismatic} \end{cases} \quad (2.14)$$

To describe the kinematics of manipulator systematically, Denavit and Hartenberg provide one convention to describe the each link with four parameters and affix frames to each link as shown in Fig. 2.4{Craig, 2005 #39}.

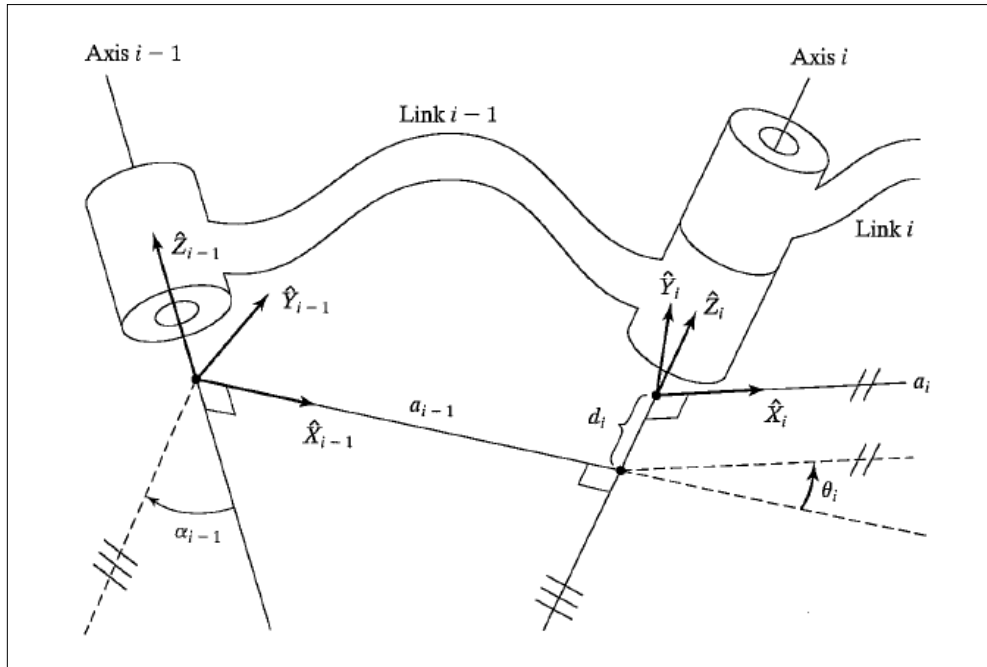


Fig. 2.4: Illustration of D-H parameters and link-attached frames

According to D-H convention, the four parameters used to describe any link of manipulator are defined as below

- Link length, i.e.  $a_{i-1}$  is defined as the distance measured along a line that is mutually perpendicular to joint axis  $i - 1$  and joint axis  $i$
- Link twist, i.e.  $\alpha_{i-1}$  is defined as the angle measured from axis  $i - 1$  to axis  $i$  in the right hand sense about  $a_{i-1}$ .
- Link offset, i.e.  $d_i$  is defined as the signed distance measured along the axis  $i$  from the point where  $a_{i-1}$  intersects the axis to the point where  $a_i$  intersects the axis.
- Joint angle, i.e.  $\theta_i$  is defined as the angle measured from the extension of  $a_{i-1}$  to  $a_i$  along axis  $i$  in right hand sense.

And for the link attached frames, it defines that frame  $\{i\}$  is attached to link  $i$ . And the assignment of each axis and origin of frame  $\{i\}$  is shown below

- $\hat{Z}_i$  is coincident with joint axis  $i$ .
- The origin of frame  $\{i\}$  is located where the  $a_i$  perpendicular intersects with the joint axis  $i$ .

- $\hat{X}_i$  points along  $a_i$  in the direction from joint  $i$  to joint  $i + 1$
- $\hat{Y}_i$  can be specified according to the right hand coordinate system rule.
- Frame  $\{0\}$  is arbitrary but for simplification,  $\hat{Z}_0$  is chosen along  $\hat{Z}_1$ .
- $\hat{X}_n$  direction freely but generally to cause as many link parameters as possible to be zero.

Once we assigned link frames properly according the convention above, then link parameters can also be specified by the axis of frames as below

- $a_{i-1}$ : the offset distance from  $\hat{Z}_{i-1}$  to  $\hat{Z}_i$  along  $\hat{X}_{i-1}$
- $\alpha_{i-1}$ : the offset angle from  $\hat{Z}_{i-1}$  to  $\hat{Z}_i$  about  $\hat{X}_{i-1}$
- $d_i$ : the distance from  $\hat{X}_{i-1}$  to  $\hat{X}_i$  along  $\hat{Z}_i$
- $\theta_i$ : the joint angle from  $\hat{X}_{i-1}$  to  $X_i$  about  $Z_i$

And based on this convention, each homogenous transformation matrix  $T_i^{i-1}$  can be given

$$T_i^{i-1} = \begin{bmatrix} c\theta_i & -s\theta_i & 0 & a_{i-1} \\ s\theta_i c\alpha_{i-1} & c\theta_i c\alpha_{i-1} & -s\alpha_{i-1} & -s\alpha_{i-1}d_i \\ s\theta_i s\alpha_{i-1} & c\theta_i s\alpha_{i-1} & c\alpha_{i-1} & c\alpha_{i-1}d_i \\ 0 & 0 & 0 & 1 \end{bmatrix} \quad (2.15)$$

Where  $c$  means *cosine* function and  $s$  means *sine* function and  $i$  starts from 1

So for an n-link manipulator, the transformation matrix from frame  $\{N\}$  to base frame  $\{0\}$  can be given below

$$T_n^0 = T_1^0 T_2^1 \dots T_n^{n-1} \quad (2.16)$$

And based on this we can express any point on the manipulator in base frame or inertia frame as shown below which is very useful when finding position of gravity center of each link for deriving the dynamics equation of manipulator.

$$r^0 = T_n^0 r^n \quad (2.17)$$

Where  $r^0$  is  $[P^0, 1]^T$  and  $r^n$  is  $[P^n, 1]^T$  and  $P^0$  and  $P^n$  is the position vector of any point in the frame  $\{N\}$  expressed in frame  $\{0\}$  and frame  $\{N\}$  respectively.

In order to define the position of end-effector of manipulator, we attached a tool frame at the end of manipulator and defined as frame  $\{N+1\}$ . The direction of all the axis of the tool frame is same as frame  $\{N\}$  and the origin is at the end of the manipulator.

In the previous section of this part, we has discussed how to determine the end effector's position and orientation in terms of the joint angles. However, there are many situations such as realization control of manipulator and design actuators for manipulator where we need to know joint variables for a given orientation and position of the end effector. The general

problem involving inverse kinematics is quite difficult, it may have not only one set of configurations for a given position and orientation or no solution if it is out of the reachable workspace. But it turns out it is possible to decouple the inverse kinematics into inverse position kinematics and inverse orientation kinematics. It can be solved by closed-form solution and numerical solution. Because this is not the concentration of this thesis, so we will not go into details about how to solve the inverse kinematics problem. For a thorough study of this field, the reader is advised to consult Craig (2005) and Spong (2006).

But in engineering application, although we have some mathematical solutions for inverse kinematics problems, we have to take the reality constraints such as working space, physical properties of actuators or safety operation into consideration when design a manipulator.

### 2.2.3 Jacobians

Jacobian is a matrix that generalizes the notion of the ordinary derivative of scalar function and the notation for it is  $J$ . In the field of manipulators, it defines the relation from joints velocities to the angular and linear velocity of manipulator links. It is composed of two parts, i.e. linear velocity Jacobian and angular velocity Jacobian which are denoted as  $J_v$  and  $J_w$ .

$$J = \begin{bmatrix} J_v \\ J_w \end{bmatrix} \quad (2.18)$$

And the body velocities denoted as  $\xi$  can be divided into two parts, i.e. linear velocity  $v$  and angular velocity  $\omega$ . The joints' displacement and velocity are defined as  $q$  and  $\dot{q}$  respectively. For an  $n$ -link manipulator, the number for the tool frame axis is  $N + 1$ . So the relation between end-effector velocity expressed in frame  $\{0\}$  and joints' velocities can be given

$$\xi_{n+1}^0 = \begin{bmatrix} v_{n+1}^0 \\ \omega_{n+1}^0 \end{bmatrix} = J \dot{q} \quad (2.19)$$

Where  $J$  is a  $6 \times n$  matrices and  $\dot{q}$  is  $[q_1, q_2, \dots, q_n]^T$ .

The linear velocity of the end effector of  $n$ -link manipulator is denoted as  $\dot{o}_{n+1}^0$  given below

$$\dot{o}_{n+1}^0 = \sum_{i=1}^n \frac{\partial o_{n+1}^0}{\partial q_i} \dot{q}_i \quad (2.20)$$

Where the  $\dot{o}_{n+1}^0$  means the velocity of the origin of tool frame  $\{N+1\}$  is expressed in inertia frame or base frame  $\{0\}$  and  $q_i$  and  $\dot{q}_i$  means the  $i$ th joint displacement and  $i$ th joint velocity respectively.

Then we can find that the  $i$ th column of  $J_v$  denoted as  $J_{v_i}$  can be given



$$J_{v_i} = \frac{\partial o_{n+1}^0}{\partial q_i} \quad (2.21)$$

Considering the contribution of joints for  $J_v$ ,  $J_{v_i}$  can be expressed as below

$$J_{v_i} = \begin{cases} z_i^0 \times (o_{n+1}^0 - o_i^0) & \text{for revolute joint } i \\ z_i^0 & \text{for prismatic joint } i \end{cases} \quad (2.22)$$

Where  $z_i^0$  is the  $\hat{Z}$  axis of frame  $i$  expressed in frame  $\{0\}$ ,  $o_i^0$  is the origin of frame  $\{i\}$  expressed in frame  $\{0\}$  and  $i \in [1, n]$ .

And the linear Jacobian for end effector is given

$$J_v = [J_{v_1}, J_{v_2}, \dots, J_{v_n}] \quad (2.23)$$

For the angular velocity of the end effector, we know that when a rigid body rotate, every point on the body has the same angular velocity. And based on skew theory, the angular velocity of end-effector expressed in frame  $\{0\}$  denoted by  $\omega_{n+1}^0$  can be expressed as

$$\omega_{n+1}^0 = R_1^0 \omega_1^1 + R_2^0 \omega_2^2 + \dots + R_n^0 \omega_n^n \quad (2.24)$$

Where the superscripts of  $\omega_n^n$  means the angular velocity of frame  $\{N\}$  and the subscripts means that in which frame the angular velocity of frame  $\{N\}$  is expressed.

And we know that angular velocity of frame  $\{N\}$   $\omega_n^n$  can also be written as

$$\omega_n^n = \dot{q}_i \hat{Z}_i^i$$

Where  $\hat{Z}_i^i$  is the  $\hat{Z}$  axis of frame  $\{i\}$  expressed in frame  $\{i\}$ , i.e.  $[0,0,1]^T$ .

Then we have

$$\omega_{n+1}^0 = \rho_1 \dot{q}_1 R_1^0 z_1^1 + \rho_2 \dot{q}_2 R_2^0 z_2^2 + \dots + \rho_n \dot{q}_n R_n^0 z_n^n \quad (2.25)$$

$$\omega_{n+1}^0 = \rho_1 \dot{q}_1 z_1^0 + \rho_2 \dot{q}_2 z_2^0 + \dots + \rho_n \dot{q}_n z_n^0 \quad (2.26)$$

Where  $\rho_i$  is equal to one if the joint is revolute and 0 if it is prismatic

So the angular Jacobian for the end-effector of an n-link manipulator is given as

$$J_\omega = [J_{\omega_1}, J_{\omega_2}, \dots, J_{\omega_n}] \quad (2.27)$$

Where the  $i$ th column of  $J_\omega$ , i.e.  $J_{\omega_i}$  is

$$J_{\omega_i} = \begin{cases} z_i^0 & \text{for revolute joint } i \\ 0 & \text{for prismatic joint } i \end{cases} \quad (2.28)$$

The linear and angular Jacobian can also be extended to any point on the manipulator. Recall Equation 2.17, we know that for any point P on the  $i$ th link of an n-link manipulator, it has

$$[P_{p_i}^0, 1]^T = T_i^0 [P_{p_i}^i, 1]^T \quad (2.29)$$

Where  $P_{p_i}^i$  means the position vector of point P in frame  $\{i\}$  expressed in frame  $\{i\}$  and  $P_{p_i}^0$  means the position vector of point P expressed in frame  $\{0\}$

So the Jacobian, i.e.  $J^{p_i}$  for any point P on  $i$ th frame of an n-link manipulator is given below

$$J^{p_i} = [J_1^{p_i}, J_2^{p_i}, \dots, J_n^{p_i}] \quad (2.30)$$

Where  $k \in [1, n]$  and the  $k$ th column of  $J^{p_i}$ , i.e.  $J_k^{p_i}$  is

$$J_k^{p_i} = \begin{cases} J_{v_k}^{p_i} & \begin{cases} \text{if } k \leq i & \begin{cases} z_k^0 \times (P_{p_i}^0 - o_k^0) & \text{for revolute joint } i \\ z_k^0 & \text{for prismatic joint } i \end{cases} \\ \text{if } k > i & 0 \end{cases} \\ J_{\omega_k}^{p_i} & \begin{cases} \text{if } k \leq i & \begin{cases} z_k^0 & \text{for revolute joint } i \\ 0 & \text{for prismatic joint } i \end{cases} \\ \text{if } k > i & 0 \end{cases} \end{cases} \quad (2.31)$$

## 2.3 Manipulator Dynamics

Dynamics is the field of studying the external forces or torques required to cause motion of manipulators. In this section, we will introduce the basic theories of compute the dynamics equation of manipulator and how to implement the dynamics equation with bond-graph into 20-sim software. These are necessary and important for manipulator design, modeling and simulation of manipulator motion, and design of control algorithms. The following theories of this section are mainly from Spong (2006) and Craig (2005) .

### 2.3.1 Euler-Lagrange Equation

Euler-Lagrange Equations is an energy-based approach to derive the dynamics equation of manipulators. In order to determine the Euler-Lagrange Equation of a specific system, one has to form the Lagrangian of the system, which is the difference between the kinetic energy and the potential energy of the system as shown below

$$\mathcal{L} = \mathcal{K} - \mathcal{P} \quad (2.32)$$

Where  $\mathcal{L}$ ,  $\mathcal{K}$  and  $\mathcal{P}$  are the notation for Lagrangian, total kinetic energy and total potential energy of the system respectively.

With the formulation of Lagrangian, the dynamics of the manipulator can be described in terms of a set so-called generalized coordinates, i.e. the joint variables rather than reference frames as shown below

$$q = [ q_1, q_2, \dots, q_n ] \quad (2.33)$$

$$\tau = [ \tau_1, \tau_2, \dots, \tau_n ] \quad (2.34)$$

$$\frac{d}{dt} \frac{\partial \mathcal{L}}{\partial \dot{q}_i} - \frac{\partial \mathcal{L}}{\partial q_i} = \tau_i \quad (2.35)$$

Where  $q$  and  $\dot{q}$  denotes joints' variable displacements and joints' velocity respectively;  $\tau$  is the generalized forces corresponding to generalized coordinates. Equation 2.35 is called Euler-Lagrange Equation.

As we shall see, the Lagrangian approach provides an easier way for deriving the dynamic equations for complex systems such as multi-link manipulator.

### 2.3.2 Kinetic and Potential Energy of an N-Link Manipulator

The general form of kinetic energy for a rigid body in space can be expressed as

$$\mathcal{K} = \frac{1}{2} m v^T v + \frac{1}{2} \omega^T I_b \omega \quad (2.36)$$

Where  $m$  is the total mass of the rigid body,  $v$  and  $\omega$  are the linear and angular velocity vectors expressed in inertia frame, and  $I_b$  is the symmetric  $3 \times 3$  matrices called the inertia tensor expressed in inertia frame.

For a manipulator, usually the given inertia tensor denote as  $I$  for the link is expressed in the body-attached frame as

$$I = \begin{bmatrix} I_{xx} & I_{xy} & I_{xz} \\ I_{yx} & I_{yy} & I_{yz} \\ I_{zx} & I_{zy} & I_{zz} \end{bmatrix} \quad (2.37)$$

Where the diagonal terms are called principal moments of inertia and the rest are called cross products of inertia.

Since both linear and angular velocity are expressed in inertia frame in the calculation of kinetic energy, so the inertia tensor for  $ith$  link of manipulator should be expressed in inertia frame as well shown below

$$I_{b_i} = R_i^0 I_i R_i^{0T} \quad (2.38)$$

Where  $I_i$  and  $I_{b_i}$  denote the inertia tensor relative to the mass center of  $ith$  link expressed in body attached frame and inertia frame, i.e.  $\{0\}$  frame respectively.

Here we denote the angular velocity and linear velocity of the gravity center of  $ith$  link expressed in inertia frame as  $v_{ci}^0$  and  $\omega_{ci}^0$ . Then the total kinetic energy of the  $n$ -link manipulator can be given as

$$\mathcal{K} = \frac{1}{2} \sum_{i=0}^n \left( m_i v_{ci}^0 v_{ci}^{0T} + \omega_{ci}^0 I_{bi} \omega_{ci}^{0T} \right) \quad (2.39)$$

And according to the Jacobians, the linear and angular velocity of  $ith$  link gravity center are given as

$$v_{ci}^0 = J_v^{ci} \dot{q} \quad (2.40)$$

$$\omega_{ci}^0 = J_\omega^{ci} \dot{q} \quad (2.41)$$

Where  $\dot{q}$  is the velocities of joints' variables, i.e.  $[\dot{q}_1, \dot{q}_2, \dots, \dot{q}_n]$ ; and  $J_v^{ci}$  and  $J_\omega^{ci}$  can be given based on Equation 2.30 and Equation 2.31.

Therefore, the total kinetic energy of the  $n$ -link manipulator can be rewritten as

$$\mathcal{K} = \frac{1}{2} \dot{q}^T \left[ \sum_{i=1}^n \left\{ m_i J_v^{ci}(q)^T J_v^{ci}(q) + J_\omega^{ci}(q)^T R_i^0(q) I_i R_i^0(q)^T J_\omega^{ci}(q) \right\} \right] \dot{q} \quad (2.42)$$

$$\mathcal{K} = \frac{1}{2} \dot{q}^T D(q) \dot{q} \quad (2.43)$$

Where

$$D(q) = \left[ \sum_{i=1}^n \left\{ m_i J_v^{ci}(q)^T J_v^{ci}(q) + J_\omega^{ci}(q)^T R_i^0(q) I_i R_i^0(q)^T J_\omega^{ci}(q) \right\} \right] \quad (2.44)$$

Here,  $D(q)$  is a  $n \times n$  configuration dependent matrix called the inertia matrix, which is symmetric and positive, definite for any manipulator.

For total potential energy of the manipulator, it is the sum of the potential energy of each link. Since the position of gravity center of  $ith$  link of manipulator can be easily achieved from the transformation matrix  $T_i^0$  as described in Equation 2.29, then the derivation of the total potential energy of the manipulator is quite straightforward as given below

$$P = \sum_{i=1}^n -m_i g_0^T P_{ci}^0 \quad (2.45)$$

Where  $g_0$  is  $3 \times 1$  gravity acceleration vector, namely, if  $\hat{Z}_0$  is the vertical axis of the inertia frame  $\{0\}$ ,  $g_0 = [0, 0, -g]^T$  and  $P_{ci}^0$  is a  $3 \times 1$  position vector of  $ith$  link gravity center expressed in inertia frame  $\{0\}$ .

### 2.3.3 Bond Graph Modeling of Manipulator Motion Dynamics

Up to now, we have introduced how to derive the total kinetic energy and potential energy of an n-link manipulator. However, in order to model the manipulator motion dynamics with bond graph approach we have to rewrite the Euler-Lagrange Equation into Hamiltonian form. Because the Hamiltonian form not only more useful for computation but also is more compatible with bond graph formalism (Karnopp, Margolis et al. 2012).

Based on Equation 2.32 and Equation 2.35, Euler-Lagrange Equation can be rewritten as

$$\frac{d}{dt} \frac{\partial \mathcal{K}}{\partial \dot{q}} - \left( \frac{\partial \mathcal{K}}{\partial q} - \frac{\partial P}{\partial q} \right) = \tau \quad (2.46)$$

Based on Equation 2.43, the items on the left side of Equation 2.46 can be given as followings

$$\frac{d}{dt} \frac{\partial \mathcal{K}}{\partial \dot{q}} = \frac{d}{dt} (D(q) \dot{q}) \quad (2.47)$$

Similarly

$$\frac{\partial \mathcal{K}}{\partial q} = \frac{1}{2} \dot{q}^T \frac{\partial D(q)}{\partial q} \dot{q} \quad (2.48)$$

And the potential energy differentiated with respect to the generalized coordinates is the vector of restoring forces denoted by  $g(q)$  (Sciavicco 2000).

$$\frac{\partial P}{\partial q} = g(q) \quad (2.49)$$

So the Euler-Lagrange Equation is given by inserting Equation 2.47 , 2.48 and 2.49 above

$$\frac{d}{dt} (D(q) \dot{q}) - \left( \frac{1}{2} \dot{q}^T \frac{\partial D(q)}{\partial q} \dot{q} - g(q) \right) = \tau \quad (2.50)$$

Where  $(D(q) \dot{q})$  is the generalized momentum denoted by  $p$  as below

$$p = D(q) \dot{q} \quad (2.51)$$

Hence, we have

$$\dot{q} = D(q)^{-1} p \quad (2.52)$$

Because  $D(q)$  is a symmetric matrix, so  $(D(q)^{-1})^T = D(q)^{-1}$ . And by inserting Equation 2.51 and 2.52 into Equation 2.50, we obtain

$$\dot{p} = \frac{1}{2} p^T D(q)^{-1} \frac{\partial D(q)}{\partial q} D(q)^{-1} p - g(q) + \tau \quad (2.53)$$

$$\dot{p} = e'(p, q) + \tau \quad (2.54)$$

Where

$$e'(p, q) = \frac{1}{2} p^T D(q)^{-1} \frac{\partial D(q)}{\partial q} D(q)^{-1} p - g(q) \quad (2.55)$$

Therefore, we have the state space equation as

$$\begin{aligned} \dot{q} &= D(q)^{-1} p \\ \dot{p} &= e'(p, q) + \tau \end{aligned} \quad (2.56)$$

We can find that the space state equation 2.56 is the constitutive relation for the IC-field as described in Fig. 2.5 below and the flow of 1-junction is set by  $p1. f = \dot{q} = D(q)^{-1} p$

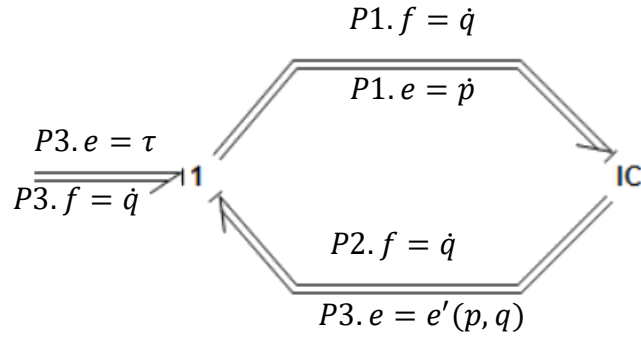


Fig. 2.5 Illustration of modeling manipulator dynamics with bond-graph

As a conclusion of this section, we can see that by rewriting the Euler-Lagrange Equation of manipulator into Hamiltonian form, we can obtain the constitutive relation for IC-field. And then we can easily model the motion dynamics of manipulator with a compact and clear structure with bond-graph.

### 3 Gangway Design

The purpose of this chapter is to introduce the gangway that used a basis for modeling, simulation and control of gangway operation in the later chapters of the thesis. It includes the design requirements, conceptual design and strength analysis. In order to shorten the report, the strength analysis of the designed gangway is given in Appendix A rather than here.

#### 3.1 Design requirements

The initial design stage is to identify the technical requirements and study relative standards relating to design. DNVGL-ST-0358 (2015) was carefully followed during the design process. And the technical design requirements is given based on the small type of gangway of Uptime company (UPTIME-Brochure) as below.

- The range of operating lengths is 7m – 10m
- Operation angle is +25 degrees and -15 degrees
- Walkway width is 0.8 m
- Achieve the lowest weight possible which will meet the certification requirements

For the ability of motion compensation, due to time limitation and considering the purpose of this thesis is about the modeling, simulation and control of gangway system, we only consider the ship motion in X and Z axis . And the simplified general function of these two motion are given as below

- $X = 0.5\sin\left(\frac{2\pi}{12}t\right)$  m
- $Y = 0$  m
- $Z = \sin\left(\frac{2\pi}{12}t\right)$  m

#### 3.2 Conceptual Design

The mechanical structure consists of four parts, which include the pedestal, slewing king, luffing boom and telescopic boom. The slewing king is actuated by hydraulic motor and luffing boom and telescopic boom are actuated by hydraulic cylinders. In order to reduce the total weight of the total gangway structure, the material for each part is chosen as shown in Table 3.1 . And the connection between aluminum parts and steel parts will be made by bolts and Nuts.

Table 3.1 Materials used for each part of gangway

Parts	Material
Pedestal	Steel_S355J2G3
Slewing King	Steel_S355J2G3
Luffing Boom	Aluminum 5086
Telescopic Boom	Aluminum 5086
Lugs and Joints	Steel_S355J2G3
Handrails	Aluminum 5086

Considering all the requirements, the 3D model of concept design is given below based on the Uptime small type gangway in the following Fig. 3.1 .

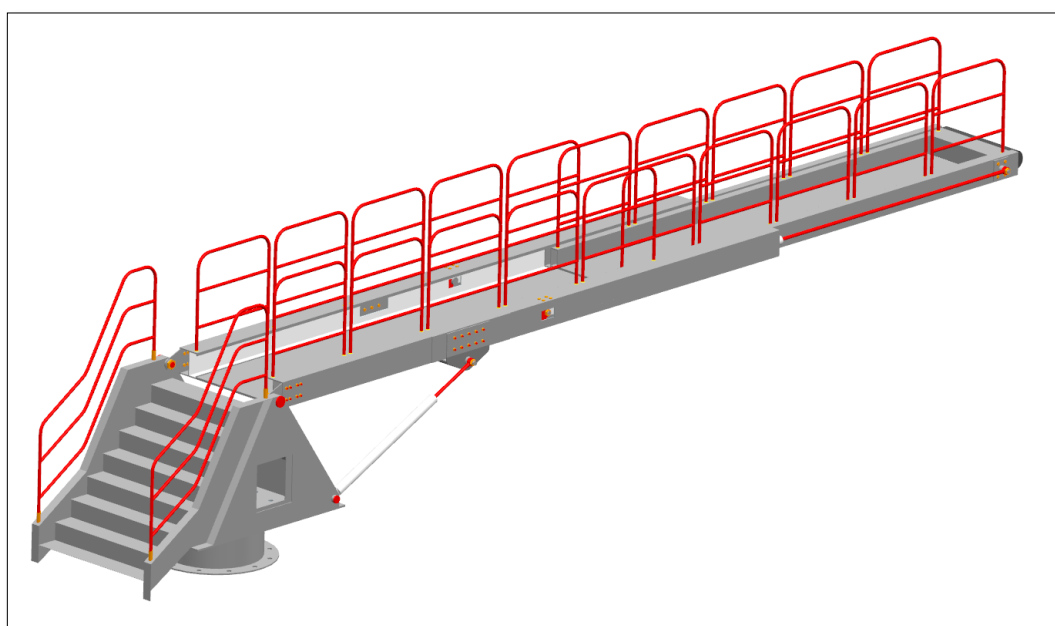


Fig. 3.1 3D model of designed gangway

We can see that the slewing king sits on the pedestal and luffing boom is connected to slewing king by bolts and bearings. The telescopic boom is sliding inside the luffing boom. The total mass of the gangway structure except pedestal and stair is about 1718 kg according to our design. Interested readers can visit the 3D model of gangway named “3D Model of Gangway” in the attached CD.



## **4 Mechanical Model of Gangway**

In this chapter, the mechanical model of gangway will be derived mathematically and implemented in 20-sim software with bond graph form. It includes the simplification that made in order to simplify the overall model of gangway system, the kinematic model of gangway and dynamic model of gangway based on that simplification. The parameters for calculating kinematics and dynamics of gangway were given in Appendix B

### **4.1 Simplifications**

In order to simplify the overall mathematical model of gangway system, the simplification of mechanical system of gangway is needed. First, we assume that the mass distribution of each part is symmetric with respect to the body-attached frame at the center of mass, which is parallel to the link frame in D-H sketches. As a result, it only has principal moments of inertia about X, Y and Z-axes of the body-attached frame respectively. But the torque or force that is needed to actuate each joint will be slightly wrong compared to the actual gangway system. However, the focus of this thesis is not on finding the exactly right amount torque or force of each actuator but on the modeling, simulation and control of such system, so this simplification is acceptable. Second, all the bodies are considered as rigid bodies and the flexibility and deformation is neglected. Consequently, the gangway tip position might be slightly different compared to that of the gangway in real operation. However, this difference is quite small compared to other dimensions of gangway, so it can also be neglected.

### **4.2 Kinematics of the Gangway**

In this section, we present the kinematic algorithms that are necessary to map variable between task-space, joint-space and actuator space. This is important in our project because it allowed high-level coordinated commands to be mapped into low-level actuator commands during the transferring operation of gangway. It included the forward kinematics, Jacobian transforms and inverse kinematics, which describe the relation of position and velocity between joint space and task space. And the transformation between joint variables and actuator variables were presented as well.

#### **4.2.1 Forward Kinematics and Jacobian Transformation**

According to the designed gangway in chapter 3, we can see that it has three joint variables, which includes the pedestal king revolute joint, the luffing main boom revolute joint and the

prismatic joint of telescopic boom. If we take the center of pedestal bottom as the base frame {0} origin, then L1 is 1.82 m and L4 is 5.65 m based on our design.

According to the design requirements, the operational range of each joint is shown in following in the Table 4.1

Table 4.1 The operational range of joint variables

Joint	1	2	3
Variables	$\theta_1$	$\theta_2$	$d_3$
Range	[0,360] deg	[255,295] deg	[2.15, 5.15] m

And the joint variables is defined according to D-H conventions as shown in the simplified sketch of gangway in the following Fig. 4.1.

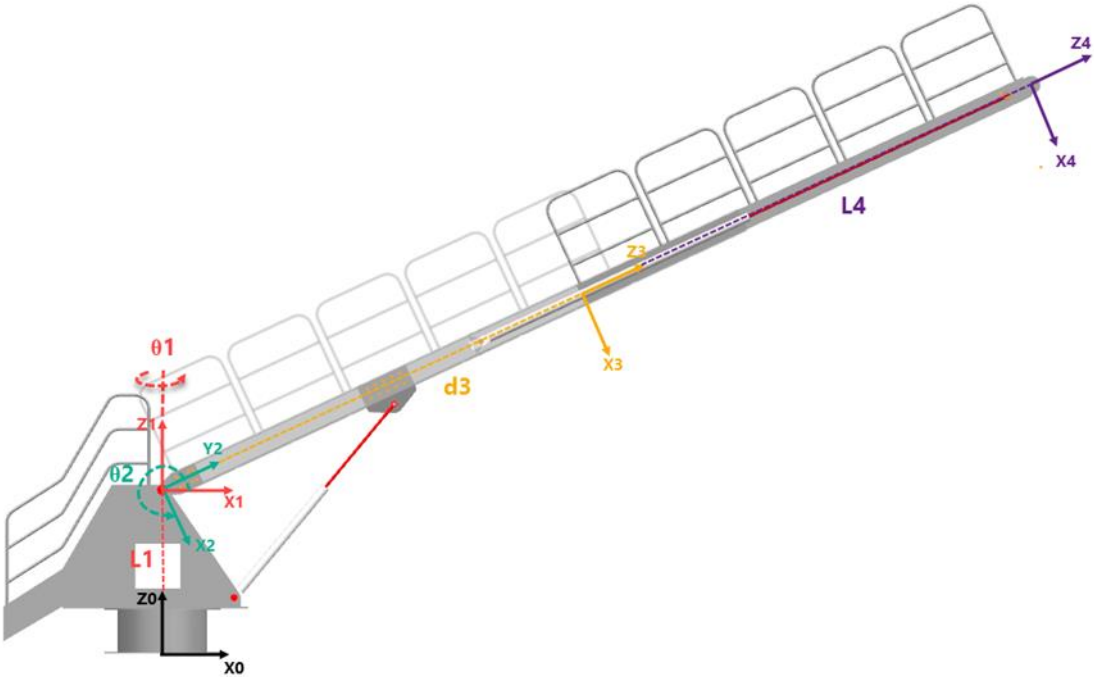


Fig. 4.1 The D-H sketch of simplified gangway system

And based on D-H convention, the D-H parameters are given in Table 4.2 below.

Table 4.2 D-H parameters of redefined gangway sketch

$i$	$a_{i-1}$	$\alpha_{i-1}$	$d_i$	$\theta_i$
1	0	0	L1	$\theta_1$
2	0	$\frac{\pi}{2}$	0	$\theta_2$
3	0	$-\frac{\pi}{2}$	$d3$	0
4	0	0	L4	0

Then the transformation matrices can be given as below according to Equation 2.15

$$T_1^0 = \begin{bmatrix} c1 & -s1 & 0 & 0 \\ s1 & c1 & 0 & 0 \\ 0 & 0 & 1 & L1 \\ 0 & 0 & 0 & 1 \end{bmatrix} \quad (4.1)$$

$$T_2^1 = \begin{bmatrix} c2 & -s2 & 0 & 0 \\ 0 & 0 & -1 & 0 \\ s2 & c2 & 0 & 0 \\ 0 & 0 & 0 & 1 \end{bmatrix} \quad (4.2)$$

$$T_3^2 = \begin{bmatrix} 1 & 0 & 0 & 0 \\ 0 & 0 & 1 & d3 \\ 0 & -1 & 0 & 0 \\ 0 & 0 & 0 & 1 \end{bmatrix} \quad (4.3)$$

$$T_4^3 = \begin{bmatrix} 1 & 0 & 0 & 0 \\ 0 & 1 & 0 & 0 \\ 0 & 0 & 1 & L4 \\ 0 & 0 & 0 & 1 \end{bmatrix} \quad (4.4)$$

Then the transformation matrices of each link frame to gangway base frame {0} is given below

$$T_1^0 = \begin{bmatrix} c1 & -s1 & 0 & 0 \\ s1 & c1 & 0 & 0 \\ 0 & 0 & 1 & L1 \\ 0 & 0 & 0 & 1 \end{bmatrix} \quad (4.5)$$

$$T_2^0 = T_1^0 T_2^1 = \begin{bmatrix} c1c2 & -c1s2 & s1 & 0 \\ s1c2 & -s1s2 & -c1 & 0 \\ s2 & c2 & 0 & L1 \\ 0 & 0 & 0 & 1 \end{bmatrix} \quad (4.6)$$

$$T_3^0 = T_1^0 T_2^1 T_3^2 = \begin{bmatrix} c1c2 & -s1 & -c1s2 & -c1s2d3 \\ s1c2 & c1 & -s1s2 & -s1s2d3 \\ s2 & 0 & c2 & L1 + d3c2 \\ 0 & 0 & 0 & 1 \end{bmatrix} \quad (4.7)$$

$$T_4^0 = T_1^0 T_2^1 T_3^2 T_4^3 = \begin{bmatrix} c1c2 & -s1 & -c1s2 & -c1s2(d3 + L4) \\ s1c2 & c1 & -s1s2 & -s1s2(d3 + L4) \\ s2 & 0 & c2 & L1 + (d3 + L4)c2 \\ 0 & 0 & 0 & 1 \end{bmatrix} \quad (4.8)$$

Then the rotation matrix of each frame can be obtained from the transformation matrix

$$R_1^0 = \begin{bmatrix} c1 & -s1 & 0 \\ s1 & c1 & 0 \\ 0 & 0 & 1 \end{bmatrix} \quad (4.9)$$

$$R_2^0 = \begin{bmatrix} c1c2 & -c1s2 & s1 \\ s1c2 & -s1s2 & -c1 \\ s2 & c2 & 0 \end{bmatrix} \quad (4.10)$$

$$R_3^0 = R_4^0 = \begin{bmatrix} c1c2 & -s1 & -c1s2 \\ s1c2 & c1 & -s1s2 \\ s2 & 0 & c2 \end{bmatrix} \quad (4.11)$$

So the gangway tip position expressed in gangway base frame {0} is given from Equation 4.8

$$\begin{aligned} P_{tip_x} &= -c1s2(d3 + L4) \\ P_{tip_y} &= -s1s2(d3 + L4) \\ P_{tip_z} &= L1 + (d3 + L4)c2 \end{aligned} \quad (4.12)$$

And the linear Jacobian of gangway tip is given as following

$$J_{v_{tip}} = \begin{bmatrix} s1s2(d3 + L4) & -c1c2(d3 + L4) & -c1s2 \\ -c1s2(d3 + L4) & -s1c2(d3 + L4) & -s1s2 \\ 0 & -s2(d3 + L4) & c2 \end{bmatrix} \quad (4.13)$$

## 4.2.2 Inverse Kinematics

We know the purpose of heave compensation is to maintain the gangway tip still during transferring process of people. It means we have to make the gangway tip move in the counter direction of ship motion. Then to find the desired joint displacement for a desired tip position is necessary. And this can be done via inverse kinematics.

Based on Equation 4.12, we have following equations for a desired gangway tip position in task space expressed in gangway base frame {0}

$$P_{tip_x} = -c1s2(d3 + L4) \quad (4.14)$$

$$P_{tip_y} = -s1s2(d3 + L4) \quad (4.15)$$

$$P_{tipz} = L1 + (d3 + L4)c2 \quad (4.16)$$

By solving system equation above and consider the operational range according the our requirement, we have the following expressions for the desired joint displacement for the a given gangway tip position

$$\theta_1 = atan2(P_{tipy}, P_{tipx}) \quad (4.17)$$

$$\theta_2 = atan2( P_{tipx}, \cos(\theta_1) \cdot (L1 - P_{tipz}) ) + \pi \quad (4.18)$$

$$d_3 = \frac{P_{tipx}}{-\cos(\theta_1) \cdot \sin(\theta_2)} - L4 \quad (4.19)$$

Where the function  $atan2(Y, X)$  in 20-sim is a four quadrant arctangent of the elements of Y and X, and it produces results in the range  $[-\pi, \pi]$ .

Then the desired joint velocity corresponding to a given gangway tip velocity can be given by using equation 4.13 as below

$$\begin{bmatrix} \dot{\theta}_1 \\ \dot{\theta}_2 \\ \dot{d}_3 \end{bmatrix} = inverse(J_{vtip}) \cdot \begin{bmatrix} v_{tipx} \\ v_{tipy} \\ v_{tipz} \end{bmatrix} \quad (4.20)$$

Where  $\dot{\theta}_1, \dot{\theta}_2$  and  $\dot{d}_3$  is the desired joint velocity for the corresponding gangway tip velocity  $v_{tipx}, v_{tipy}$  and  $v_{tipz}$ .

### 4.2.3 Joint-Space to Actuator-Space kinematics

To find the relation between joint variable and actuator variable is important to calculate the desired input for the hydraulic system. Based on our design, the slewing joint is actuated by a motor with gearbox, luff revolute joint is actuated by a cylinder and the telescopic joint is actuated by a cylinder as well. So the relation between the joint space and actuator space can be given respectively as below.

For the slewing joint the actuator velocity can be given as below

$$S_{motor} = \theta_1 r \quad (4.21)$$

$$\dot{S}_{motor} = \dot{\theta}_1 r \quad (4.22)$$

Where  $r$  is the gear ratio of slewing motor,  $S_{motor}$  is the angle of motor and  $\dot{S}_{motor}$  is the velocity of motor. For the luffing main boom, the geometry relation between cylinder length and joint angle is shown in the following Fig. 4.2

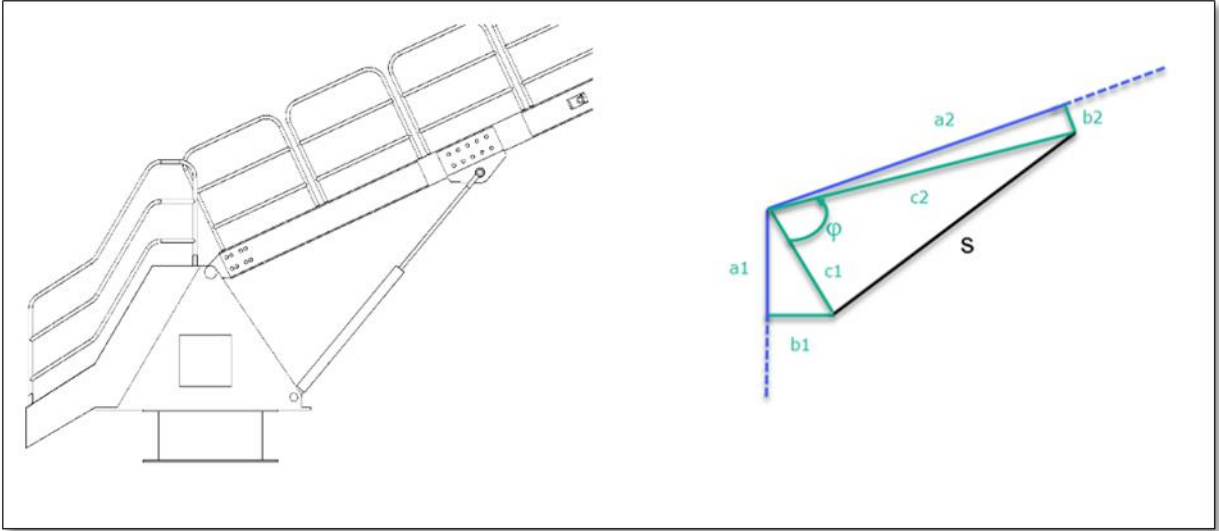


Fig. 4.2 The geometry relation of luffing joint

Then the relation between joint angle ( $\theta_2$ ) and cylinder length ( $s_{luff}$ ) can be given as below

$$s_{luff} = \sqrt{c_1^2 + c_2^2 - 2c_1c_2 \cos(\varphi)} \quad (4.23)$$

Where  $c_1 = \sqrt{a_1^2 + b_1^2}$ ,  $c_2 = \sqrt{a_2^2 + b_2^2}$  and  $\varphi = \theta_2 - \pi - \arctan\left(\frac{b_1}{a_1}\right) - \arctan\left(\frac{b_2}{a_2}\right)$

Then the velocity of main boom cylinder can be given

$$\dot{s}_{luff} = \frac{c_1c_2 \sin(\varphi)}{\sqrt{c_1^2 + c_2^2 - 2c_1c_2 \cos(\varphi)}} \dot{\theta}_2 \quad (4.24)$$

For the telescopic boom, it has the following equations since the cylinder is aligned with the telescopic boom.

$$s_{tele} = s_{shortest} + d_3 + L_4 - L_{min} \quad (4.25)$$

$$\dot{s}_{tele} = \dot{d}_3 \quad (4.26)$$

Where  $s_{shortest}$  the shortest length of telescopic cylinder,  $L_4$  is is length of telescopic boom and  $L_{min}$  is the total minimum length of gangway.

### 4.3 Dynamics of the Gangway

In this section, the dynamics equation of motion is derived with Euler-Lagrange method and then rewritten into Hamiltonian form in order to implement in 20-sim with bond graph. It includes the derivation of Jacobian of the mass center of each link of gangway, the calculation of kinetic and potential energy of gangway and the derivation Hamilton form of equation of motion.

### 4.3.1 Jacobian Derivation

In order to form the Euler-Lagrange equation of gangway system, the Jacobian of mass center of each link of gangway is needed. And the Jacobian will be split into linear velocity Jacobian and angular velocity Jacobian and they will be calculated separately.

Then the Jacobian matrix can be derived by Equation 2.31. Because the gangway has three joints, so the complete Jacobian forms a 6 x 3 matrix. And all the parameters needed to calculate the Jacobian in Equation 2.31 can be found from Equation 4.5 to Equation 4.11

$$\begin{aligned}
 o_1^0 &= \begin{bmatrix} 0 \\ 0 \\ L1 \end{bmatrix} & o_2^0 &= \begin{bmatrix} 0 \\ 0 \\ L1 \end{bmatrix} \\
 o_3^0 &= \begin{bmatrix} -c1s2d3 \\ -s1s2d3 \\ L1 + d3c2 \end{bmatrix} \\
 Z_1^0 &= \begin{bmatrix} 0 \\ 0 \\ 1 \end{bmatrix} & Z_2^0 &= \begin{bmatrix} s1 \\ -c1 \\ 0 \end{bmatrix} \\
 Z_3^0 &= \begin{bmatrix} -c1s2 \\ -s1s2 \\ c2 \end{bmatrix}
 \end{aligned} \tag{4.27}$$

And the coordinate of mass center of each link expressed in link-attached frame is given as below

$$\begin{aligned}
 P_{c1}^1 &= \begin{bmatrix} 0 \\ 0 \\ Z_{c1} \end{bmatrix} & P_{c2}^2 &= \begin{bmatrix} 0 \\ Y_{c2} \\ 0 \end{bmatrix} \\
 P_{c3}^3 &= \begin{bmatrix} 0 \\ 0 \\ Z_{c3} \end{bmatrix}
 \end{aligned} \tag{4.28}$$

And then the position of mass center of each link expressed in gangway base frame {0} can be obtained

$$\begin{aligned}
 P_{c1}^0 &= T_1^0 P_{c1}^1 = \begin{bmatrix} 0 \\ 0 \\ L1 + Z_{c1} \end{bmatrix} & P_{c2}^0 &= T_2^0 P_{c2}^2 = \begin{bmatrix} -Y_{c2}c1s2 \\ -Y_{c2}s1s2 \\ L1 + Y_{c2}c2 \end{bmatrix} \\
 P_{c3}^0 &= T_3^0 P_{c3}^3 = \begin{bmatrix} -(Z_{c3} + d3)c1s2 \\ -(Z_{c3} + d3)s1s2 \\ L1 + (Z_{c3} + d3)c2 \end{bmatrix}
 \end{aligned} \tag{4.29}$$

Then the Jacobian  $J_v^{ci}$  and  $J_w^{ci}$  are given below based on Equation 2.31

$$J_v^{c1} = \begin{bmatrix} 0 & 0 & 0 \\ 0 & 0 & 0 \\ 0 & 0 & 0 \end{bmatrix} \quad (4.30)$$

$$J_v^{c2} = \begin{bmatrix} Y_{c2}s1s2 & -Y_{c2}c1c2 & 0 \\ -Y_{c2}c1s2 & -Y_{c2}s1c2 & 0 \\ 0 & -Y_{c2}s2 & 0 \end{bmatrix} \quad (4.31)$$

$$J_v^{c3} = \begin{bmatrix} (Z_{c3} + d3)s1s2 & -(Z_{c3} + d3)c1c2 & -c1s2 \\ -(Z_{c3} + d3)c1s2 & -(Z_{c3} + d3)s1c2 & -s1s2 \\ 0 & -(Z_{c3} + d3)s2 & c2 \end{bmatrix} \quad (4.32)$$

$$J_w^{c1} = \begin{bmatrix} 0 & 0 & 0 \\ 0 & 0 & 0 \\ 1 & 0 & 0 \end{bmatrix} \quad (4.33)$$

$$J_w^{c2} = J_w^{c3} = \begin{bmatrix} 0 & s1 & 0 \\ 0 & -c1 & 0 \\ 1 & 0 & 0 \end{bmatrix} \quad (4.34)$$

### 4.3.2 Kinetic Energy of the Gangway

As described in Equation 2.46, the equation of motion is expressed below

$$\frac{d}{dt} \frac{\partial \mathcal{K}}{\partial \dot{q}} - \left( \frac{\partial \mathcal{K}}{\partial q} - \frac{\partial P}{\partial q} \right) = \tau \quad (4.35)$$

Where the kinetic energy is

$$\mathcal{K} = \frac{1}{2} \dot{q}^T \left[ \sum_{i=1}^n \left\{ m_i J_v^{ci}(q)^T J_v^{ci}(q) + J_w^{ci}(q)^T R_i^0(q) I_i R_i^0(q)^T J_w^{ci}(q) \right\} \right] \dot{q} \quad (4.36)$$

$$\mathcal{K} = \frac{1}{2} \dot{q}^T D(q) \dot{q}$$

We can see that the kinetic energy is the sum of kinetic energy of three links and the contributions of  $D(q)$  are also come from these three links. So  $D(q)$  will be split into three parts, which are relative to each link of gangway. To do this calculation, we denote the mass of slewing king, main boom and telescopic boom as  $m_1$ ,  $m_2$  and  $m_3$ . For the inertia of each link of gangway, it only has principal moments of inertia about x, y and z axes of the body-attached frame at mass center which are parallel to link frame at their joints based on the simplification we made. So the inertia tensor of each link is given as below

$$I_1 = \begin{bmatrix} I_{xx1} & 0 & 0 \\ 0 & I_{yy1} & 0 \\ 0 & 0 & I_{zz1} \end{bmatrix} \quad (4.37)$$

$$I_2 = \begin{bmatrix} I_{xx2} & 0 & 0 \\ 0 & I_{yy2} & 0 \\ 0 & 0 & I_{zz2} \end{bmatrix} \quad (4.38)$$



$$I_3 = \begin{bmatrix} I_{xx3} & 0 & 0 \\ 0 & I_{yy3} & 0 \\ 0 & 0 & I_{zz3} \end{bmatrix} \quad (4.39)$$

Then  $D(q)$  can be expressed as below

$$D(q) = D(q)_1 + D(q)_2 + D(q)_3 \quad (4.40)$$

Where  $D(q)_1, D(q)_2$  and  $D(q)_3$  are the contribution of slewing king, main boom, telescopic boom separately.

And the contribution of each link of gangway for  $D(q)$  is given as following by inserting Equation 4.29- 4.34 and Equation 4.37- 4.39

$$\begin{aligned} D(q)_1 &= m_1 J_v^{c1T} J_v^{c1} + J_\omega^{c1T} R_1^0 I_1 R_1^{0T} J_\omega^{c1} \\ &= \begin{bmatrix} I_{zz1} & 0 & 0 \\ 0 & 0 & 0 \\ 0 & 0 & 0 \end{bmatrix} \end{aligned} \quad (4.41)$$

$$\begin{aligned} D(q)_2 &= m_2 J_v^{c2T} J_v^{c2} + J_\omega^{c2T} R_2^0 I_2 R_2^{0T} J_\omega^{c2} \\ &= \begin{bmatrix} (I_{xx2} + m_2 Y_{c2}^2) s^2 + I_{yy2} c^2 & 0 & 0 \\ 0 & m_2 Y_{c2}^2 + I_{zz2} & 0 \\ 0 & 0 & 0 \end{bmatrix} \end{aligned} \quad (4.42)$$

$$\begin{aligned} D(q)_3 &= m_3 J_v^{c3T} J_v^{c3} + J_\omega^{c3T} R_3^0 I_3 R_3^{0T} J_\omega^{c3} \\ &= \begin{bmatrix} (I_{xx3} + m_3 (Z_{c3} + d_3)^2) s^2 + I_{zz3} c^2 & 0 & 0 \\ 0 & I_{yy3} + m_3 (Z_{c3} + d_3)^2 & 0 \\ 0 & 0 & m_3 \end{bmatrix} \end{aligned} \quad (4.43)$$

Recall Equation 4.40, the  $D(q)$  can be written as

$$\begin{aligned} D(q) &= D(q)_1 + D(q)_2 + D(q)_3 \\ D(q) &= \begin{bmatrix} d_{11} & d_{12} & d_{13} \\ d_{21} & d_{22} & d_{23} \\ d_{31} & d_{32} & d_{33} \end{bmatrix} \end{aligned} \quad (4.44)$$

Where

$$\begin{aligned} d_{11} &= I_{zz1} + (I_{yy2} + I_{zz3}) c^2 + (I_{xx2} + I_{xx3} + m_2 Y_{c2}^2 + m_3 (Z_{c3} + d_3)^2) s^2 \\ d_{12} &= d_{21} = d_{13} = d_{31} = d_{23} = d_{32} = 0 \\ d_{22} &= I_{zz2} + I_{yy3} + m_2 Y_{c2}^2 + m_3 (Z_{c3} + d_3)^2 \\ d_{33} &= m_3 \end{aligned} \quad (4.45)$$

### 4.3.3 Hamiltonian-Lagrange Equation and Bond Graph Implementation

Then next step is to derive the state space equation of motion in Hamiltonian form. Recall Equation 2.49 and Equation 2.50, the Lagrange equation can be given

$$\frac{d}{dt}(D(q) \dot{q}) - \left( \frac{1}{2} \dot{q}^T \frac{\partial D(q)}{\partial q} \dot{q} - g(q) \right) = \tau \quad (4.46)$$

Where

$$g(q) = \frac{\partial P}{\partial q} \quad (4.47)$$

And the second part of the left side of Equation 4.46 can be calculated separately as below

$$\frac{1}{2} \dot{q}^T \frac{\partial D(q)}{\partial q} \dot{q} = \frac{1}{2} \begin{bmatrix} \dot{q}^T \frac{\partial D(q)}{\partial \theta 1} \dot{q} \\ \dot{q}^T \frac{\partial D(q)}{\partial \theta 2} \dot{q} \\ \dot{q}^T \frac{\partial D(q)}{\partial d 3} \dot{q} \end{bmatrix} = \frac{1}{2} \begin{bmatrix} \dot{q}^T D(q)_{11} \dot{q} \\ \dot{q}^T D(q)_{22} \dot{q} \\ \dot{q}^T D(q)_{33} \dot{q} \end{bmatrix} \quad (4.48)$$

Where  $D(q)_{11}$ ,  $D(q)_{22}$  and  $D(q)_{33}$  is the partial derivative of  $D(q)$  with respect to  $\theta 1$ ,  $\theta 2$  and  $d 3$  respectively, and  $\dot{q} = [\dot{\theta} 1; \dot{\theta} 2; \dot{d} 3]$ .

Then  $D(q)_{11}$ ,  $D(q)_{22}$  and  $D(q)_{33}$  can be calculated as below

$$D(q)_{11} = \frac{\partial D(q)}{\partial \theta 1} \quad (4.49)$$

$$= \begin{bmatrix} 0 & 0 & 0 \\ 0 & 0 & 0 \\ 0 & 0 & 0 \end{bmatrix}$$

$$D(q)_{22} = \frac{\partial D(q)}{\partial \theta 2} \quad (4.50)$$

$$= \begin{bmatrix} (m_2 Y_{c2}^2 + m_3 (Z_{c3} + d_3)^2 + I_{xx2} + I_{xx3} - I_{yy2} - I_{zz3}) 2s_2 c_2 & 0 & 0 \\ 0 & 0 & 0 \\ 0 & 0 & 0 \end{bmatrix}$$

$$D(q)_{33} = \frac{\partial D(q)}{\partial d 3} \quad (4.51)$$

$$= \begin{bmatrix} (2m_3 (Z_{c3} + d_3)) s_2^2 & 0 & 0 \\ 0 & 2m_3 (Z_{c3} + d_3) & 0 \\ 0 & 0 & 0 \end{bmatrix}$$

We know that  $g(q)$  is partial derivative of potential energy with respect to respect to  $\theta 1$ ,  $\theta 2$  and  $d 3$  respectively. To calculate it, the gravity acceleration is defined as following

$$g_0 = \begin{bmatrix} 0 \\ 0 \\ -g \end{bmatrix} \quad (4.52)$$

Where  $g$  is value of gravity acceleration in Z direction and  $g = 9.81 \text{ m/s}^2$

Then  $g(q)$  can be calculated as below by inserting Equation 4.29- 4.34

$$\begin{aligned} g(q) &= \frac{\partial P}{\partial q} = - \left( J_v^{c1T} m_1 g_0 + J_v^{c2T} m_2 g_0 + J_v^{c3T} m_3 g_0 \right) \\ &= \begin{bmatrix} 0 \\ -(m_2 Y_{c2} + m_3 (Z_{c3} + d_3)) g \\ m_3 g c_2 \end{bmatrix} \end{aligned} \quad (4.53)$$

Up to now, we have all the equations needed to form the Hamilton form of equation of motion of gangway system. Recall Equation 2.56, the state space equation of gangway system is given as below

$$\dot{q} = \begin{bmatrix} \dot{\theta}_1 \\ \dot{\theta}_2 \\ \dot{d}_3 \end{bmatrix} = D(q)^{-1} p \quad (4.54)$$

Where  $\dot{q}$  is the joint velocity vector and the  $p$  is the momentum vector of the joints

$$\dot{p} = e'(p, q) + \tau \quad (4.55)$$

Where

$$e'(p, q) = \frac{1}{2} \begin{bmatrix} \dot{q}^T D(q)_{11} \dot{q} \\ \dot{q}^T D(q)_{22} \dot{q} \\ \dot{q}^T D(q)_{33} \dot{q} \end{bmatrix} - g(q) \quad (4.56)$$

So the bond graph implementation with IC field can be given as below

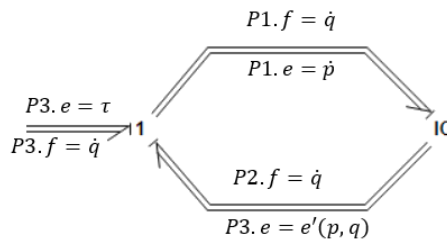


Fig. 4.3 Bond graph implementation of gangway dynamics with IC-field



## 5 Modeling and Design of Hydraulic Systems of Gangway

In this chapter, we will present the basic hydraulic system of offshore AMC gangway and the system model based on bond graph method. First, the hydraulic system description regarding the basic components of hydraulic system for slewing king, luffing boom and telescopic boom will be introduced. Then a design process regarding how to select proper hydraulic motor, hydraulic cylinders and pump and relative valves will be given. At last, the bond graph modeling of each components and overall system will be presented.

### 5.1 Description of Hydraulic System of Gangway

According to the mechanical design and operational requirement, we know that the gangway has three degrees of freedom, which come from the three joints. They are the slewing king rotation joint, luffing boom rotation joint and telescopic prismatic joint. For our design, we use hydraulic motor to actuate slewing boom and hydraulic cylinders to actuate luffing boom and telescopic boom.

For offshore lifting application, it is common to have the pressure compensator valve (PCV) together with directional control valve (DCV). Then the motion of the actuator will be proportional to opening of DCV and become much easier to control. For such application where it has negative loads such as gravity acting on the actuator, a counter balance valve (CBV) is necessary in the side of hydraulic circuit before hydraulic actuator to prevent it from over-running. In addition, since these hydraulic actuators usually share the same hydraulic power unit, so an individual pressure relief valve is necessary before actuator in hydraulic circuit to prevent from over load.

Based on these principles, we can configure the hydraulic system based on their mechanical properties and operational features as followings

- Slewing king

Based on our design, the range of slewing is  $[0 - 2\pi]$ , there is no negative loads acting any side of hydraulic motor. So CBV is not necessary. But two-pressure relief valve should be include on both sides of hydraulic motor in the hydraulic to prevent it from over load. Of course, DCV and PCV are necessary for control purpose.

- Luffing boom

According to design, the hydraulic cylinder always suffers the negative load during the lower operation of gangway. So a CBV is necessary except DCV and PCV. In addition, the relief valve should be include in the cylinder head side to prevent from over load.

- Telescopic boom

We know that, during gangway operation, it will swing up and down. So it is clear that the telescopic cylinder will suffer negative on both sides during operation. So two CBV will be include on both sides of the hydraulic circuits of the hydraulic circuit except DCV and PCV. And because when the gangway will be operate at bumper mode where the gangway tip push against the platform. So a pressure relief valve should be included in the cylinder head side of hydraulic circuit.

We know that, in our design we have two cylinders for luffing boom and telescopic boom respectively, but in our hydraulic circuit we just represent them as one cylinder for simplification. And we will model them as one cylinder for luffing boom and telescopic boom for simplification. Based on these consideration and analysis of the sub-systems, an overall hydraulic systems is given in following Fig. 5.1

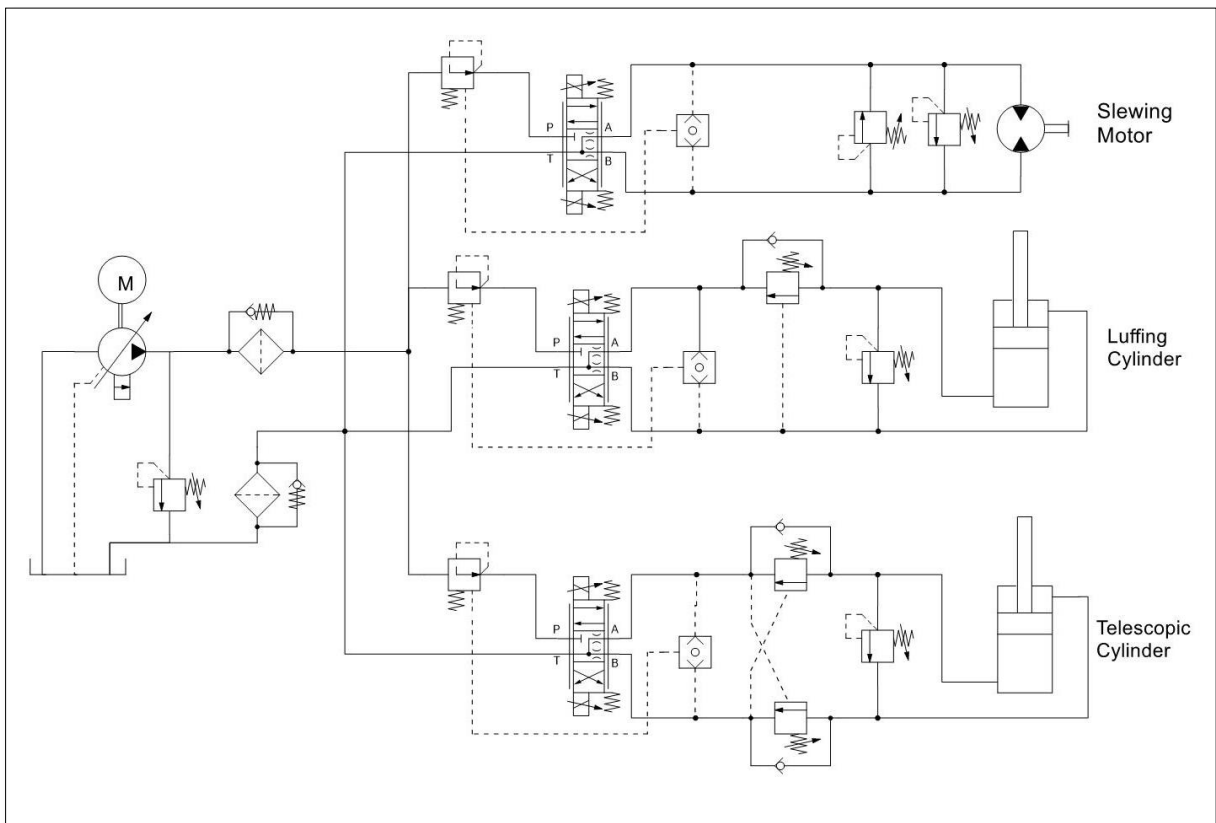


Fig. 5.1 Overall Hydraulic circuit of gangway system

## 5.2 Specification of Parameters of Hydraulic Components

In this section, we will give an introduction regarding how to calculate and select the proper actuators and valves for our hydraulic system. As we mentioned, the main hydraulic components of our system are hydraulic pumps, hydraulic motors, hydraulic cylinders and relative valves. And due to time limitation and lack of knowledge of valves, we will focus on how to select actuators and pumps and give a brief introduction on selection of relative valves. According to our design, the slewing motor, luffing cylinder and telescopic cylinder share the same HPU, so we will present the calculation and selection of these actuators first, then selection and calculation of pumps and valves will be given.

### 5.2.1 Slewing Motor

Generally, the selection of hydraulic motor is based on the required speed and acceleration. Usually, for a gangway with coordinated control of multiple actuators, inverse kinematics can be applied to find the operating cycles for individual actuators. However, since we don't define the required coordinate motion in Y axis, so based on industrial experiences and application the independent operating cycles of slewing king is defined as followings

Table 5.1 Operating cycles of slewing king

Velocity ( <i>RPM</i> )	Acceleration Time ( <i>s</i> )
2	4

The procedures to find the suitable hydraulic motors for specified operating requirements are given below

- Calculating angular acceleration based on the operational requirement
- Calculating required torque for obtain such acceleration, which includes the torque for acceleration, and torque for overcoming friction. But usually the torque for overcoming friction is quite small and it can be negligible.
- Finding the proper slewing bearing and gear ratio
- Finding the proper gearbox
- Calculating the motor size and selecting the suitable motor

The process of selecting the right motor is an iterative process in order to match the requirement and select proper slewing bearing, gearbox, and motor from existing standard products of suppliers.

In our design, we will simplify this process due to time limit. Based on advices from supervisors, the total gear ratio is take as 500 and this will be used for our calculation. And the rotation inertia of designed gangway can be obtained from NX software. Because the slewing motor is usually oversized, so the friction will be neglected as well and the efficiency is taken as one. Then the data used for calculating motor size is given below

Table 5.2 Data for calculating motor size

Slewing Velocity (RPM)	Acceleration Time (s)	Rotation Inertia (kgm <sup>2</sup> )	Total Gear Ratio
2	4	39900	500:1

Then required acceleration torque for motor can be given

$$\tau_{motor} = I_z \cdot \frac{2\pi n}{60 \cdot t \cdot r} = 4.2 (Nm) \quad (5.1)$$

Where  $I_z(kgm^2)$  is the rotation inertia,  $n(RPM)$  is the required slewing velocity,  $t (s)$  is the time for acceleration,  $r$  is total gear ratio

Because the total inertia is quite small, so we assume the inlet working pressure is 50 bar and outlet pressure is zero, then the displacement of motor can be given

$$V_{motor} = \frac{\tau_{motor}}{\Delta P} \cdot 2\pi \cdot 10^6 = 5.3(cm^3/rev) \quad (5.2)$$

Where  $V_{motor} (cm^3/rev)$  is the pump displacement per revolution,  $\Delta P(Pa)$  is pressure difference over motor

We can see that the displacement of motor we get is quite small, which is very hard to find such kind of motor. So we can scale the pump displacement into following

$$V_{motor} = 20 (cm^3/rev) \quad (5.3)$$

And then if we want to make the slewing king operate at 2 RPM, the required flow for hydraulic motor can be given

$$Q_m = \frac{V_{motor} \cdot n \cdot r}{10^3} = 20 (liter/min) \quad (5.4)$$

Where  $Q_m$  is required flow for motor per minute.



## 5.2.2 Luffing Cylinder and Telescopic Cylinder

Because in our design, the gangway is able to compensate the heave and sway ship motion caused by wave. So the operating cycle of this two cylinder should be determined by inverse kinematics. And the diameter of luffing cylinders and telescopic cylinders should be calculated individually based on the worst load case. So the calculation regarding piston diameter of luffing cylinder and telescopic cylinder will be given first, then a calculation about the required flow for this two cylinder will be present.

For luffing cylinder, the worst load case is load case NO-PT-I as defined in Appendix A where the gangway is operated at -15 degree and push against windmill platform with 10KN force. Because we have two luffing cylinders, so the force acting on one luffing cylinder is given as below

$$F_{luffmax} = \frac{\tau_{luffmax}}{2 \cdot h} = \frac{106203}{2 \cdot 1.31} = 40666 \text{ N} = 40.7 \text{ KN} \quad (5.5)$$

Where  $F_{luffmax}$  is the maximum force acting on one luffing cylinders,  $\tau_{luffmax}$  is the maximum torque that two luffing cylinder should supply and  $h$  is the force arm in this load case.

If we assume the inlet pressure cylinder is 150 bar, outlet pressure is zero and neglect the friction and leakage. The luffing cylinder piston diameter can be given

$$D_p = \frac{1}{1000} \cdot \sqrt{\frac{4}{\pi} \cdot \frac{F_{luffmax}}{\Delta P}} = 58.75 \text{ (mm)} \quad (5.6)$$

Where  $D_p$  (mm) is the luffing piston diameter and  $\Delta P$  (Pa) is the pressure difference over the luffing piston.

And the rod diameter should be calculated by formula of Euler buckling for an ideal beam in order to avoid bucking of cylinder (Bak and Hansen 2013). However, instead of calculating rod diameter, it is preferable to choose standard cylinder from supplier as reference. For our application, the operating angle of luffing boom is  $[-15, 25] \text{ deg}$ . So the length range of luffing cylinder can be given based on Equation 4.23

$$s_{luff} = [1.818, 2.802] \text{ m} = [1818, 2802] \text{ mm} \quad (5.7)$$

Where  $s_{luff}$  is the length of luffing cylinder.

Then a cylinder (part No.25ca-65/35-1300/85) from company “PMC hydraulics” can be selected as reference. The details of this cylinder is given in Appendix C and the relative data of cylinder used for our modeling are given below

- $D_p = 65 \text{ (mm)}$
- $D_r = 35 \text{ (mm)}$

We can see that, the length of this selected cylinder is not perfectly fit our designed cylinder range. But the length of cylinder can be customized to fit our requirement.

For telescopic cylinder, the worst load case is NO-PT-C as defined in Appendix A where the gangway is operated in cantilever position and push against the platform with 10 KN force. And if we assume the inlet pressure cylinder is 150 bar, outlet pressure is zero and neglect the friction and leakage. The telescopic cylinder piston diameter can be given

$$D_p = \frac{1}{1000} \cdot \sqrt{\frac{4}{\pi} \cdot \frac{F_{telemax}}{\Delta P * 2}} = 21 \text{ (mm)} \quad (5.8)$$

But we know that based on our design the cylinder stroke is 3 meter, so considering the buckling problem of such long cylinder the calculated piston diameter is not applicable. Also by checking with the cylinder with such long stroke made of steel, the piston diameter is quite big and the weight is quite heavy. So in order to reduce the weight of cylinder and find the reasonable piston diameter for our application, the composite cylinders made of fiber from company “Parker” can be selected. This type of cylinder is up to 50% lighter than comparable standard steel designs and much stronger. The details of the selected cylinder (part No.LC TS 380 D 080 036 3000 00) is given in Appendix C and the relative data used for our modeling is given below. By choosing such cylinder, the operating pressure should be quite low considering the large piston area.

- $D_p = 80 \text{ (mm)}$
- $D_r = 36 \text{ (mm)}$
- $Stroke = 3000 \text{ (mm)}$

In order to find the required flow for luffing and telescopic cylinder, the operating velocity should be calculated. When the gangway operate in AMC mode, the gangway tip should be able to lower in Z-axis or extend in X axis with a controllable speed relative to the world frame. The maximum operational velocity in Z-axis and X-axis is defined as 0.05 m/s in the world frame during the approaching process. And this operational velocity can be included in the ship motion with a scaling factor based on defined ship motion function. Usually, the gangway is operating at horizontal position and the telescopic boom is extended to the operational range. And in this condition, the required actuator velocity can be given by inverse kinematics. The

following table defines the required gangway tip velocity in world frame coordinate system based on operational requirements.

Table 5.3 Desired gangway tip velocity

X axis	Y axis	Z axis
$-1.2 \cdot \frac{2\pi}{24} \cdot \cos\left(\frac{2\pi}{12} t\right) m/s$	0	$-1.1 \cdot \frac{2\pi}{12} \cdot \cos\left(\frac{2\pi}{12} t\right) m/s$

The inverse kinematic model for finding luffing cylinder velocity and telescopic cylinder velocity can be given as below based on Equation 4.20, 4.22, 4.24 and 4.26

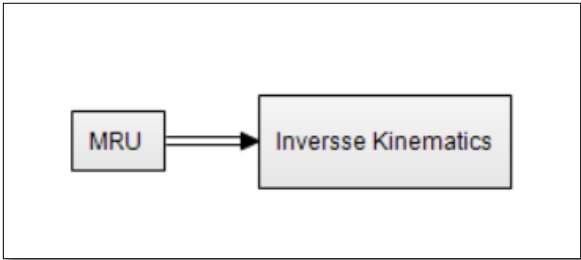


Fig. 5.2 Inverse kinematics model of gangway

The equation in block “MRU” is the defined wave motion velocity with scaling factors and the equations inside “Inverse Kinematics” block is the inverse kinematic equation for finding the corresponding actuator velocity based on requirement.

Since the ship motion in Y-axis is given as zero, so the velocity of slewing motor will be zero, then we will only present the luffing cylinder velocity and telescopic cylinder velocity as below

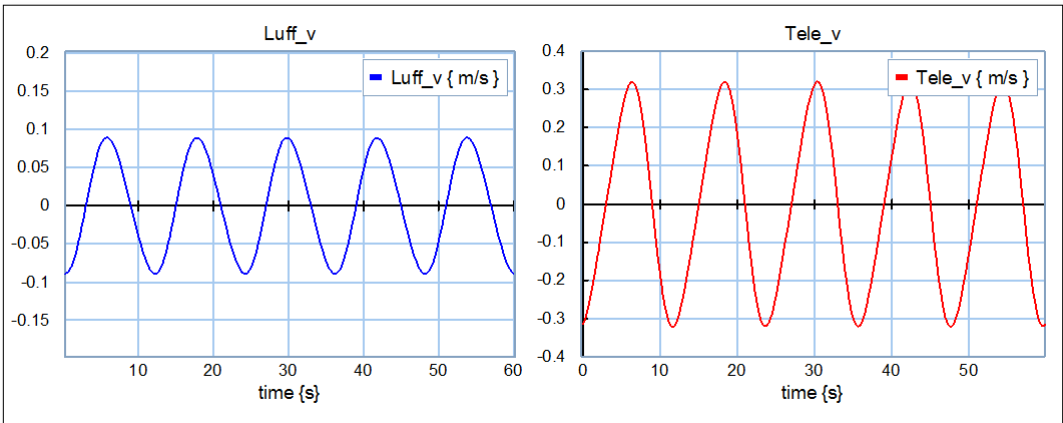


Fig. 5.3 Required luffing and telescopic velocity

From Fig. 5.3 we can see that the maximum required velocity for luffing cylinder and telescopic cylinder are about 0.1m/s and 0.32 m/s respectively.

For safety consideration, we define the maximum velocity for luffing cylinder and telescopic cylinder as below

- $V_{luffmax} = 0.15 \text{ m/s}$
- $V_{telemax} = 0.35 \text{ m/s}$

Readers may find in the datasheet of telescopic cylinder, the maximum allowable speed is  $0.3 \text{ m/s}$  for working pressure  $380 \text{ bar}$ . But for our application, the working pressure is lower than  $100 \text{ bar}$ , the velocity we defined is allowable.

Since we have two luffing cylinders and two telescopic cylinders, so the required flow for luffing cylinders and telescopic cylinders is given as below

$$Q_{luff} = 2 \cdot \frac{\pi D_{pluff}^2}{4} \cdot V_{luffmax} = 60 \text{ (liter/min)} \quad (5.9)$$

Where  $Q_{luff}$  is the flow for the two luffing cylinders and  $D_{pluff}$  is the piston diameter of luffing cylinder

$$Q_{tele} = 2 \cdot \frac{\pi D_{ptele}^2}{4} \cdot V_{telemax} = 210 \text{ (liter/min)} \quad (5.10)$$

Where  $Q_{tele}$  is the flow for the two telescopic cylinders and  $D_{ptele}$  is the piston diameter of telescopic cylinder

### 5.2.3 Hydraulic Pump

Hydraulic pump is the core components of HPU, so it is quite crucial for the overall performance of hydraulic system. The pump we selected for our application is pressure compensated pump due to its high efficiency. This type pump maintain the preset pressure at its outlet by adjusting the delivered flow according to the pressure.

The maximum flow of pump can be determined by the sum of flow of actuators.

$$Q_{pump} = (Q_{motor} + Q_{luff} + Q_{tele}) = 290 \text{ (liter/min)} \quad (5.11)$$

The pump runs at constant speed and it will be driven by a four-pole 60 Hz electric motor. Considering the slip, the rated speed of pump is given as below

$$n_{pump} = 1776 \text{ RPM} \quad (5.12)$$

If we assume the pump efficiency is 0.95, then the required pump displacement is given below

$$V_{pump} = 1000 \cdot \frac{Q_{pump}}{\eta_{pump} n_{pump}} = 171 \text{ (cm}^3/\text{rev)} \quad (5.13)$$

Then the pump can be selected from the company “Parker”. The details of the selected pump (part No. PV180) will be given in the Appendix C The maximum displacement of this pump is given as below

$$V_{pump} = 180 (cm^3/rev) \quad (5.14)$$

#### 5.2.4 Relative Valves and Pipes

We know that the valves in our hydraulic circuits include PCV, DCV, CBV and relief valve. The sizing and selecting of these valves are based on the maximum flow of corresponding actuators. Due to the lack of knowledge of these valves and time limitation, we just assume the maximum flow of these valves is the same as the maximum flow of corresponding actuators. And the pressure drop over these valves are assumed as 5 bar at maximum flow.

The selecting of pressure pipe and return pipe of hydraulic system should be based on the maximum flow and maximum allowable flow speed. Based on this, the calculated inner diameter of pressure and return pipe are given below

Table 5.4 Calculated inner diameter of pressure pipe and return pipe

Pipe	Pressure pipe	Return pipe
Maximum velocity ( $m/s$ )	8	4
Maximum flow ( $liter/min$ )	320	320
Pipe inner diameter (mm)	29.1	41.2

We assume the pipe is made of steel, by checking the product catalogue of company “GS-Hydro”, the following pipe has been selected and the details can be find in Appendix C

Table 5.5 Data of selected pressure pipe and return pipe

Pipe	Part No	Outer Diameter (mm)	Wall thickness(mm)
Pressure pipe	35X2.5AISI316L	35	2.5
Return pipe	50X3AISI316L	50	3

#### 5.3 Bond Graph Modeling of Hydraulic System Components

After identification and specification the main parameters of hydraulic components, in this chapter will present the modeling of these components with bond graph method. We know that

the hydraulic system has complex dynamics with non-linear properties. However, a good model is the model, which can catch the main properties that are important to the operation and analysis, not the model that contains all the details of the system. Thus, some reasonable assumptions and simplifications can be made to simplify the hydraulic model. In our model, the hydraulic components are modeled based on basic principle of fluid dynamics. Fluid inertia and capacitance are the main dominant for modeling of flow in pipe and cylinder and all the valves are modeled as orifices. Then the junction element in bond graph is used to connect these components and forms the complete hydraulic system. The modeling method for hydraulic system is mainly based on Chu, Æsøy et al. (2014) , Bak and Hansen (2013) and Pedersen and Engja (2014).

### 5.3.1 HPU

The HPU mainly consists of a pressure compensated pump with internal leakage. The outlet flow of pump is adjusted based on the outlet pressure. If the pressure is less than the preset pressure, the outlet flow is proportional to the pressure deviation. In bond graph model, the pump is modelled as flow source element (Sf-element) and the leakage is modelled with an R-element, which represent the leakage orifice. The constitutive law of pump is given below

$$Q_{max} = \frac{V_{pump}}{2\pi} \omega \quad (5.15)$$

$$f = \frac{P_{set} - e}{\Delta P_{dev}} Q_{max} \quad (5.16)$$

Where  $V_{pump}$  is the displacement of pump ( $m^3 / rev$ ),  $\omega$  is the pump rotational velocity ( $rad/s$ ),  $P_{set}$  is the set point of the outlet pressure of pump and  $\Delta P_{dev}$  is the pressure deviation from the set point where the pump is required to give full flow.

Based on the principle of fluid dynamics, the flow and pressure relationship of orifices can be given

$$Q = C_d A \sqrt{\frac{2}{\rho} \Delta P} \quad (5.17)$$

Where  $Q$  is the flow rate,  $C_d$  is the discharge coefficient and  $A$  is the discharge area,  $\Delta P$  is the pressure drop cross the orifice,  $\rho$  is the density of the fluid.

Because  $C_d$  is a constant value, for an orifice with constant flow area, we can take  $C_d$  as one for simplification. Then the flow area of the pump leakage orifice can be given

$$A = \frac{(1 - \eta_{pump})Q_{max}}{\sqrt{\frac{2}{\rho} P_{set}}} \quad (5.18)$$

Where  $\eta_{pump}$  is the volume efficiency of pump.

So the constitutive law for the pump leak orifice is given as below

$$f = A \sqrt{\frac{2}{\rho} e} \quad (5.19)$$

So based on the analysis, bond graph model of HPU is given as below

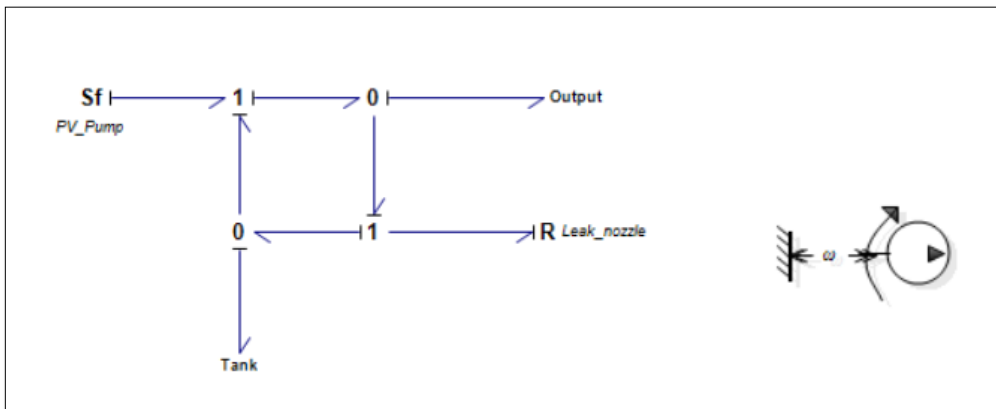


Fig. 5.4 Bond graph model of HPU

### 5.3.2 Pipe

In our hydraulic system model, we only consider the pipe between the pump and PCV. It includes the pressure line to from pump to DCV and return line from DCV to tank. The bond graph model of hydraulic pipe accounts for the friction loss along the pipe, fluid inertia and compressibility. As shown in the bond graph model below, the I-element and R-element is used to represent the inertia of fluid and friction loss. For the compressibility, it is represented by two C-element in order to avoid causality error.

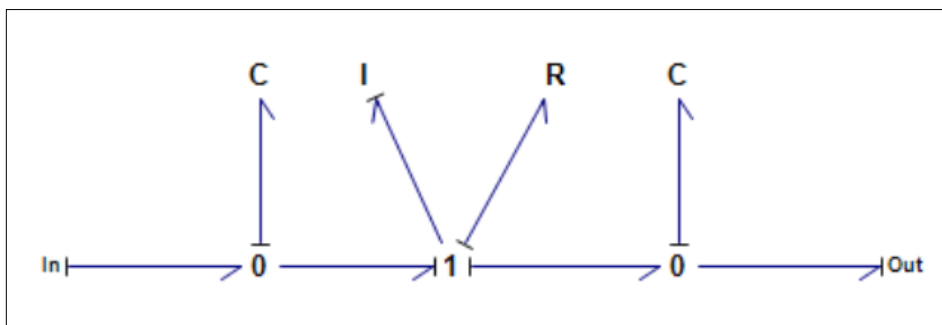


Fig. 5.5 Bond graph model of hydraulic pipe

The constitutive law of power variables for C-element, I-element and R-element of hydraulic pipe are given below respectively.

C-element

$$e = \frac{\beta}{l} \int f dt \quad (5.20)$$

Where  $\beta$  is the bulk modulus,  $A$  is the section area of the pipe and  $l$  is length of the pipe.

I-element

$$f = \frac{A}{\rho l} \int e dt \quad (5.21)$$

Where  $A$  is section area of the pipe,  $\rho$  is the fluid density,  $l$  is the length of the pipe segment.

R-element

$$e = \frac{1}{2} k \frac{\rho l f^2}{d A^2} \cdot \text{sign}(f) \quad (5.22)$$

Where  $k$  is friction factor,  $\rho$  is the fluid density,  $l$  is the length of pipe segment,  $d$  is the diameter of pipe and  $A$  is the section area of pipe.

The friction factor  $k$  is determined by the flow type through Colebrook–White equation approximation given by Swamee–Jain

$$k = \begin{cases} \frac{64}{R_e} & \text{for laminar flow: } R_e < 2100 \\ \frac{1}{4 \cdot \left( \log_{10} \left( \frac{\varepsilon/d}{3.7} + \frac{5.74}{R_e^{0.9}} \right) \right)^2} & \text{for turbulent flow: } R_e \geq 2100 \end{cases} \quad (5.23)$$

Where  $\varepsilon$  is the roughness of pipe and Reynolds number ( $R_e$ ) can be calculated

$$R_e = \text{abs}(f) \frac{d}{A\nu} \quad (5.24)$$

Where  $\nu$  is the kinematic viscosity of fluid.

### 5.3.3 Valves

For the hydraulic system of gangway, all the hydraulic valves are modelled as variable orifices with linear opening characteristics. Recall equation 5.17, the pressure and flow relationship of valves can be given



$$Q = \xi \cdot C_{nom} \sqrt{\frac{2}{\rho} \Delta P} \quad (5.25)$$

$$C_v = C_d A_{nom} \quad (5.26)$$

Where  $Q$  is the flow rate,  $\xi$  is the relative opening of valve,  $C_{nom}$  is the flow coefficient at the nominal flow,  $\Delta P$  is the pressure drop across the valve,  $\rho$  is the density of the fluid,  $C_d$  is the discharge coefficient and  $A_{nom}$  is the nominal discharge area.

Usually, the discharge coefficient  $c_d$  and flow area at nominal flow  $A_{nom}$  is not specified on the datasheet. But the flow coefficient at nominal flow can be given as below

$$C_{nom} = \frac{Q_{nom}}{\sqrt{\frac{2}{\rho} \Delta P_{nom}}} \quad (5.27)$$

Where the valve is fully open, and  $Q_{nom}, P_{nom}$  is nominal flow and pressure drop respectively.

Then the bond graph model of pressure compensator valve, directional control valve, counter balance valve and relief valve can be given in the following.

#### Pressure compensator valve

The PCV is flow control valve. It is used to maintain the pressure difference over the DCV at the set point to minimize the influence of pressure on the flow rate of DCV. The valve will be modeled as an R element. It has two input signal ports receiving the pressure signal from both sides of DCV. The pressure signal coming after DCV should be on the higher-pressure sides provided by a logic-selecting valve. The bond graph model of counter balance valve is given in following Fig. 5.6.

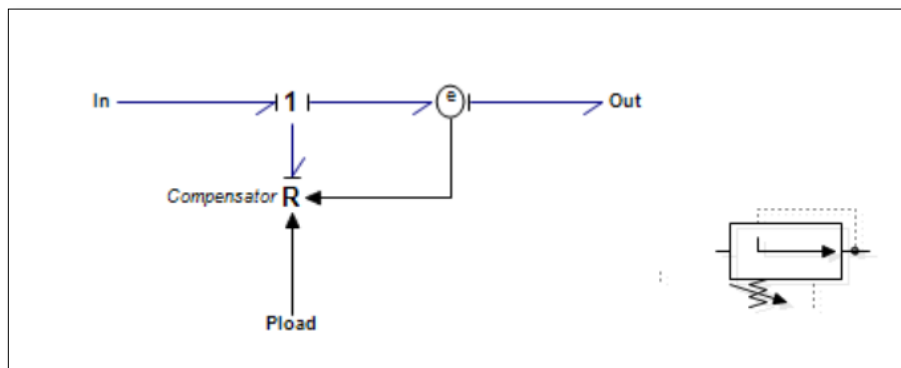


Fig. 5.6 Bond graph model of pressure compensator valve

The relative opening of PCV is given

$$\xi_{pcv} = \frac{\Delta P_{set} - \Delta P_{dcv}}{\Delta P_{set}} \quad (5.28)$$

Where  $\Delta P_{set}$  and  $\Delta P_{dcv}$  is the set point of pressure difference and measured pressure difference over DCV respectively.

Recall equation 5.25 to equation 5.27, the power variables relation of PCV can be given

$$f = \xi_{pcv} C_{pcv} \sqrt{\frac{2}{\rho} abs(e)} \quad (5.29)$$

Where  $C_{pcv}$  is the nominal flow coefficient of PCV.

Directional control valve

The function of DCV is to control the flow direction and then control the load motion. Since there is a pressure compensated valve before DCV, so ideally the flow should be only proportional to the spool position, which is controlled by the input control signal. In our hydraulic system, a 3-way-4-port DCV is used. The four port is represented by four R-element and three C-element to avoid causality error in bond graph model as below.

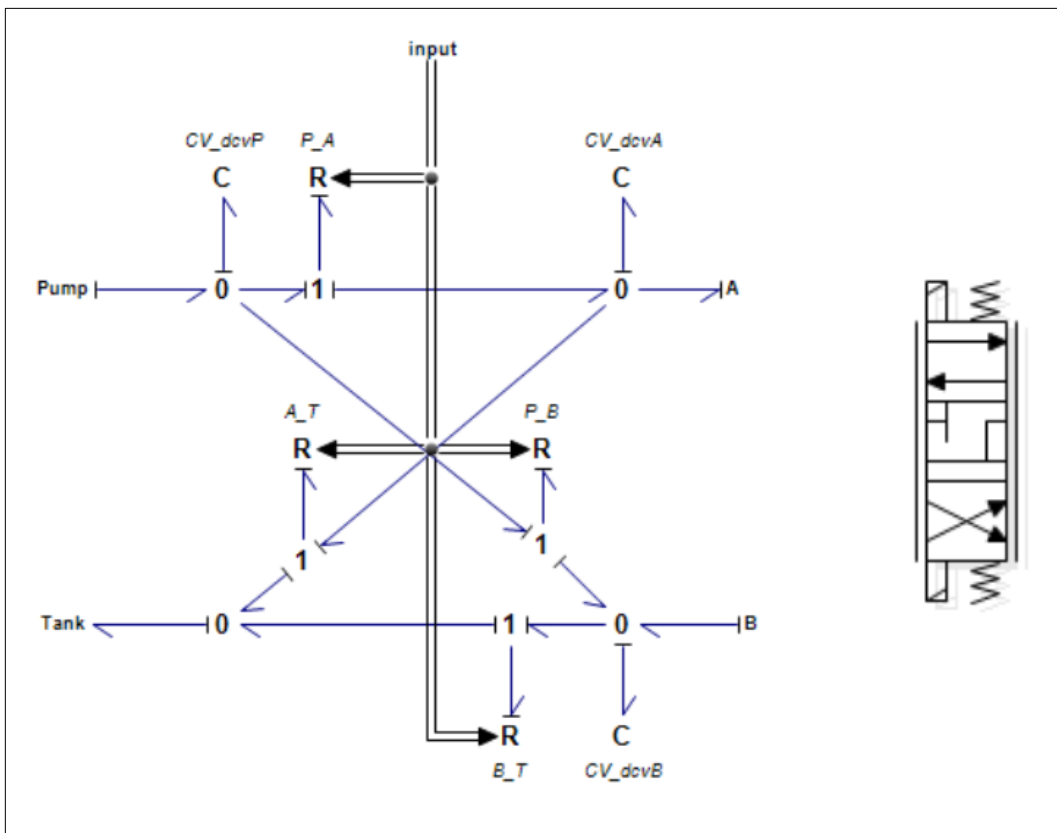


Fig. 5.7 Bond graph model of DCV

Recall equation 5.27, the constitutive relation of valve R-element is given as below

$$f = \xi_{dcv} C_{dcv} \sqrt{\frac{2}{\rho} \text{abs}(e)} \cdot \text{sign}(e) \quad (5.30)$$

Where the relative opening of port  $\xi_{dcv}$  is signaled by slide position, which controlled by external controller and  $C_{dcv}$  is the nominal opening area.

The constitutive law for the control volume C-element is given as below

$$e = \frac{\beta}{V} \int f dt \quad (5.31)$$

Where  $\beta$  is the bulk modulus of fluid and  $V$  is the controlled volume.

Counter balance valve

The model of CBV consists of check valve and pressure control valve (the CBV itself). The modelling equations of both valve are written in the same R-element. It has a pressure signal input from load side. The bond graph model is given below.

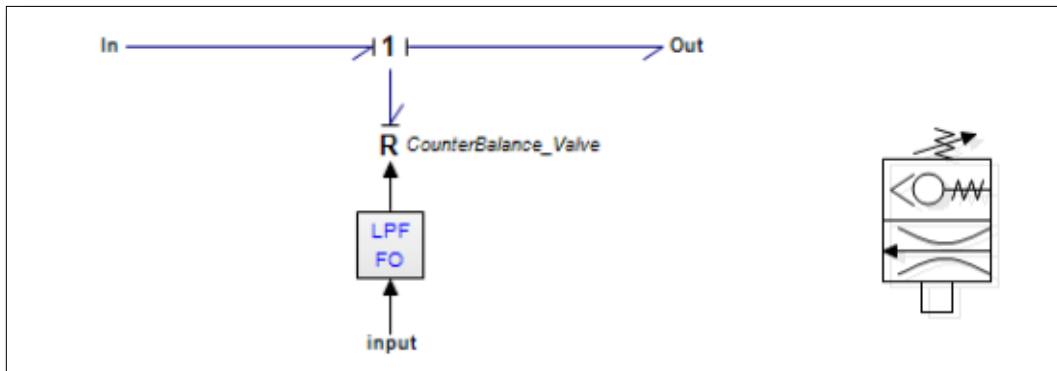


Fig. 5.8 Bond graph model of counter balance valve

Based on Equation 5.25 and Equation 5.27, the check valve model is simplified as below

$$f_{cv} = \begin{cases} C_{cv} \sqrt{\frac{2}{\rho} \text{abs}(e)} & \text{for } e > 0 \\ 0 & \text{for } e \leq 0 \end{cases} \quad (5.32)$$

Where  $f_{cv}$  is the flow through check valve,  $C_{cv}$  is the nominal flow coefficient of check valve.

The relative opening of pressure control valve is given as below

$$\xi_{cbv} = \begin{cases} 0 & \text{for } P_{pilot} \leq P_{cr,cbv} \\ \min\left(1, \frac{P_{pilot} - P_{cr,cbv}}{P_{full,cbv} - P_{cr,cbv}}\right) & \text{for } P_{pilot} > P_{cr,cbv} \end{cases} \quad (5.33)$$

Where  $P_{pilot}$  is the pressure signal,  $P_{cr,cbv}$  is the crack opening pressure and  $P_{full,cbv}$  is the fully opening pressure.

The flow through pressure control valve is given

$$f_{cbv} = \xi_{cbv} C_{cbv} \sqrt{\frac{2}{\rho} \text{abs}(e)} \cdot \text{sign}(e) \quad (5.34)$$

Where  $C_{cbv}$  is the nominal flow coefficient of pressure control valve

So the flow variable of power of the CBV is given below

$$f = f_{cv} + f_{cbv} \quad (5.35)$$

Relief valve

The relief valve is used to prevent the pressure over the set point. The bond graph model of relief valve contains an R element and C element for avoiding causality error as shown below

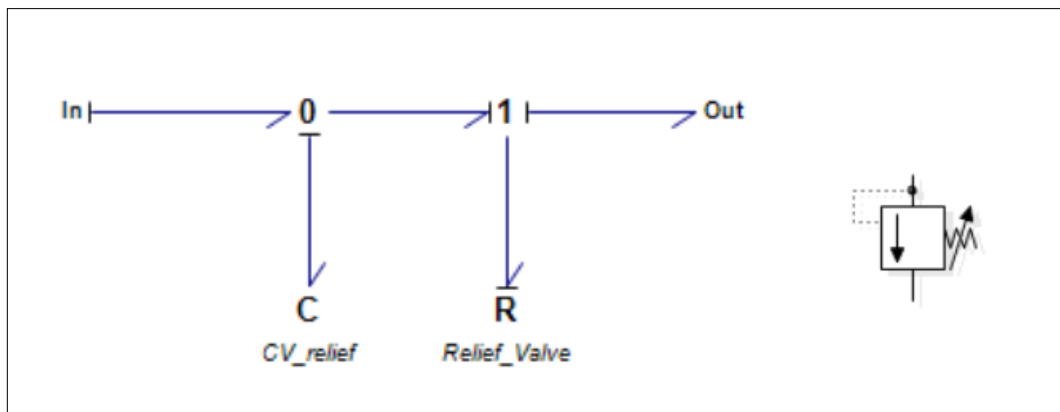


Fig. 5.9 Bond graph model of relief valve

The modeling equation of control volume C-element is the same as equation 5.31.

And constitutive law of relief valve is given below

$$f = \begin{cases} 0 & \text{for } e \leq P_{cr,rv} \\ C_{rv} \sqrt{\frac{2}{\rho} \text{abs}(e - P_{cr,rv})} & \text{for } e > P_{cr,rv} \end{cases} \quad (5.36)$$

Where  $C_{rv}$  is the nominal flow coefficient and  $P_{cr,rv}$  is the crack opening pressure of relief valve.

### 5.3.4 Hydraulic Motor

The hydraulic motor is modeled as transformer-element with friction loss as below

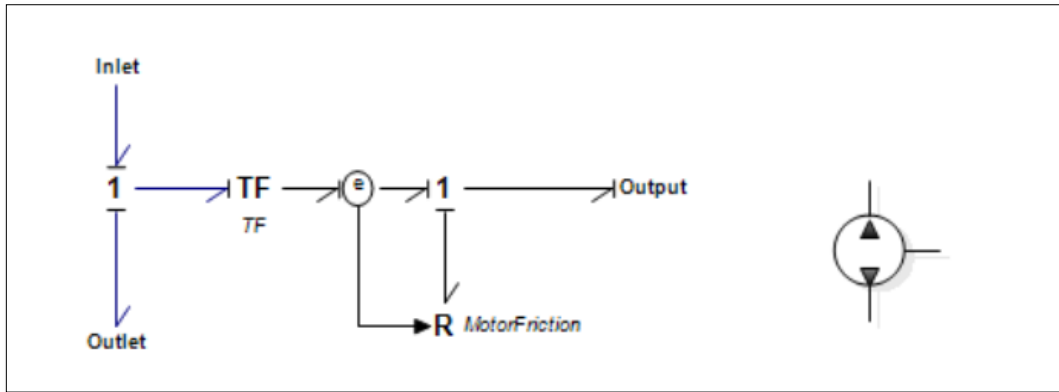


Fig. 5.10 Bond graph model of hydraulic motor

The relationship of power variables of motor TF-element is given below

$$e_1 = \frac{1}{\frac{V_{motor}}{2\pi}} e_2 \quad (5.37)$$

$$f_2 = \frac{1}{\frac{V_{motor}}{2\pi}} f_1 \quad (5.38)$$

Where  $e_1$  is the hydraulic pressure at motor,  $e_2$  is the output torque of motor,  $f_1$  is the flow through motor,  $f_2$  is the motor rotational speed and  $V_{motor}$  is the displacement of motor ( $m^3/rev$ ).

The actual friction in motor is quite complex. It consists of both static and coulomb friction as well as velocity and pressure dependent friction. However, for our application, a simplified model of friction is used based on Li (2016) and Bak and Hansen (2013)

$$\tau_{friction} = \tau_s + C_p |\tau_h| \quad (5.39)$$

Where the first term is constant static friction, which may be set to,  $\tau_s \approx \frac{V_{motor}}{2\pi} \cdot 1 \cdot 10^5 Nm$  and the second term is pressure dependent friction, which may constitute 2 ... 3% of the hydraulic torque. Here we take  $C_p = 0.02$ .

To avoid the computation difficulties around zero velocity, then the constitutive law for friction R-element can be given

$$e = \begin{cases} \tau_{friction} \cdot \frac{f}{\omega_0} & \text{for } abs(f) \leq \omega_0 \\ \tau_{friction} \cdot sign(f) & \text{for } abs(f) > \omega_0 \end{cases} \quad (5.40)$$

Where  $\omega_0$  should be a very small number close to zero, here we take  $\omega_0 = 1(rad/s)$ .

### 5.3.5 Hydraulic Cylinder

The bond graph model of hydraulic cylinder include the capacitance of the chambers, friction between the piston and barrel, and end stoppers. The cylinder inlet is modelled as restriction orifice with MR-element, the capacitance of chambers are modeled as C-element, the transformation between hydraulic energy and mechanical energy on piston side and rod side is modelled as MTF-element and the end stopping cushion is modelled as MSe-element.

The bond graph model of hydraulic cylinder is shown as below in Fig. 5.11

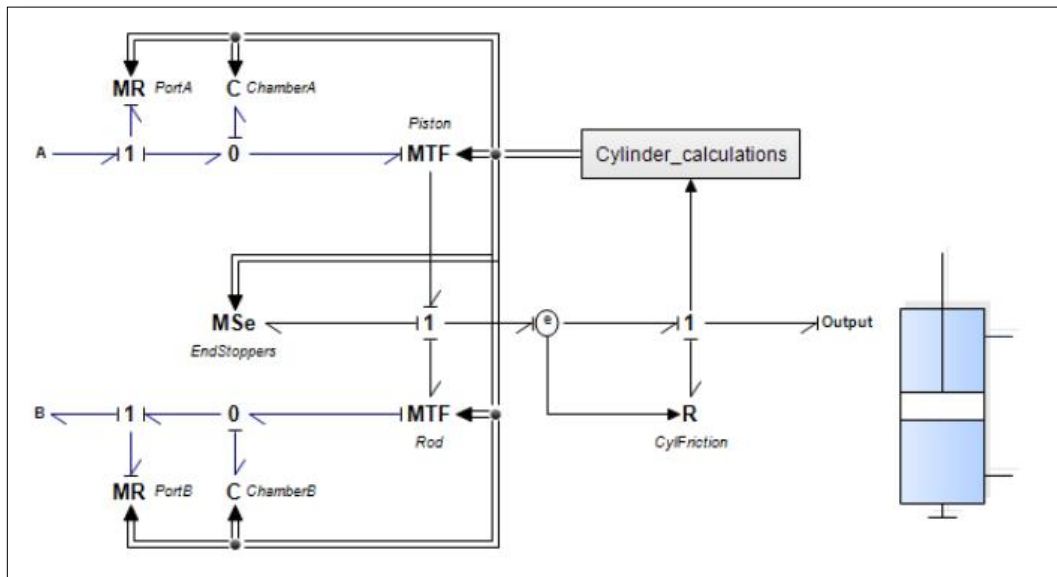


Fig. 5.11 Bond graph model of hydraulic cylinder

The constitutive relation of power variables of restriction orifice MR-element is the same as equation 5.19. And the constitutive law for other elements are given in following.

Chamber C-element

Based on equation 5.31, we have the following power variables relationship for chamber A and chamber B.

$$e = \frac{\beta}{V_A} \left( \int f dt + V_{A,ini} \right) \quad (5.41)$$

$$e = \frac{\beta}{V_B} \left( \int f dt + V_{B,ini} \right) \quad (5.42)$$

Where  $\beta$  is the bulk modulus of fluid,  $V_A$  and  $V_B$  are the chamber volumes which are function of piston position and  $V_{A,ini}$  and  $V_{B,ini}$  are the initial volume in chamber A and B respectively.

Piston and rod MTF-element

The MTF-element for piston side is given

$$e_1 = \frac{1}{A_p} e_2 \quad (5.43)$$

$$f_2 = \frac{1}{A_p} f_1 \quad (5.44)$$

Where  $e_1$  is the hydraulic pressure at piston side,  $e_2$  is the force acting on piston side,  $f_1$  is the flow into chamber of piston side,  $f_2$  is the piston velocity and  $A_p$  is the piston area.

The MTF-element for rod side is given

$$e_1 = A_r e_2 \quad (5.45)$$

$$f_2 = A_r f_1 \quad (5.46)$$

Where  $e_1$  is the force exerted on the cylinder rod,  $e_2$  is pressure in the chamber of rod side,  $f_1$  is rod velocity,  $f_2$  is the flow out of chamber of rod side and  $A_r$  is the area calculated by deducting piston area by rod area.

End stopper Mse-element

The end stopper is modeled as spring damper system and the constitutive law is given below

$$e = -k\Delta x - cf \quad (5.47)$$

Where  $k$  is the spring stiffness,  $\Delta x$  is the deflection of spring and  $c$  is the damping factor

Friction R-element

Similar to motor friction, the friction of cylinder can be given based on equation 5.39

$$F_{friction} = F_s + C_p |F_h| \quad (5.48)$$

Where the first term is constant static friction, which may be set to,  $F_s \approx A_p \cdot 1 \cdot 10^5 Nm$  and the second term is pressure dependent friction, which may constitute 2 ... 3% of the hydraulic Force. Here we take  $C_p = 0.02$ .

The constitutive relation of R-element is given

$$e = \begin{cases} F_{friction} \cdot \frac{f}{v_0} & \text{for } abs(f) \leq v_0 \\ F_{friction} \cdot sign(f) & \text{for } abs(f) > v_0 \end{cases} \quad (5.49)$$

Where  $v_0$  should be a small value, here we take  $v_0 = 0.005(m/s)$

### 5.3.6 Tank

The tank is modeled as an open effort source with one atmosphere pressure and the constitutive relation of tank model is given as below

$$e = 1 \cdot 10^5 (P_a) \quad (5.50)$$

## 5.4 Simulation and Verification of Complete Hydraulic Systems

Based on above analysis, the overall hydraulic system model integrated with gangway dynamics model is shown below in Fig. 5.12. Based on that the hydraulic system sub-model for slewing king, luffing boom and telescopic boom will be verified.



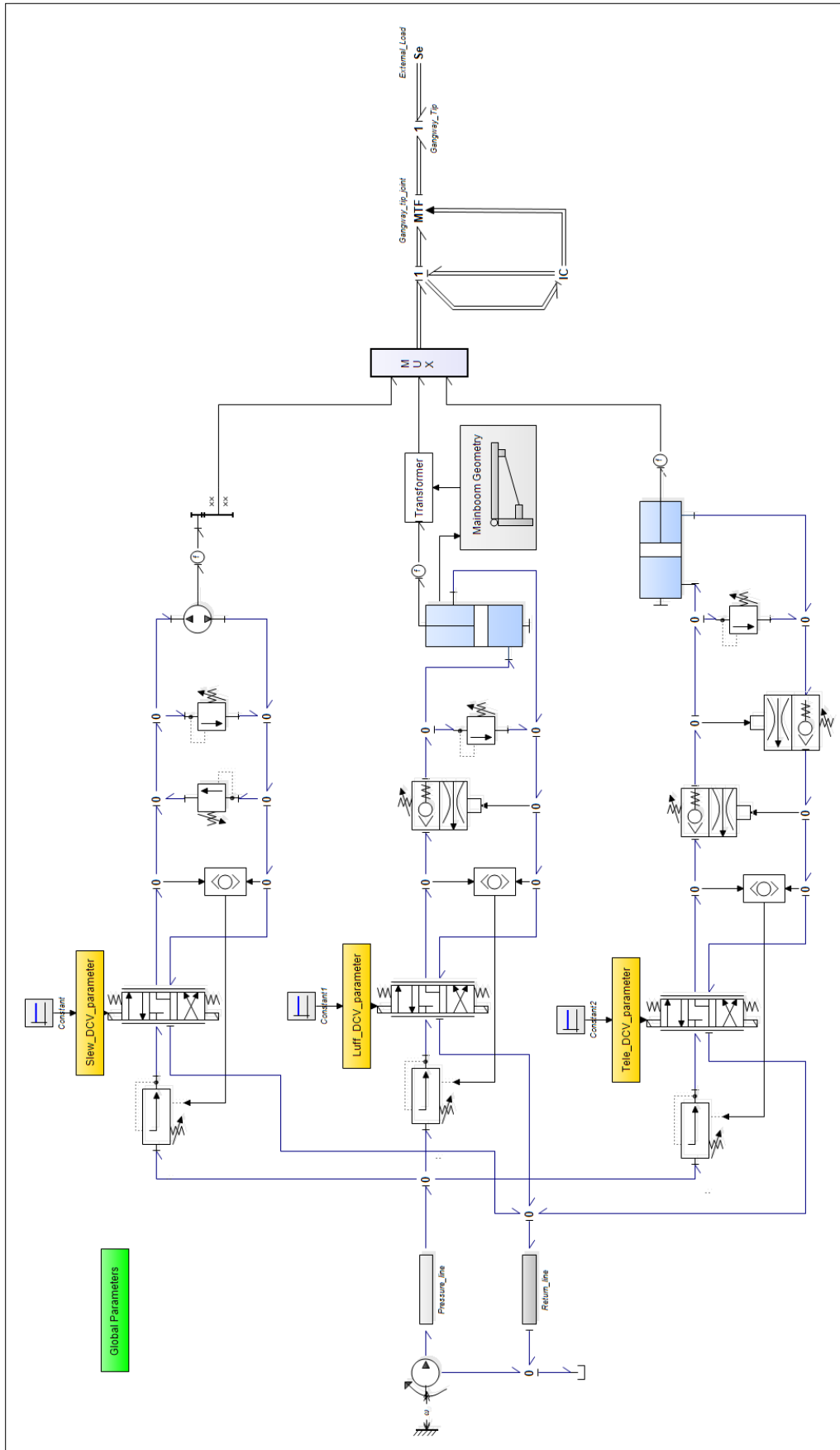


Fig. 5.12 Complete hydraulic system model integrated with gangway dynamics

### 5.4.1 Shared Pump and Pipe Parameters

Based on the calculation parameters before, the pump and pipe parameters are given below

Table 5.6 Pump and Pipe parameters

Pump	
$Q_{max} = 180 \text{ cm}^3/\text{rev}$	$RPM = 1776$
$P_{set} = 200 \text{ bar}$	$\Delta P_{dev} = 10 \text{ bar}$
$\eta_{eff} = 0.95$	
Pipe	
$l = 10 \text{ m}$	$\varepsilon = 0.0002$
$D_{pressure} = 30 \text{ mm}$	$D_{return} = 44 \text{ mm}$

### 5.4.2 Hydraulic System for Slewing King

For all the valves in our hydraulic system, we assume the nominal pressure drop corresponding the maximum nominal flow is 5 bar. And based on the calculations for the sub-hydraulic system of slewing king, the main parameters of the hydraulic components are given below

Table 5.7 Parameters of main components of slewing sub hydraulic system

Pressure compensator valve	
$Q_{max} = 100 \text{ l/min}$	$\Delta P_{set} = 5 \text{ bar}$
Directional control valve	
$Q_{max} = 20 \text{ l/min}$	Dead band: 10%
Relief valve	
$Q_{max} = 20 \text{ l/min}$	$P_{cr,rv} = 50 \text{ bar}$
Motor and gearbox	
$V_{motor} = 20 \text{ cm}^3/\text{rev}$	Gear ratio: 500

In order to check the maximum speed of the slewing king, we give the signal DCV of slewing hydraulic system to let the DCV fully open in two direction in sequence. And the luffing boom is set in horizontal position, telescopic boom in full extension and the designed live load (300 kg) is applied at the tip in minus Z-axis. Under this condition, the plot slewing speed of slewing king and the working pressure is given below

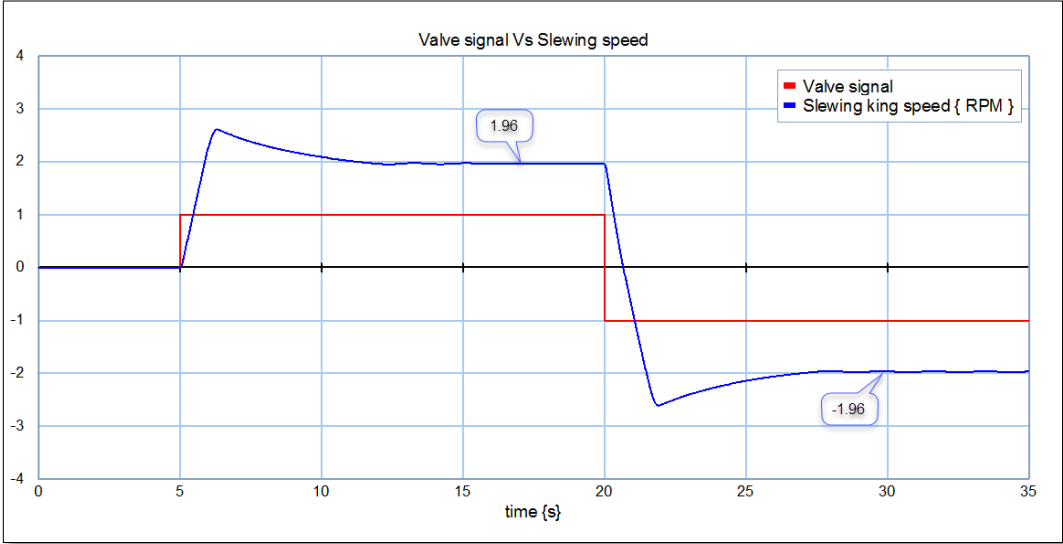


Fig. 5.13 Rotation speed of slewing king

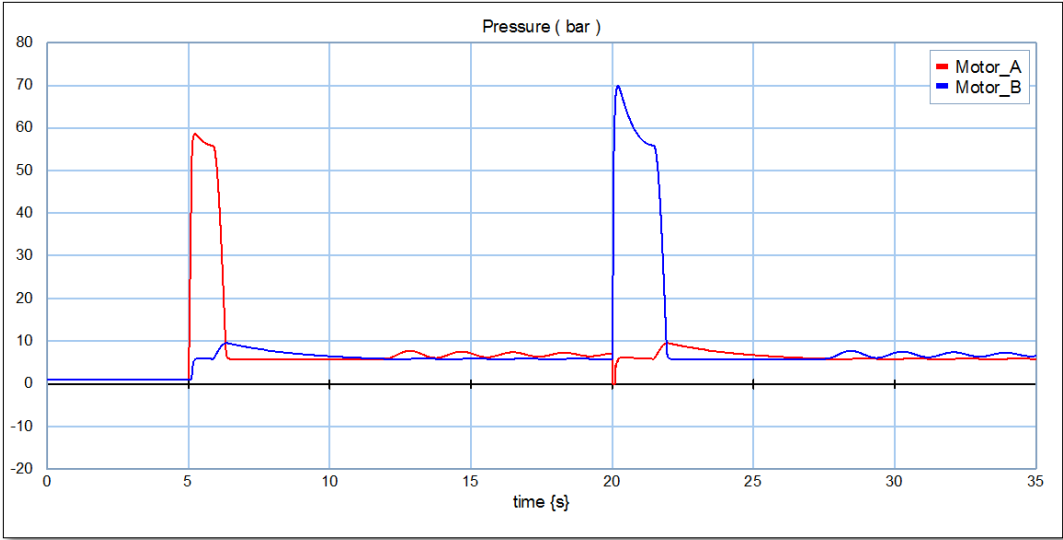


Fig. 5.14 Pressure of both sides of motor

As Fig. 5.13 shows, the maximum stabilized slewing speed of slewing king is 1.96 RPM and the acceleration time is less than two seconds, which is quite close to the requirement (2 RPM). The reason for this small velocity error is the throttling of PCV and that is why we choose a bigger capacity PCV. The bigger capacity PCV, the speed is more close to designed speed. Also

from Fig. 5.14, we can see that because we don't include the rotation friction, so the stabilized pressure difference between both sides of motor is less than 5 *bar* and the inlet and outlet pressure is less than 10 *bar*. And considering the velocity error is quite small and acceptable for our system, so we can say the designed hydraulic system is powerful enough to fulfil the gangway operation requirement. For the other information such as flow through each elements, we will not present here, and interested readers can check that in the hydraulic model named "slewing hydraulic system" in the attached CD.

### 5.4.3 Hydraulic System for Luffing Boom

As we mentioned before, we have two identical cylinders to actuate the luffing boom and the information about the required cylinder is given in section 5.2.2. But in our modeling, we modelled these two cylinders as one in order to simplify the model. The same as slewing hydraulic system, the nominal pressure drop over valves are assumed as 5 *bar*. The main parameters for components of hydraulic system are given below.

Table 5.8 Parameters for luffing hydraulic system

Pressure compensator valve	
$Q_{max} = 200 \text{ l/min}$	$\Delta P_{set} = 5 \text{ bar}$
Directional control valve	
$Q_{max} = 60 \text{ l/min}$	Dead band: 10%
Counter balance valve	
$Q_{max} = 60 \text{ l/min}$	$P_{cr,cbv} = 5 \text{ bar}, P_{full,cbv} = 160 \text{ bar}$
Relief valve	
$Q_{max} = 60 \text{ l/min}$	$P_{cr,rv} = 160 \text{ bar}$
Cylinder	
Equivalent $R_p$ : 92 mm	Equivalent $R_r$ : 50 mm

To perform the simulation of luffing sub-hydraulic system, the initial condition of gangway is set as that the telescopic boom is in full extension, luffing cylinder is fully extracted and the

designed live load (300 kg) is applied at the tip in minus Z-axis. Then the simulation result of luffing cylinder speed, rod position and working pressure in the circuit is given below.

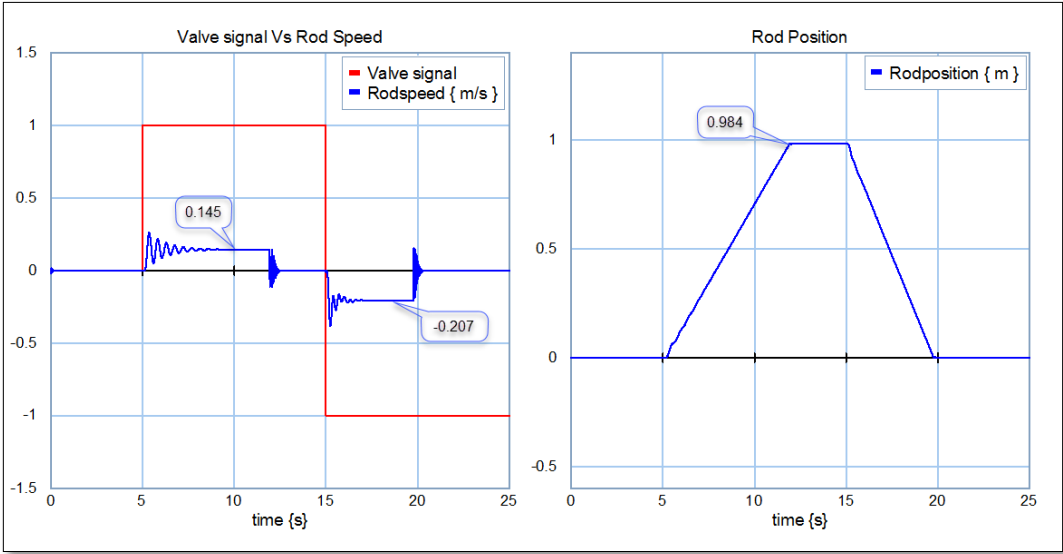


Fig. 5.15 Luffing cylinder rod speed and position

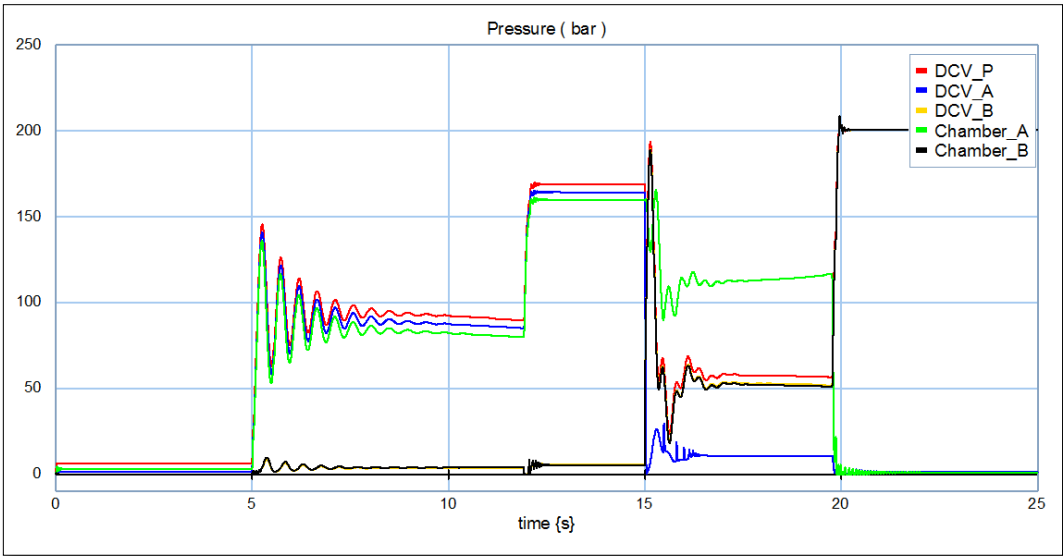


Fig. 5.16 Working pressure of luffing sub hydraulic system

As above plots show that the maximum velocity of luffing cylinder during extension and extraction is  $0.145\text{ m/s}$  and  $0.207\text{ m/s}$  respectively which can fulfil our requirement even the maximum velocity during extension is a little smaller than the designed reference in section 5.2.2. And difference between the maximum velocities is due to the asymmetric features of cylinder. Also, the plot shows the cylinder rod stopped when reaching maximum stroke (0.894 ) at around 12 seconds and the pressure of chamber-A(head side) reaches about  $160\text{ bar}$  because of the setting pressure of relief valve on the chamber-A side. At 15 seconds, the luffing cylinder

start to extract after switching valve signal and stopped at full extraction at about 20 seconds. At the same time, the pressure of chamber-B (rod side) reach about 200 *bar* (the pump setting pressure), because we have no relief valve on chamber-B side. We notice that due to the self-weight of gangway, the pressure of chamber-B is always smaller than chamber-A during normal operation, so there is no need to have relief valve on Chamber-B side. But due to CBV, the pressure of port-B of DCV is always bigger than that of port-A of DCV during extraction process. So with the help of PCV, the pressure drop over DCV in the pressure line is maintained at 5 *bar* during operation. So we can say that the designed luffing sub-hydraulic system can satisfy our requirement based on our analysis. For the other information regarding luffing system, interested readers can visit model named “luffing hydraulic system” in the attached CD.

#### 5.4.4 Hydraulic System for Telescopic Boom

Similar to the luffing cylinder, the two telescopic cylinders will be modeled as one cylinder with equivalent diameter in the hydraulic system. And the nominal pressure drop is assumed as 5 *bar* for all the valves. So based on the design parameters of telescopic cylinder in section 5.2.2 and considering the strength of gangway in Appendix A The main parameters of the hydraulic components is given below

Table 5.9 Parameters for telescopic hydraulic system

Pressure compensator valve	
$Q_{max} = 600 \text{ l/min}$	$\Delta P_{set} = 5 \text{ bar}$
Directional control valve	
$Q_{max} = 220 \text{ l/min}$	Dead band: 10%
Counter balance valve	
$Q_{max} = 220 \text{ l/min}$	$P_{cr,cbv} = 5 \text{ bar}, P_{full,cbv} = 20 \text{ bar}$
Relief valve	
$Q_{max} = 220 \text{ l/min}$	$P_{cr,rv} = 20 \text{ bar}$
Cylinder	
Equivalent $R_p$ : 113 <i>mm</i>	Equivalent $R_r$ : 51 <i>mm</i>

The initial condition for performing telescopic sub-hydraulic system is set as that the luffing boom is in horizontal position, telescopic cylinder is fully extracted and no external load applied at gangway tip. Then simulation results of the telescopic rod speed and rod position and the working pressure is give below.

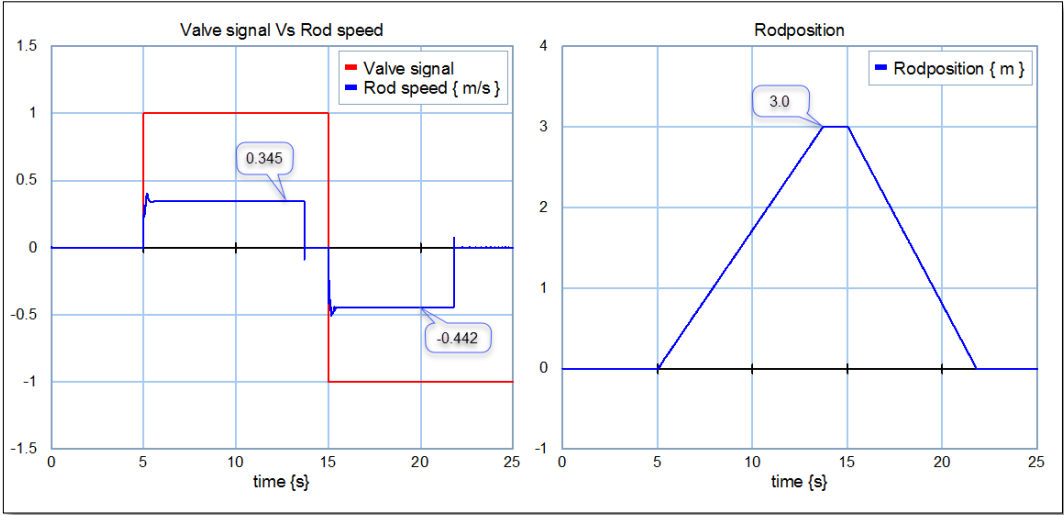


Fig. 5.17 Telescopic cylinder rod speed and position

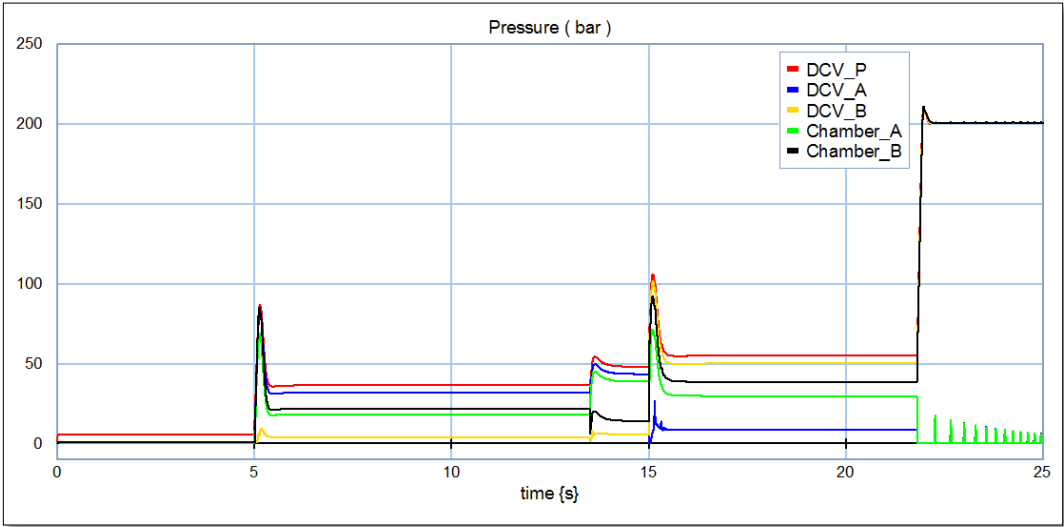


Fig. 5.18 Working pressure of telescopic sub hydraulic system

From above plots, we know that the maximum velocity during extension and extraction is  $0.345\text{m/s}$  and  $0.442\text{ m/s}$  respectively which can fulfil our requirement even the maximum velocity during extension is a little smaller than the designed reference in section 5.2.2. And the plot shows the cylinder rod stopped when reaching maximum stroke (3.0 ) at around 13.5 seconds and the pressure of chamber-A(head side) reaches about 35 bar because of the setting pressure of relief valve on the chamber-A side. At 15 seconds, the telescopic cylinder starts to

extract after switching valve signal and stopped at full extraction at about 22 seconds. At the same time, the pressure of chamber-B (rod side) reach about 200 *bar* (the pump setting pressure), because we have no relief valve on chamber-B side. We know that when pushing gangway against the windmill platform during operation, the chamber-A side is the load side. So that is why we have the relief valve on chamber-A side not chamber side. Since we donot consider the sliding friction between gangway booms, the stabilized pressure difference of the two sides of piston is very small (less than 5 bar). And the pressure drop over DCV is maintained at around 5 *bar* by PCV, so we can say the designed telescopic system fulfil our design requirement as well. For other information regarding this sub hydraulic system, interested readers can visit the model named “telescopic hydraulic system” in the attached CD.



## 6 Control of Gangway

In this chapter, we will introduce the control algorithm for the gangway operation. It includes the definition of control task, design of control algorithm for active heave compensation and design of parallel position and force controller for controlling the contact force control at desired level (4000 N suggested by supervisors) when pushing gangway tip against the wind turbine platform during transferring operation.

### 6.1 Control Task

After investigation the gangway operation procedures and talking with the engineers in ICD Company, the operation of offshore gangway can be specified as below

- Start the gangway in joint control mode
- When the gangway is close to the platform, switch to active heave compensation mode and then the gangway will be operated in coordinated control mode
- Under active heave compensation mode, the operator maneuver the gangway to approach the platform by controlling the velocity of gangway tip through joystick
- Once gangway is in contact with the platform, the bumper operation mode will be switched on. In the bumper mode operation, the controller try to maintain the setting constant contacting force between gangway tip and platform and keep motion compensation as well.
- After finishing transferring, switch to joint control mode and retract the gangway and stowed it on the vessel

Based on above operation of gangway, the operation mode of gangway can be can be classified in to three modes as below

- Joint control mode
- Active have compensation mode
- Bumper operation mode

Since when the gangway operated in joint control mode, it just feeds the signal from joystick to the individual directional control valve to move the gangway joint by joint. The controller for actuator is the same as the two other operational modes, so in this thesis we only focus on the design of controller for active motion compensation operation and bumper mode operation.

## 6.2 Active Motion Compensation Control and Simulation

### 6.2.1 Control algorithm of active motion compensation

In this section, an active motion compensation algorithm will be introduced during the AMC gangway operation. The idea is to control the gangway in the coordinate control mode. In this control mode, the signal from the input device will be the gangway tip velocity in X, Y and Z-axis in gangway foundation frame {0}, and then these signals can be converted into position and velocity of cylinder or motor by kinematics relation. And then these signals will be sent to cylinder or motor controller to control the motion of corresponding actuators. And motion compensation can be easily achieved by adding the motion signals from MRU to the controller and make the gangway tip move in the opposite direction of ship motion with the same speed. By doing this, ideally, the motion of gangway tip will be not affected by the ship motion, it will be keep still or move with a controlled speed given by operator in the world-frame {w}. To simplify the model, we assume the world-frame {w} is fixed at the initial position of gangway base frame {0}, and MRU data describes the motion of gangway base frame {0} relative to world-frame {w} as shown in following Fig. 6.1.

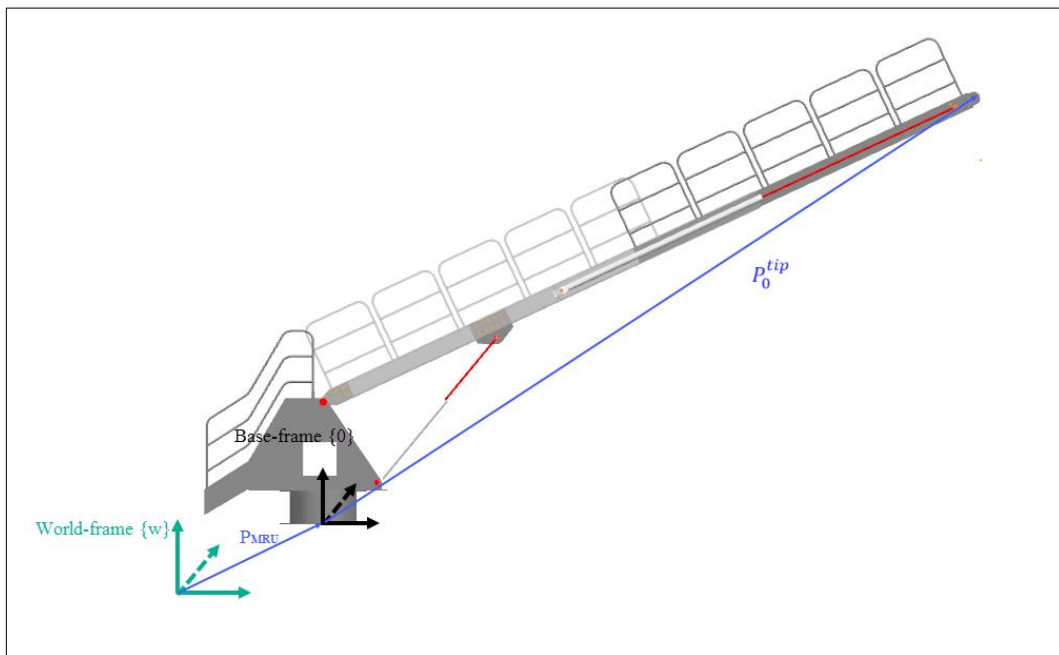


Fig. 6.1 Relation between gangway base frame and world frame

Then based on the principle description of active motion compensation above, the structure of the active motion compensation controller was given in Fig. 6.2. Due to the lack of joystick, we will use the keyboard to control the motion of gangway tip in our modeling and it can be easily replaced by joystick for interested readers.

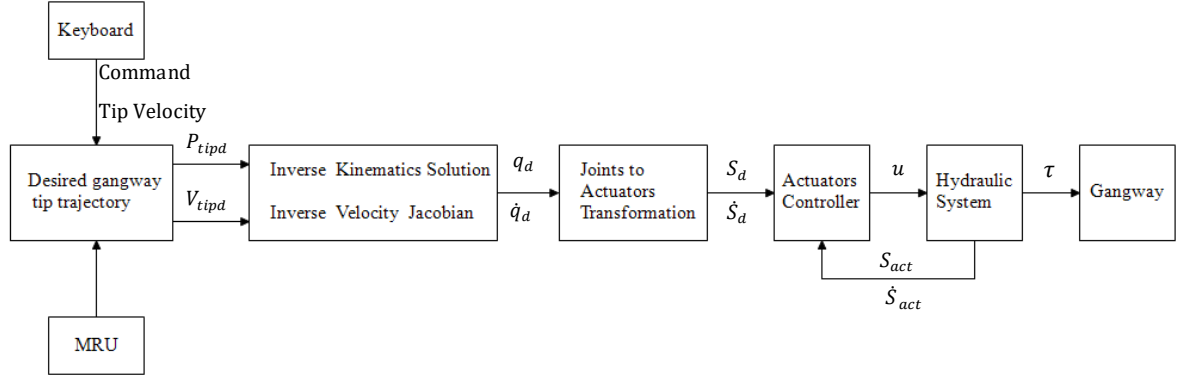


Fig. 6.2 Structure of AMC control algorithm

In Fig. 6.2,  $P_{tipd}$  and  $V_{tipd}$  are the vector of desired gangway tip velocity in gangway base frame  $\{0\}$  in order to compensate the ship motion and follow the command gangway tip trajectory in world frame  $\{w\}$ .  $q_d$  and  $\dot{q}_d$  are the vector of corresponding desired joint displacement and joint velocity calculated by inverse kinematics and inverse Jacobian as derived in 4.2.2.  $S_d$  and  $\dot{S}_d$  are vector of the corresponding desired motor angle or cylinder length and their velocity calculated by transformation relation as derived in 4.2.3,  $S_{act}$  and  $\dot{S}_{act}$  are the vector of measured motor angle or cylinder length and their velocity.  $u$  is the vector of signal from actuator controller to directional control valve of each hydraulic circuit and  $\tau$  is the actuator force or torque supplied to gangway system.

We know that the gangway tip position and velocity are affected by ship motion and maneuvering of operator. To realize the control of active motion compensation, we should obtain the desired gangway tip position and velocity in gangway base frame  $\{0\}$  for compensating ship motion and maneuvering. Based on the control structure for active heave compensation, the desired gangway tip position and velocity expressed in base frame  $\{0\}$  can be given as below

$$P_{tipd} = P_{tipr} - P_{ship} + int(input) \quad (6.1)$$

$$V_{tipd} = int(input) - V_{ship} \quad (6.2)$$

Where  $P_{tipr}$  is the vector of recorded gangway tip position expressed in base frame  $\{0\}$  when the motion compensation functions is switched on,  $P_{ship}$  and  $V_{ship}$  is the ship motion position function and velocity function in world frame  $\{w\}$ ,  $input$  is the desired gangway tip velocity given by the operator through keyboard or other input devices in world frame  $\{w\}$  and all these parameters are  $3 \times 1$  vector corresponding to X,Y and Z of their frame.

## 6.2.2 Design of Actuator Controller

As mentioned, the goal of hydraulic system is to control the motion of gangway. And the kinematics mapping relate gangway tip position and velocity to actuator position and velocity has already been discussed in section 4.2 . So we will not elaborate the details any more in this part and we will focus on how to control the motion of actuator. The control of actuator motion is achieved by adjusting the flow to the actuator through the directional control valve. In our system, we assume the response of directional control valve response fast enough and the dynamics of DCV is neglected. The control law for hydraulic actuators can be given as follows

$$u = K_{ffc}\dot{S}_d + K_p(S_d - S_{act}) + K_d(\dot{S}_d - \dot{S}_{act}) \quad (6.3)$$

Where  $u$  is the signal to DCV,  $K_{ffc}$  is the gain of velocity feedforward and  $K_p$  and  $K_d$  the proportional gain for the PD controller.

As proposed by Kjelland and Hansen (2015),Kontz (2007) andSanders (2016), the features of this controller are given as following

- Feedforward term is used to minimize the control effort generated by the feedback error signal. This term essentially make the DCV supply the exactly needed flow to follow the desired trajectory.
- The feedback PD controller is used to reject the position and velocity error.

And the feedback PD controller gains cannot be specified based on the steady state of hydraulic system and therefor they have tuned during simulation. But for our hydraulic system, due to the use of PCV, the velocity of actuator is proportional to the spool position of DCV (neglecting the deadband of valve). So the feedforward gains can be estimated based on the maximum actuator velocity given in section 5.4.

For hydraulic motors, because the magnitude of maximum velocity in two direction is the same, so the feedforward gains for hydraulic motor is given below.

$$K_{ffc} = \frac{1}{abs(V_{max})} \quad (6.4)$$

For hydraulic cylinders, due to its asymmetric features, the maximum velocity of extension and retraction is different, so the feedforward gain for the hydraulic cylinder can be given as below.

$$K_{ffc} = \begin{cases} \frac{1}{abs(V_{ext,max})} & \text{if } V_d \geq 0 \\ \frac{1}{abs(V_{rec,max})} & \text{if } V_d < 0 \end{cases} \quad (6.5)$$

Where  $V_{ext,max}$  is the maximum speed of cylinder during extension,  $V_{rec,max}$  is the maximum speed of cylinder during retraction and  $V_d$  is the desired cylinder velocity.

### 6.2.3 Performance of Gangway under Active Heave Compensation Control

To verify the effectiveness of the designed controller for active motion compensation, the ship motion is introduced into the gangway system. The initial state of gangway will be set to the specified operational condition where angle of slewing king is set to be zero, the luffing boom is at horizontal position, and the telescopic boom is extended by half stroke(1.5 m).

The initial gangway tip position in world frame {w} is given as below

- $P_{tipX}^w = 9.30 \text{ m}$
- $P_{tipY}^w = 0 \text{ m}$
- $P_{tipZ}^w = 1.82 \text{ m}$

The ship motion in world frame {w} is defined as

- $X = 0.5\sin(\frac{2\pi}{12}t) \text{ m}$
- $Y = 0 \text{ m}$
- $Z = \sin(\frac{2\pi}{12}t) \text{ m}$

The gains for actuators of sub-hydraulic system of gangway are given in the following table

	$K_{ff}$	$K_p$	$K_d$
Slewing sub-hydraulic system	$\frac{1}{102.63}$	5	3
Luffing sub-hydraulic system	$\begin{cases} \frac{1}{0.145} & \text{if } V_d \geq 0 \\ \frac{1}{0.207} & \text{if } V_d < 0 \end{cases}$	10	4
Luffing sub-hydraulic system	$\begin{cases} \frac{1}{0.345} & \text{if } V_d \geq 0 \\ \frac{1}{0.442} & \text{if } V_d < 0 \end{cases}$	10	2

The complete model of integrating controller with hydraulic model and mechanical model of gangway is given below.

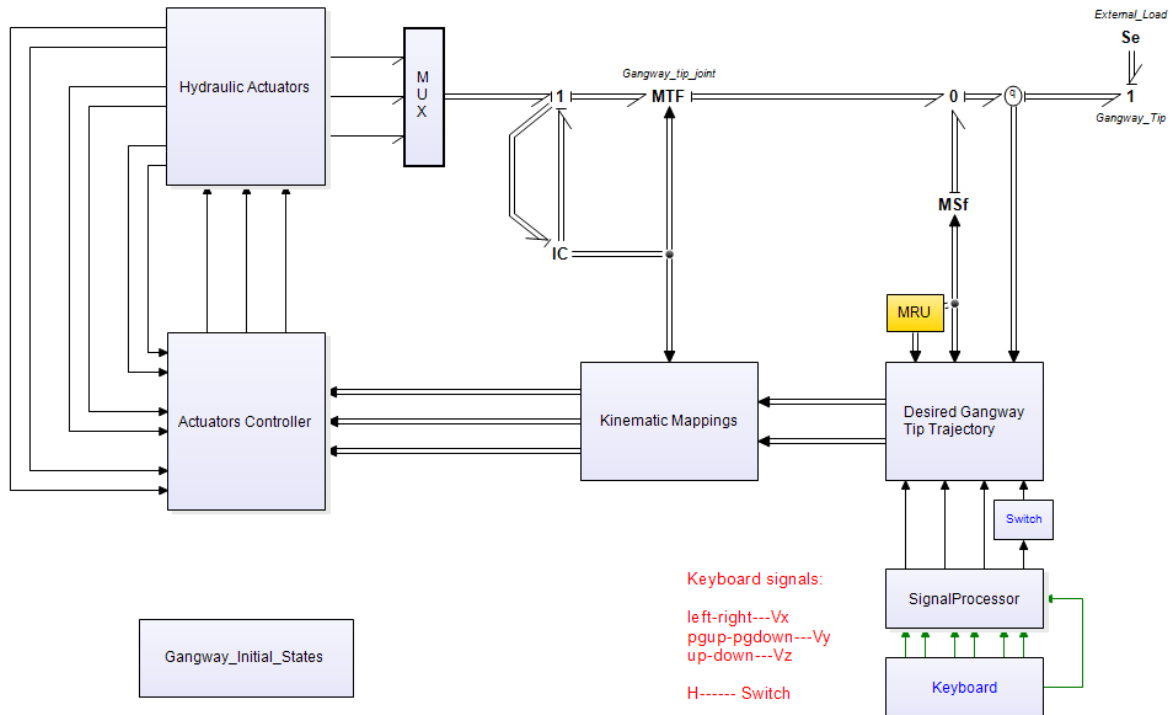


Fig. 6.3 Complete model of gangway system under active motion compensation control

In this model, the global initial states block is used to set the initial states of gangway, the keyboard is used to generate the control signal and signal processor block is used to smooth the input signals from keyboard by hold elements and low pass filter. The kinematic mappings block is used to calculate the desired actuator position and velocity by the signal receiving from block desired gangway tip trajectory. And MRU is used to generate the ship motion. IC field block is the representation of mechanical model of gangway. Se-element modelled the external load at gangway tip. And the hydraulic system is imploded into a hydraulic actuators block. Interested readers can go into each sub-model of the complete model named “Gangway with AMC Controller” in the attached CD.

The gangway performance under AMC controller are studied in the following two load cases

- Load case 1 : no external load at gangway tip
- Load case 2: 300 kg normal working live load at the gangway tip in minus Z-axis.

The simulation results regarding the gangway tip position in X-axis and Z-axis of world frame {w} and pressure of luffing cylinder and telescopic cylinder in these two different load cases are presented below.

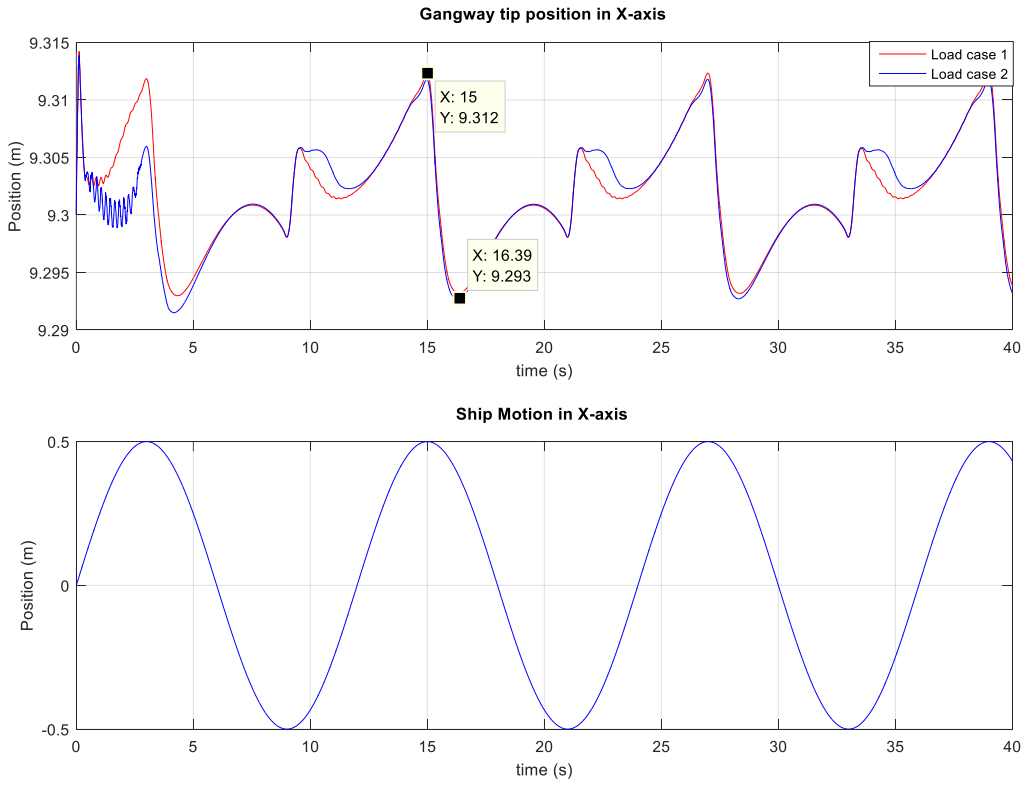


Fig. 6.4 Gangway tip position in X-axis under AMC control in two load cases

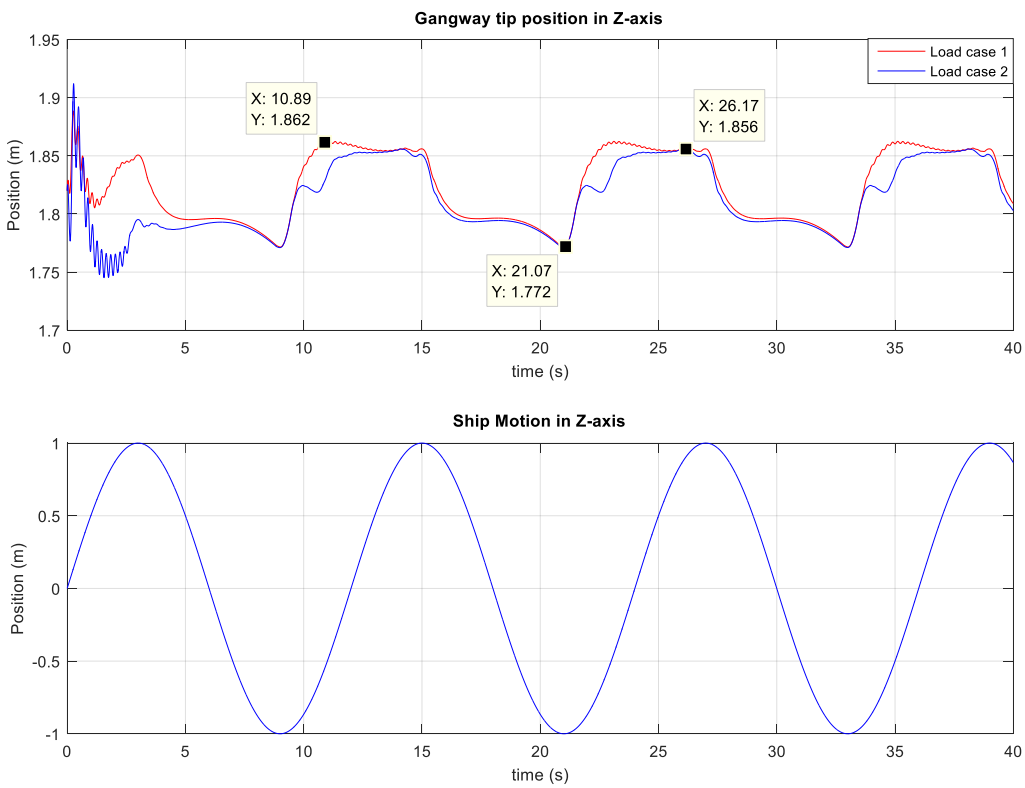


Fig. 6.5 Gangway tip position in Z-axis under AMC control in two load cases

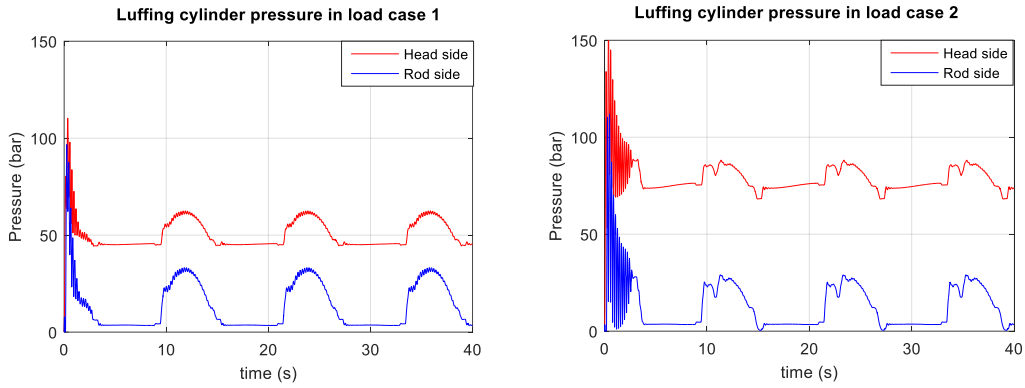


Fig. 6.6 Luffing cylinder pressure under AMC control in two load cases

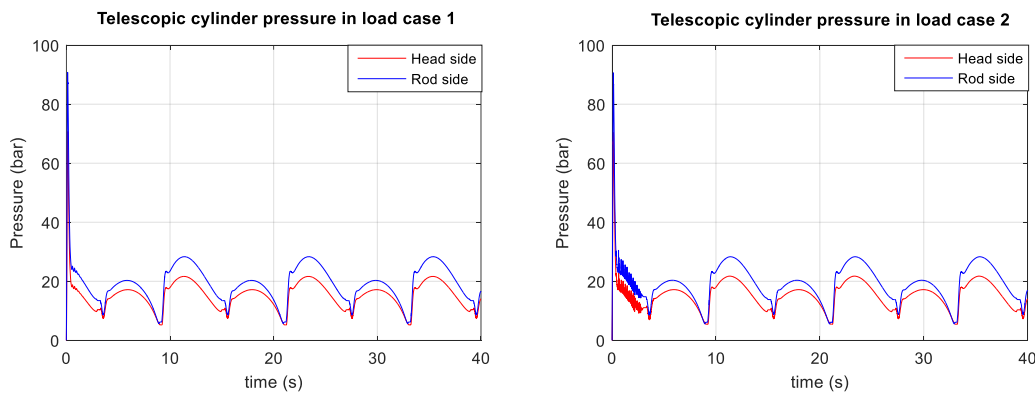


Fig. 6.7 Telescopic cylinder pressure under AMC control in two load cases

From above plots, we can see that in the two load cases, the gangway tip position in X-axis and Z-axis are all stabilized around the initial setting values after 3 seconds. In X-axis, the position errors of gangway tip and pressure of telescopic cylinder in these two load cases are nearly the same since there is no external load applied at the tip in both load cases. The position error is  $[-0.007, 0.012]$  m and the ratio of motion compensation is about 98.1 %. In Z-axis, position errors of gangway tip and pressure of luffing cylinder in the two load cases are slightly different. The position error is  $[-0.048, 0.042]$  m in load case1 where no external load applied at gangway tip and the position error is  $[-0.048, 0.036]$  m in load case 2 where 300 kg live load is applied at gangway tip in minus Z-axis. The reason for this small difference is that the controller gains were tuned for the gangway transferring operation i.e. load case 2. The luffing cylinder pressure varied in the two load cases due to the different vertical load in Z-axis. But we can see that the difference is so small that can be neglected. The ratio of motion compensation in Z-axis is about 95.8 %. So such results confirms that the control algorithm for active motion compensation is



effective. And based on this, the parallel position and force controller will be developed in the following.

### 6.3 Parallel Positon and Force Control and Simulation

The main purpose of this section is to develop a controller to make the gangway tip push against the wind turbine platform with a constant setting force (4000 N) while compensate the ship motion during the transferring operation. To realize this purpose, a parallel force and position controller is proposed based on the classic force control methods of robotic manipulator. The principle of parallel position and force control method in robotics will be given first. Then the designed parallel force and position controller for gangway will be presented and finally the performance analysis of such controller is verified via simulation.

#### 6.3.1 Principle of Parallel Position and Force Control Algorithm

The force control strategies for robotics has been developed for many years and different control algorithms has been proposed as discussed Chiaverini and Sciavicco (1993). One of the widely used control method in industrial robotic systems is called admittance control. And we are going to derive the parallel position and force control method based on such control algorithm. The control strategy for force control is to control the force by controlling the positon of end-effector of manipulator. To illustrate this principle, consider the case where a spring is attached to the end-effector of robotic as shown in Fig. 6.8. The force exerted on the constraint surface will be the stiffness of the spring multiplied by the deflection of the spring. So the contact force can be controlled by controlling the position of end effector.

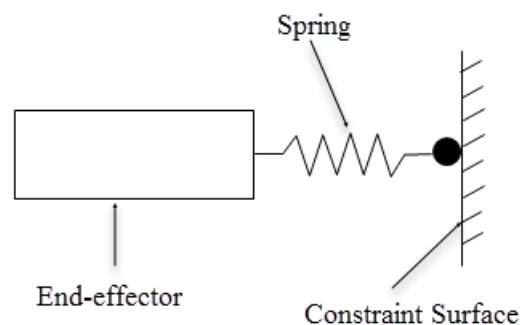


Fig. 6.8 Schematic for illustrating the concept for force control

In robotics, such controller is also called inner position loop and outer force loop controller. As proposed by Maples and Becker (1986), the general control structure of inner position loop and outer force control Cartesian based controller for robotic arms is given in the following Fig. 6.9.

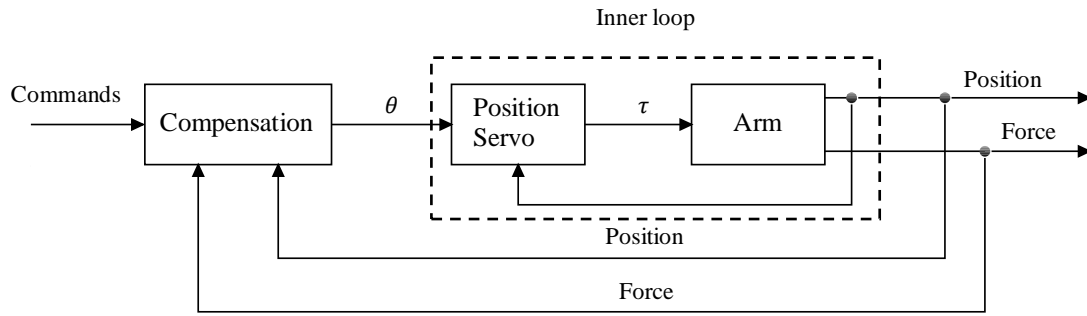


Fig. 6.9 Force servo with inner position loop

We can see that from Fig. 6.9, the principle of this controller is that the force signal is processed to become a position command to an inner position loop in order to achieve the desired contact force between end-effector of robotic arm the environment.

So based on this principle, we can develop the parallel force and position controller for gangway system during transferring operation in the next section.

### 6.3.2 Parallel Position and Force Controller Design

The proposed parallel force and position controller for our gangway system is based on the inner position loop outer force control approach described in section 6.3.1. For the gangway application, the goal is to control the contact force between gangway tip and wind turbine platform at desired value (4000 N) as well as keep the gangway tip still during the transferring operation. From section 6.2, we know that the gangway tip can be kept still with small error under the designed AMC controller. Actually, the AMC control is position control, so the idea to develop force controller is to add force controller to the designed AMC controller. Based on this idea, we propose a method that uses the force error term to modulate the desired gangway tip trajectory for active motion compensation. This approach is similar to the inner position loop outer force control approaches used in industrial manipulators Maples and Becker (1986). Fig. 6.10 presents the Structure of parallel position and force control algorithm for AMC gangway.

From figure Fig. 6.10 , we can see that the only difference of this controller from active motion compensation controller is that a position offset to achieve the desired force is added to the desired gangway tip position. And we know that once the gangway is in contact with windmill platform, the signal from joystick or keyboard will be zero. Recall equation 6.1 and 6.2, the desired trajectory of gangway tip is given based on ship motion and the command from force modulator as below

$$P_{tipd} = P_{tipd,AMC} + \begin{bmatrix} X_f \\ 0 \\ 0 \end{bmatrix} = P_{tipr} - P_{ship} + \begin{bmatrix} X_{tipf} \\ 0 \\ 0 \end{bmatrix} \quad (6.6)$$

$$V_{tipd} = V_{tipd,AMC} + \begin{bmatrix} \dot{X}_f \\ 0 \\ 0 \end{bmatrix} = -V_{ship} + \begin{bmatrix} \dot{X}_{tipf} \\ 0 \\ 0 \end{bmatrix} \quad (6.7)$$

Where  $P_{tipd}$  and  $V_{tipd}$  are the desired gangway tip position in gangway base frame  $\{0\}$ ,  $P_{tipr}$  is the recorded gangway tip position expressed in gangway base frame  $\{0\}$  when the motion compensation functions is switched on,  $P_{tipd,AMC}$  and  $V_{tipd,AMC}$  are the desired gangway tip trajectory for active motion compensation,  $P_{ship}$  and  $V_{ship}$  is the ship motion position function and velocity function in frame  $\{w\}$  and  $X_f$  is the position offset to maintain the desired force in X-axis of world frame  $\{w\}$ .

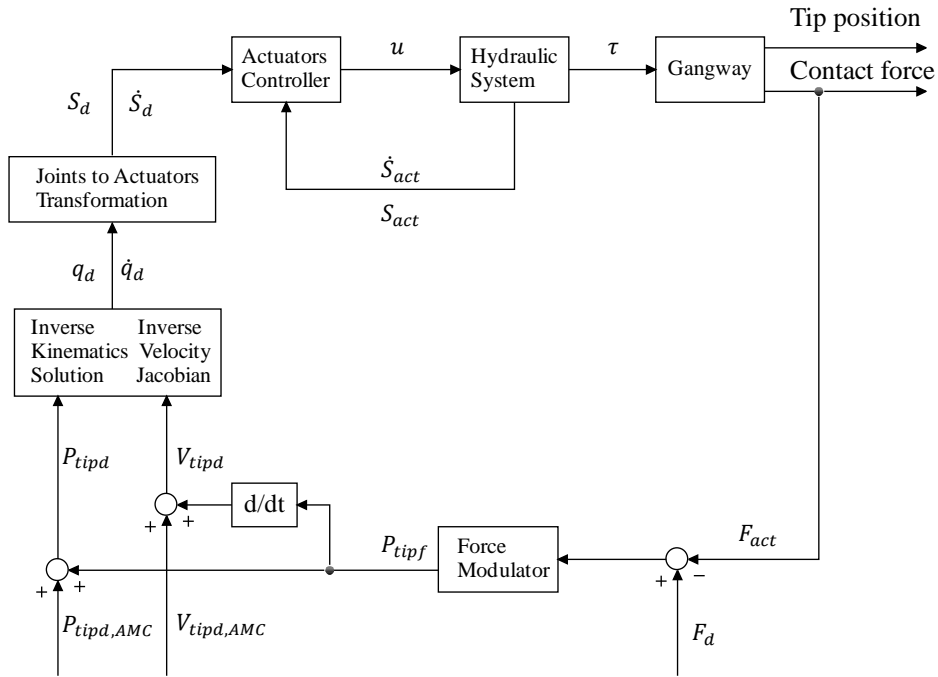


Fig. 6.10 Structure of parallel position and force control algorithm for gangway system

To maintain the contact force at desired level, a PI controller is necessary for force modulator.

So the function of force modulator can be given below

$$X_f = \frac{F_d}{K_{bumper}} + K_f(F_d - F_{act}) + K_{fi} \int (F_d - F_{act}) dt \quad (6.8)$$

Where  $F_d$  and  $F_{act}$  is the desired force and actual force exerted on platform by gangway,  $K_{bumper}$  is the approximate stiffness of the rubber bumper,  $K_f$  and  $K_{fi}$  are the controller gains.



To perform the simulation, the initial state of gangway and the ship motion profile is the same as that in section 6.2.3. We also assume the gangway tip and windmill platform are in contact in the initial and the coordinate of gangway tip, and windmill platform in world frame  $\{w\}$ , and the desired contact force and controller gains and rubber bumper stiffness are given as below

- Gangway tip :  $[9.30; 0; 1.82]m$
- Windmill platform:  $[9.29; 0; 1.82]m$
- Desired contact force: 4000 N (suggested by supervisor)
- $K_{bumper} = 10^6 N/m$ ,  $K_f = 10^{-7}$  and  $K_{fi} = 10^{-4}$

In order to verify the effectiveness of the force controller, a comparison study between the active motion controller and parallel position and force controller is made. And the simulation results regarding the gangway tip position and contact force and cylinder pressure under these two control methods are present as below.

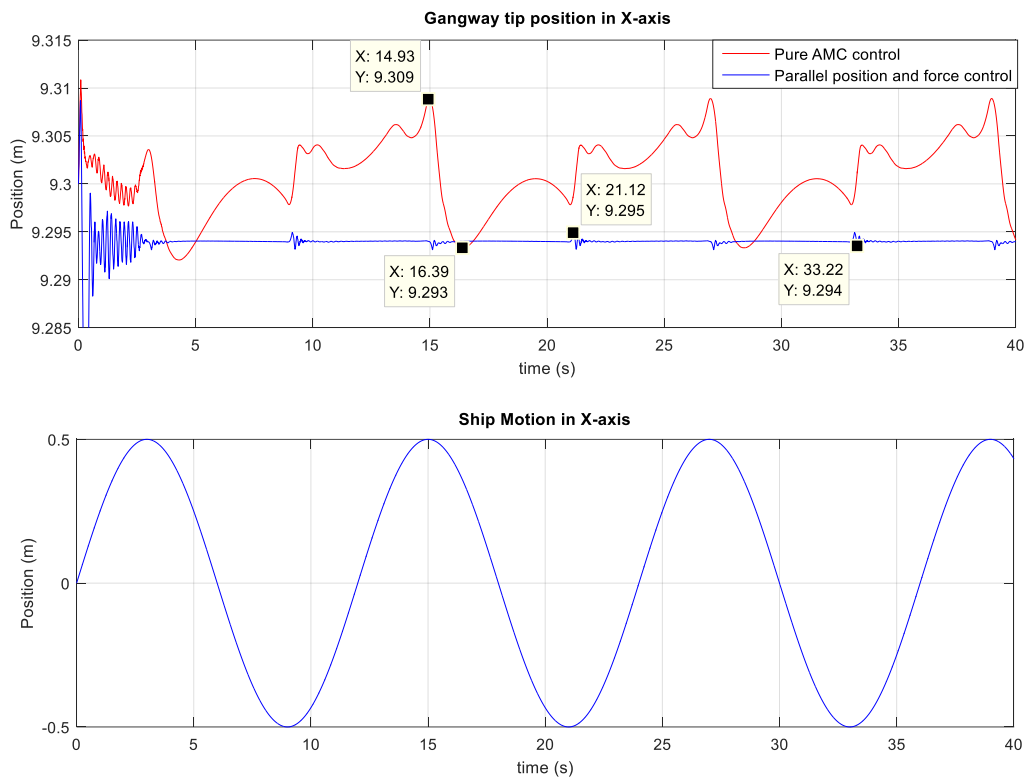


Fig. 6.12 Gangway tip position Vs ship motion in X-axis under two control algorithms

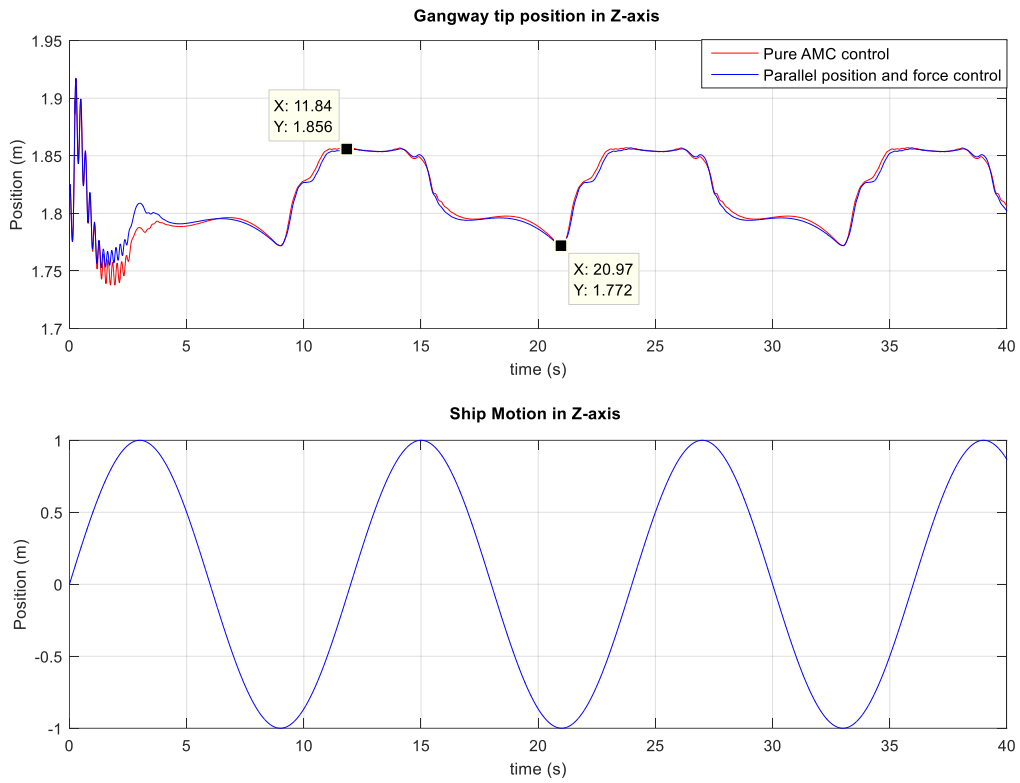


Fig. 6.13 Gangway tip position Vs ship motion in Z-axis under two control algorithms

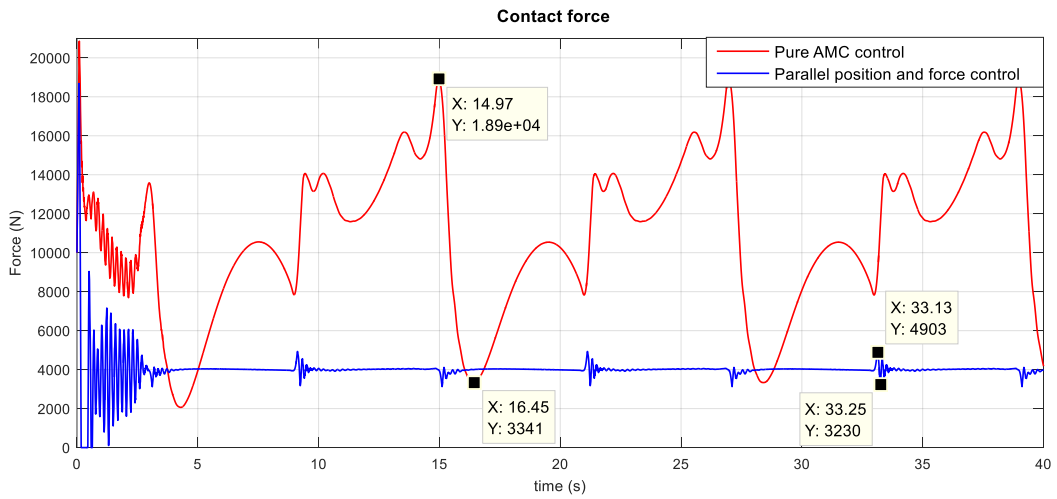


Fig.6.14 Contact force under two control algorithms in X-axis

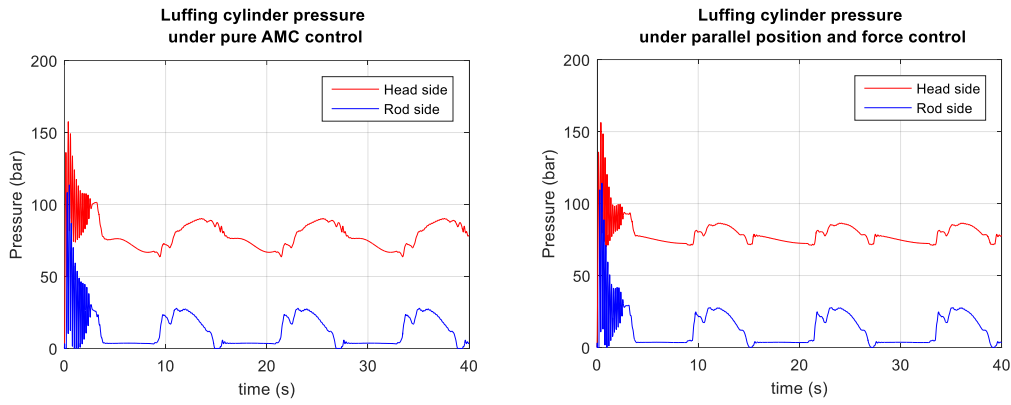


Fig. 6.15 Luffing cylinder pressure under two control methods

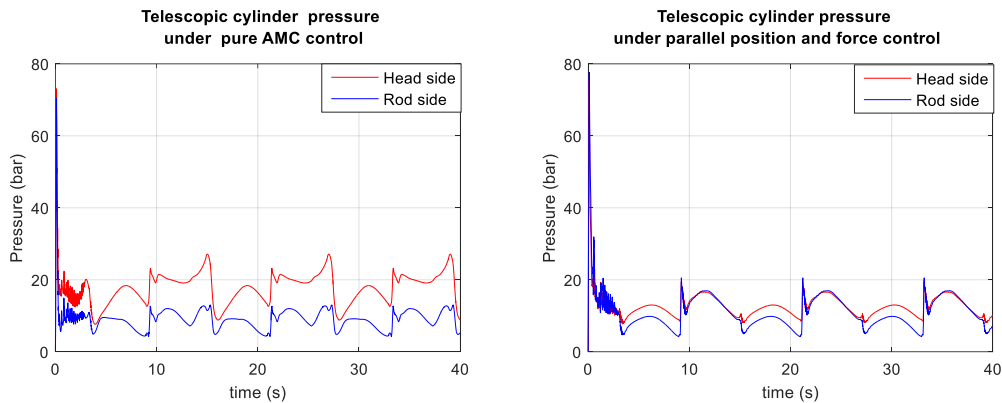


Fig. 6.16 Telescopic cylinder pressure under two control methods

From above figures, we can see that when the gangway is only under AMC controller, the position error from initial values are  $[-0.007, 0.009]$  m in X-axis and  $[-0.048, 0.036]$  m in Z-axis. Consequently, due to these small position errors, the contact force when the gangway is connected to the wind turbine varies between  $[3341, 18900]$  N in X-axis. In contrast, under parallel position and force controller, the gangway tip position is stabilized at around the desired value within  $[-0.001, 0.001]$  m in X-axis and  $[-0.048, 0.036]$  m in Z-axis. The contact force between the gangway tip and the platform is stabilized at  $[3230, 4903]$  N. These cyclic oscillations of gangway tip position and contact force in X-axis under parallel position and force control are mainly due to the DCV transition across the dead band and the fluid dynamics between the DCV and the cylinder. The pressure characteristics of luffing cylinder under both controllers are nearly the same since no force controller in Z-axis and for the pressure characteristics of telescopic cylinder under both cases, the pressure change is much less using the parallel control algorithm. These results confirms that the designed parallel position and force controller for gangway transferring operation is effective.

## 6.4 Summery

In this chapter, two controller were designed for offshore gangway operation. One is the controller for active motion compensation and another is for controlling the contact force as well as compensating the ship motion during transferring operation.

The designed active motion compensation controller is based on the principle of solving the inverse kinematics and inverse Jacobian of gangway to make the gangway tip move in the counter direction of ship motion and thus keep the gangway tip still at the desired position. The desired gangway tip position and velocity for compensating the ship motion were mapped to the desired actuator position and velocity through kinematic relations and then the actuators were controlled by position and velocity feedback with velocity feedforward controller to actuate the gangway tip to the desired position. The advantages of such controller are that the feedforward term minimize the control effort generated by the feedback error signal and make the system response very quick and the feedback PD controller is used to reject the position and velocity error. Based on the simulation results with two different loads applied at gangway tip under active motion compensation control, we know that the ship motion in X-axis ( $[-0.5,0.5] m$ ) can be compensated up to 98 % and ship motion in Z-axis ( $[-1,1]m$ ) can be compensated up to 95 %. Such results confirms that the AMC controller is robust and effective.

The designed parallel position and force controller for controlling the contact force and compensating ship motion was based on the principle of inner position loop outer force control approach in robotics. The force is controlled by adjusting the desired gangway tip trajectory to achieve the desired contact force. To achieve this goal, we propose a method that uses the force error term to modulate the desired gangway tip trajectory for active motion compensation. To maintain the contact force at desired level, the force modulator consists of a feedforward term and a PI controller. The feedforward term is used to make the controller response quickly and PI controller is used to stabilize the system and reject disturbance. The effectiveness of this controller was verified by comparison the contact force and gangway tip position under pure AMC controller and parallel position and force controller. The simulation results shows that the contact force can be maintained at the setting values ( $4000 N$ ) with acceptable error ( $[-770,903]N$ ) and the gangway tip position is maintained still with smaller error under parallel position and force controller. Considering the high contact stiffness ( $10^6 N/m$ ), this result is acceptable. So we can say the designed controller is feasible for our application.



## 7 Conclusions and Future Work

### 7.1 Conclusions

The focus of this thesis was to develop the integrated model of offshore gangway model including multi-body dynamics model and hydraulic system model. And based on that model, active motion compensation control approach was developed in order to compensate the ship motion during gangway operation and further more a parallel position and force control method was proposed to make the gangway tip maintain constant contact force with windmill platform as well as compensate ship motion during transferring process.

As start to the gangway model, we initially designed the offshore gangway based on relative rules (DNVGL-ST-0358 2015) and existing products from Uptime company (UPTIME-Brochure) and verified with finite element analysis using NX software. Then we derived the equations of motion in traditional Euler-Lagrange method and rewritten it into Hamiltonian form. And the multi-body dynamics model was built in 20-sim software with IC-field based on the derived equations of motion.

We then designed the hydraulic system for gangway based on the specific operational requirements and relative parameters of hydraulic components are calculated and discussed. The modeling method with bond graph of each hydraulic components were explained and an complete hydraulic system model with multi-body dynamics model of gangway was developed and verified with the operational requirements and designed parameters.

Further, based on the developed model of gangway system, the active motion compensation control algorithm was developed. The idea is to make the gangway tip to track the opposite trajectory of ship motion, which can be obtained from MRU. This was done by mapping the desired gangway tip position and velocity to actuator position and velocity via the derived kinematic mapping relations. Then the actuators were controlled by proportional-derivative controller with velocity feedforward. Under such control method, the simulation results showed that the gangway tip was maintained still with small acceptable error with disturbance from ship motion.

At last, the parallel position and force controller was proposed in order to make the gangway tip contact with the windmill platform with constant force as well as compensate the ship motion. This controller is based on the active motion compensation controller. The idea is to adjust the desired gangway tip trajectory by the force modulator to achieve the desired contact force. And the force modulator is a PI controller with a feedforward term. Under such controller, the

simulation results showed that the gangway tip was maintained still with even smaller error than that of pure active motion compensation controller. And the contact force was maintained at the desired level with acceptable error.

## **7.2 Future Work**

In this section, we provides the recommendation of future work for the interested readers to further optimize and improve the work in this thesis.

- Include the friction and flexibility model of gangway into the multi-body dynamic model
- More detailed modeling of each hydraulic components
- Develop advanced control algorithms to compensate the deadband of directional control valve
- Connect the gangway model with ship model and analysis the interact dynamics

## 8 Bibliography

- Bak, M. K. and M. R. Hansen (2013). "Model Based Design Optimization of Operational Reliability in Offshore Boom Cranes." International Journal of Fluid Power **14**(3): 53-65.
- Cerda Salzmann, D. J. (2010). Ampelmann: Development of the Access System for Offshore Wind Turbines, TU Delft, Delft University of Technology.
- Chiaverini, S. and L. Sciavicco (1993). "The parallel approach to force/position control of robotic manipulators." IEEE Transactions on Robotics and Automation **9**(4): 361-373.
- Chu, Y., V. Aesøy, H. Zhang and O. Bunes (2014). Modelling And Simulation Of An Offshore Hydraulic Crane. ECMS.
- Craig, J. J. (2005). Introduction to robotics : mechanics and control. Upper Saddle River, N.J, Pearson Prentice Hall.
- DNVGL-ST-0358 (2015). certification of offshore gangways for personnel transfer.
- Fatemi, S. A., V. J. Majd and M. R. Ebrahimpour (2012). Parallel force and position control with the aid of variable impedance model in robot manipulators. Electrical Engineering (ICEE), 2012 20th Iranian Conference on, IEEE.
- Karnopp, D. C., D. L. Margolis and R. C. Rosenberg (2012). System Dynamics : Modeling, Simulation, and Control of Mechatronic Systems. Chichester, Wiley.
- Kesner, S. B. and R. D. Howe (2011). Force control of flexible catheter robots for beating heart surgery. Robotics and Automation (ICRA), 2011 IEEE International Conference on, IEEE.
- Kjelland, M. B. and M. R. Hansen (2015). "Offshore Wind Payload Transfer Using Flexible Mobile Crane." Modeling, Identification and Control **36**(1): 1.
- Kontz, M. E. (2007). Haptic control of hydraulic machinery using proportional valves, Georgia Institute of Technology.
- Li, Y. (2016). Component-based Modelling and Simulation for Marine Crane System Design.
- Maples, J. and J. Becker (1986). Experiments in force control of robotic manipulators. Robotics and Automation. Proceedings. 1986 IEEE International Conference on, IEEE.
- Pedersen, E. and H. Engja (2014). Mathematical modelling and simulation of physical systems : lecture notes in course TMR4275 modelling, simulation and analysis of dynamic systems. Trondheim, Department of Marine Technology. Norwegian University of Science and Technology.
- Rokseth, B. (2014). A bond graph approach for modelling systems of rigid bodies in spatial motion, Institutt for marin teknikk.

- Salen, I. M. (2016). Apparatus and method for providing active motion compensation control of an articulated gangway, Google Patents.
- Sanders, R. (2016). "Modelling and simulation of traditional hydraulic heave compensation systems."
- Sciavicco, L. (2000). Modelling and control of robot manipulators. B. Siciliano and SpringerLink, Springer London : Imprint: Springer.
- Skaare, B. and O. Egeland (2006). "Parallel force/position crane control in marine operations." IEEE Journal of Oceanic Engineering **31**(3): 599-613.
- Spong, M. W. (2006). Robot modeling and control. Hoboken, N.J, Wiley.
- Su, H.-J., B.-O. Choi and K. Krishnamurthy (1990). "Force control of high-speed, lightweight robotic manipulators." Mathematical and Computer Modelling **14**: 474-479.
- Subramanian, K. "Design of a lightweight FRP T-boom for an offshore gangway, and development of a fatigue model for prediction of its service life."
- UPTIME-Brochure. from <http://www.uptime.no/wp-content/uploads/brochure-a41.pdf>.
- Wijnheijmer, F. (2009). Active Tension Control For Heave Compensation Systems. Offshore Mediterranean Conference and Exhibition, Offshore Mediterranean Conference.
- WindEUROPE (2017). The European offshore wind industry - key trends and statistics 2016 | WindEurope, WindEUROPE.
- Zhang, H. (2015). Lecture Notes in IP501508 Mechatronics, Robots and Deck Machines.
- Zhang, W. (2015). Dynamic Modelling, Simulation and Visualization of Marine Crane Operations on DP Vessels.

## 9 Appendix

### Appendix A Strength Analysis of Designed Gangway

#### A.1 Definition of Load Cases

The gangway is designed to be operated against the platform or in cantilever position. And due to the lack of knowledge of environment, the effect of environment is not considered during the calculation in this thesis. So based on this the load cases is defined as below

- Normal operation for people transfer in cantilever position (NO-PT-C)  
In this case, the gangway is operated horizontally with maximum extension and the designed live load is 300 kg at the gangway tip and external horizontal reaction force 10 KN is applied at the gangway tip
- Normal operation for people transfer with luffing boom inclined -15 degree (NO-PT-I)  
In this case, the gangway is operated in the worst case where the luffing boom is operated at -15 degree with maximum extension of gangway. The designed live load is 300 kg at the gangway tip and external horizontal reaction force 10 KN is applied at the gangway tip
- Emergency Operation (EO)  
In this case, the gangway is operated horizontally with maximum extension. The designed live load is 350 kg at the gangway tip

The following Table 9.1 summarizes the load cases as defined above.

Table 9.1 Load cases for gangway design

Load case	NO-PT-C	NO-PT-I	EO
LL at tip (kg)	300	300	350
Acceleration (Z axis) $m/s^2$	-0.274	-0.274	-0.274
Contact force (X axis) KN	-10	-10	0
Dynamic factor ( Z axis)	1.1	1.1	1.1

## A.2 Strength and Deflection Requirements

According to DNVGL-ST-0358 (2015), the strength requirement and deflection requirement are given below.

Table 9.2 Permissible Stress for materials used in gangway design

Material	Yield Strength (Mpa)	Safety Factor	Permissible Stress(Mpa)
Steel_S355J2G3	355	1.5	237
Aluminum_Al5086	217	1.5	145

Table 9.3 Allowed deflection of designed gangway

Gangway Type	Maximum Extension Length (mm)	Allowed Maximum Defection at Tip (mm)
Cantilever Gangway	$L$	$\frac{L}{100}$
	10800	108

## A.3 Finite Element Analysis

In this thesis, only global analysis is performed in order to check the strength of gangway under different load cases. We assume the pedestal is strong enough, so for simplification, the stair and pedestal are not included in our model. And a fixed constrain will be applied at the support area of the bottom of slewing king.

For the connection between luffing boom and slewing king, we simulate the connection with RBE2 elements and CBAR elements in the FEA model, which can provide the relative rotation movements during FEA analysis. The cylinders are assumed strong enough and they are modelled as RBE2 elements. The connections between slewing king, cylinder and luffing boom is made with same mechanism as the connection between slewing king and luffing boom. For all the connection between aluminum parts and steel parts made by bolts in our model, they are simulated with RBE2 connection as well. We know that the telescopic boom slides inside the luffing boom, so it will be supported by the luffing boom during FEA analysis. And these connections are made by RBE2 elements too. Because we assume the cylinder is strong enough, so the telescopic cylinder will not be included in the FEA model for the load cases analysis.

And because the plate thickness of gangway is quite small compared to other dimensions, so the whole mesh of gangway is made by shell elements and it will save a lot of time for finite element analysis calculation.

The following Fig. 9.1 shows the details of mesh model of gangway as mentioned above

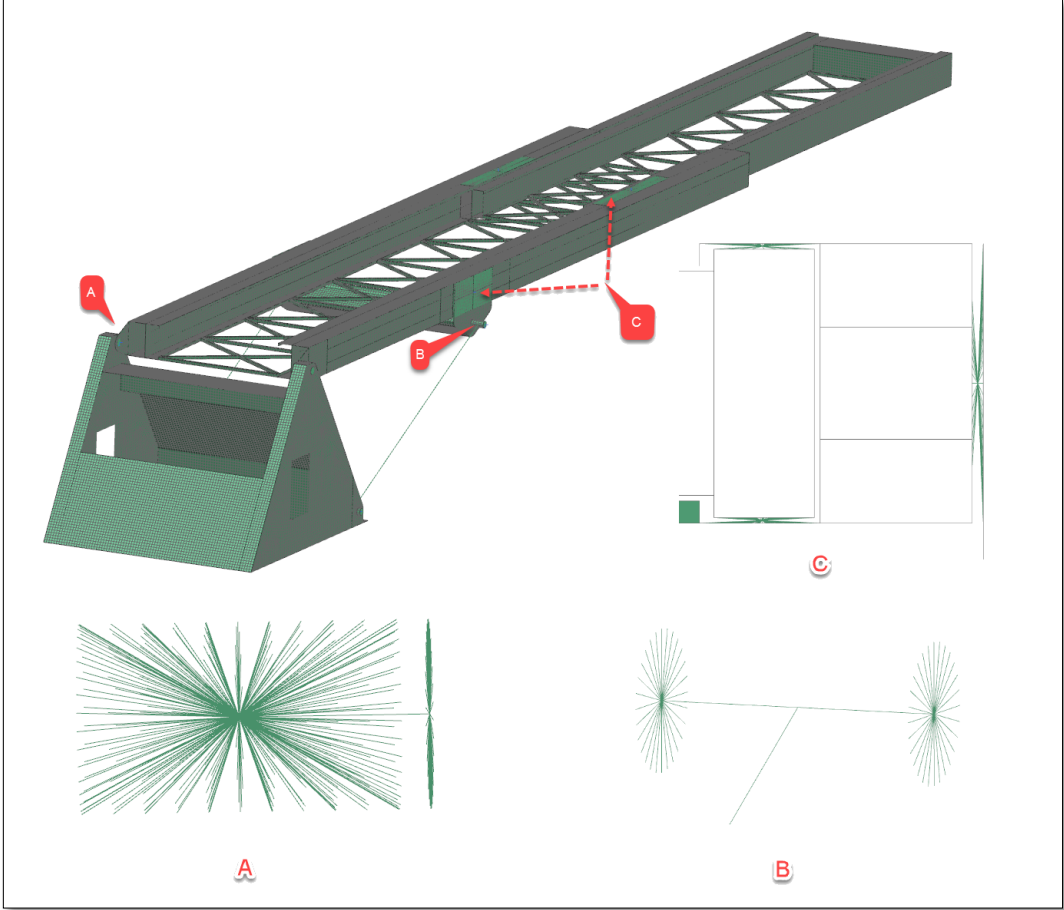


Fig. 9.1 Mesh model of gangway structure

Since the gangway is made of two different materials, so the stress analysis result will be presented for the whole structure first to see whether it can meet the steel permissible stress requirements. And then if the stress higher than aluminum stress requirement, the steel parts will be removed to check whether the aluminum part will fulfill the aluminum stress requirements. Finally, the deflection results will be presented.

The results for these three load cases are presented as below in the following sequence. The FEA analysis models named “FEA Model of Gangway” were enclosed in attached CD.

Load case: NO-PT-C

Load case: NO-PT-I

Load case: EO

## Load case: NO-PT-C

### Constraints and load set up

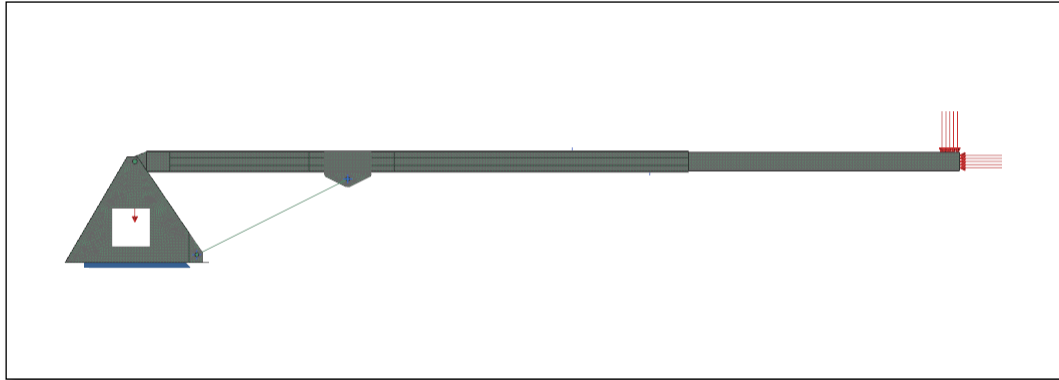


Fig. 9.2 Constraints and load set up for load case NO-PT-C

### Stress for overall structure including steel and aluminum parts

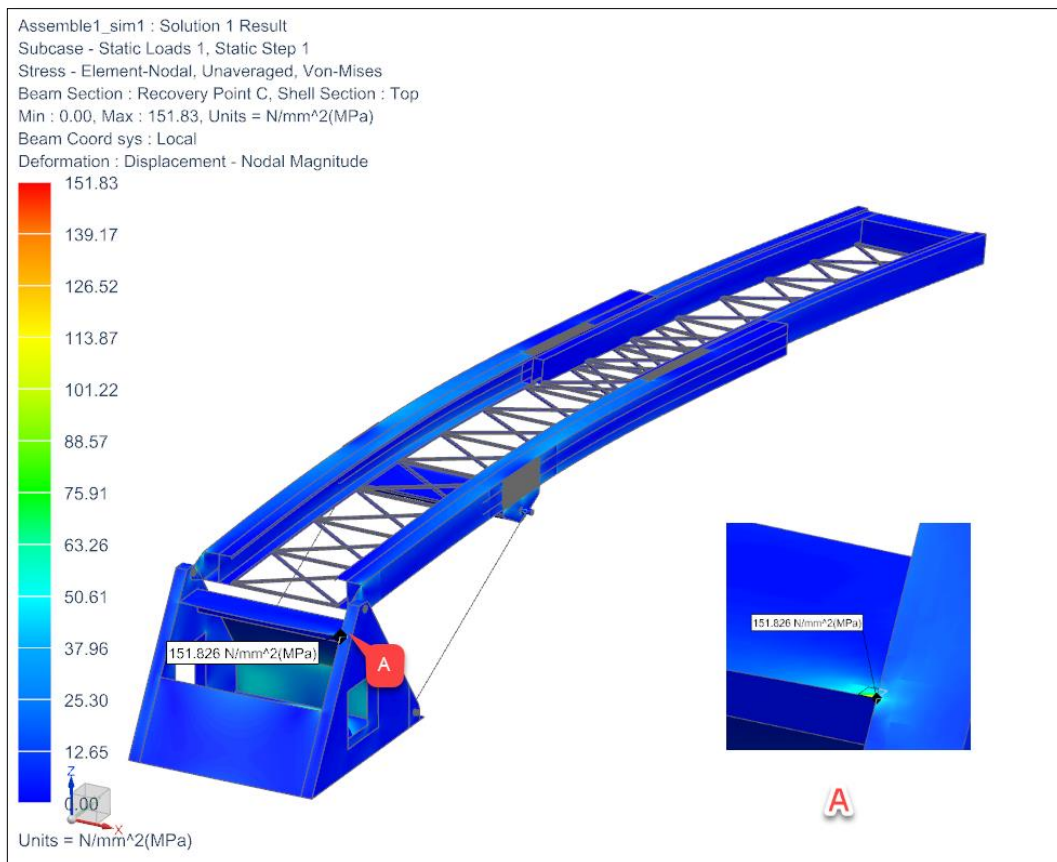


Fig. 9.3 Stress of overall structure of gangway under load case NO-PT-C



Stress for aluminum parts

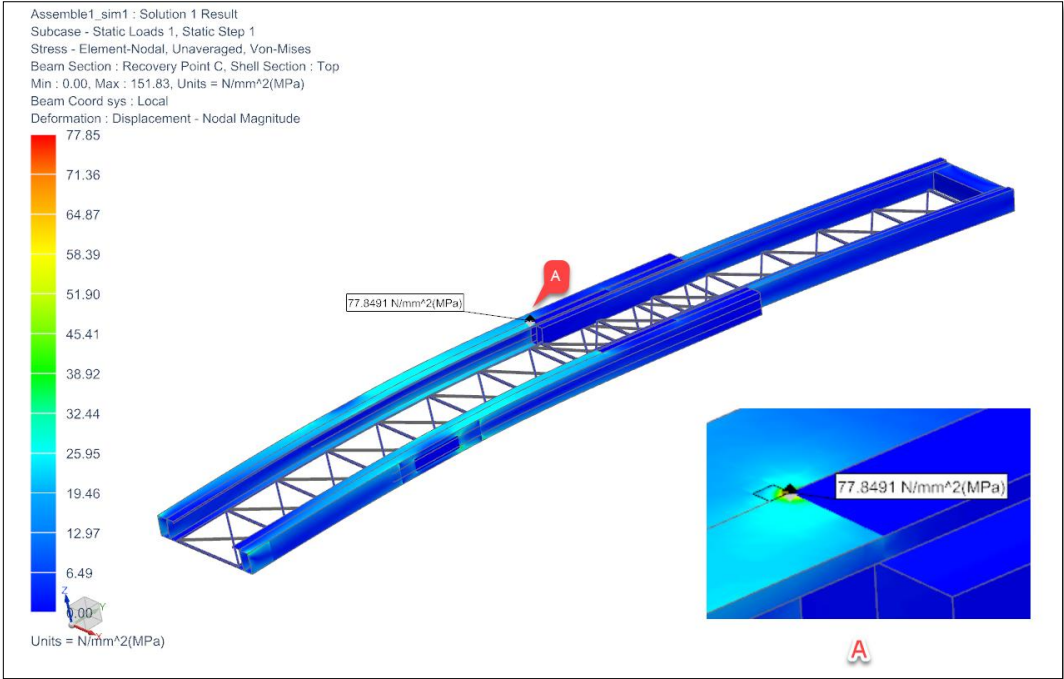


Fig. 9.4 Stress for aluminum parts of gangway under load case NO-PT-C

Deflection of overall structure

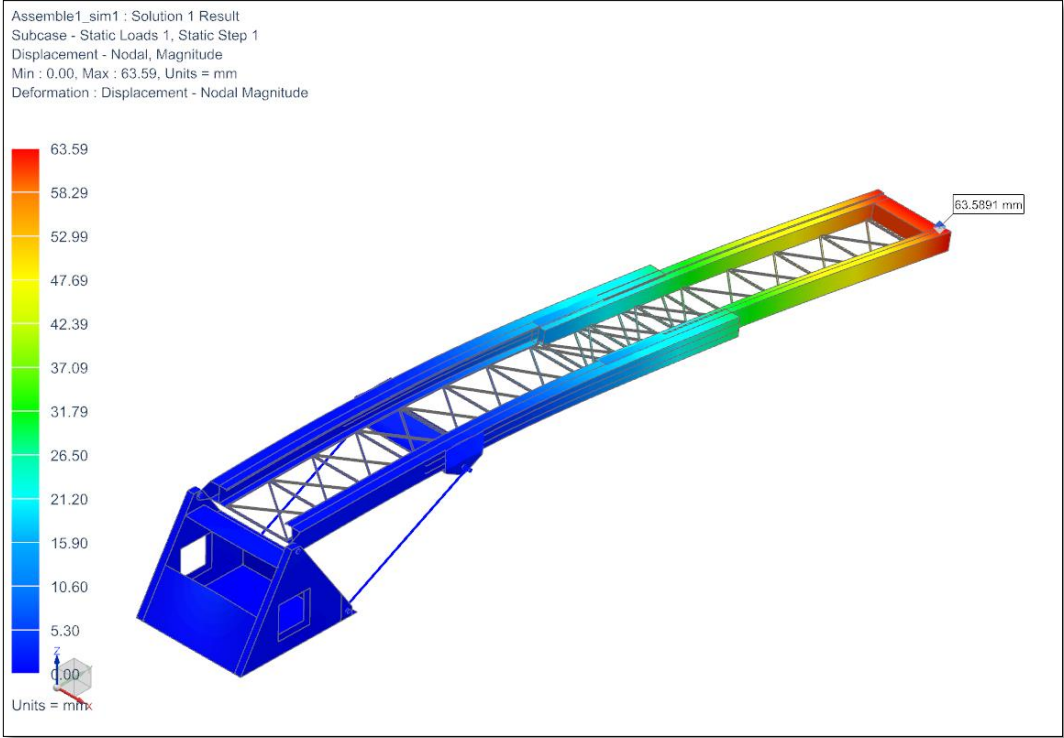


Fig. 9.5 Deflection of gangway under load case NO-PT-C

## Load case: NO-PT-I

### Constraints and load set up

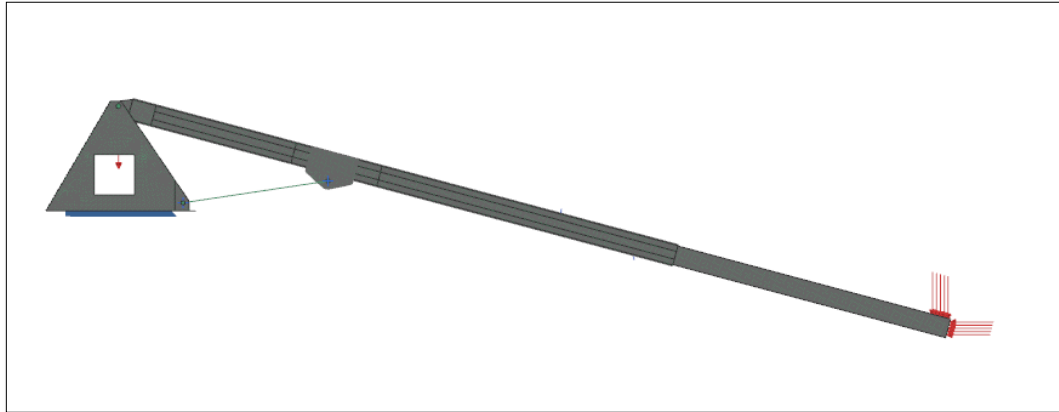


Fig. 9.6 Constraints and load set up for load case NO-PT-I

### Stress for overall structure including steel and aluminum parts

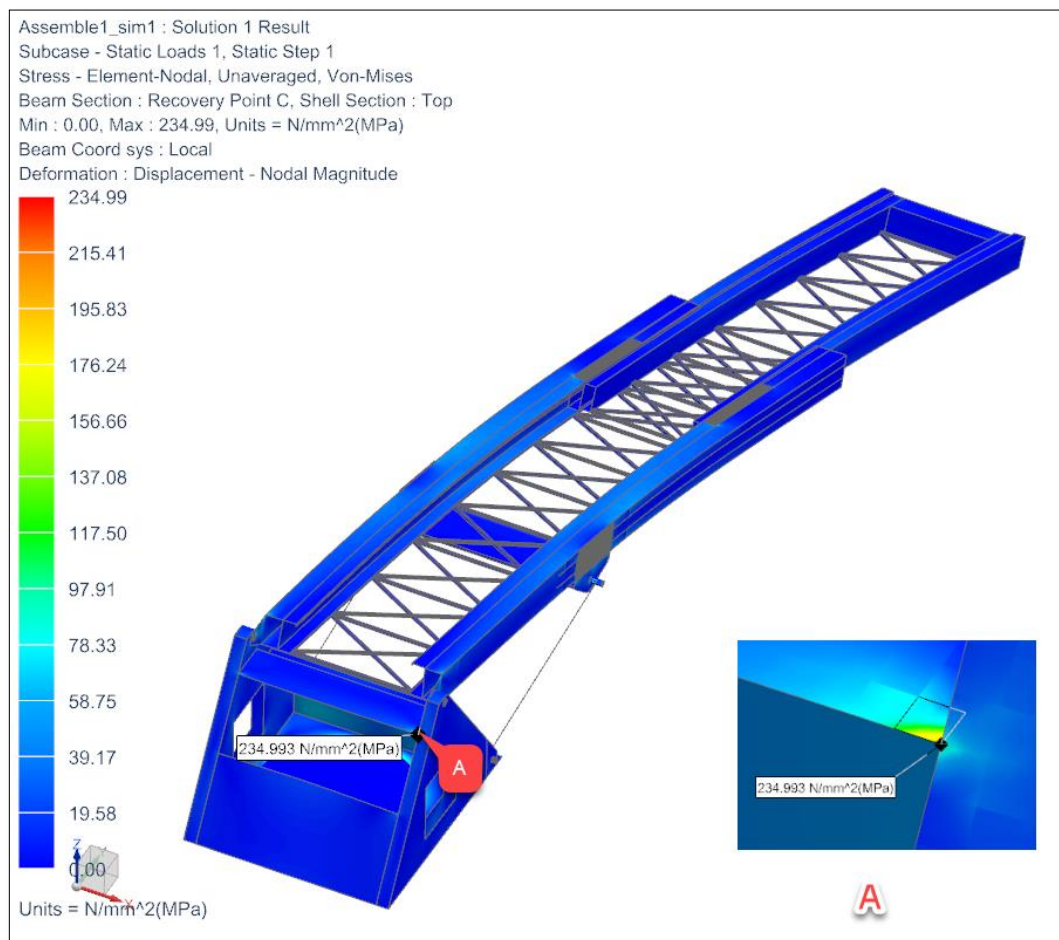


Fig. 9.7 Stress of overall structure of ganway under load case NO-PT-I

## Stress for aluminum parts

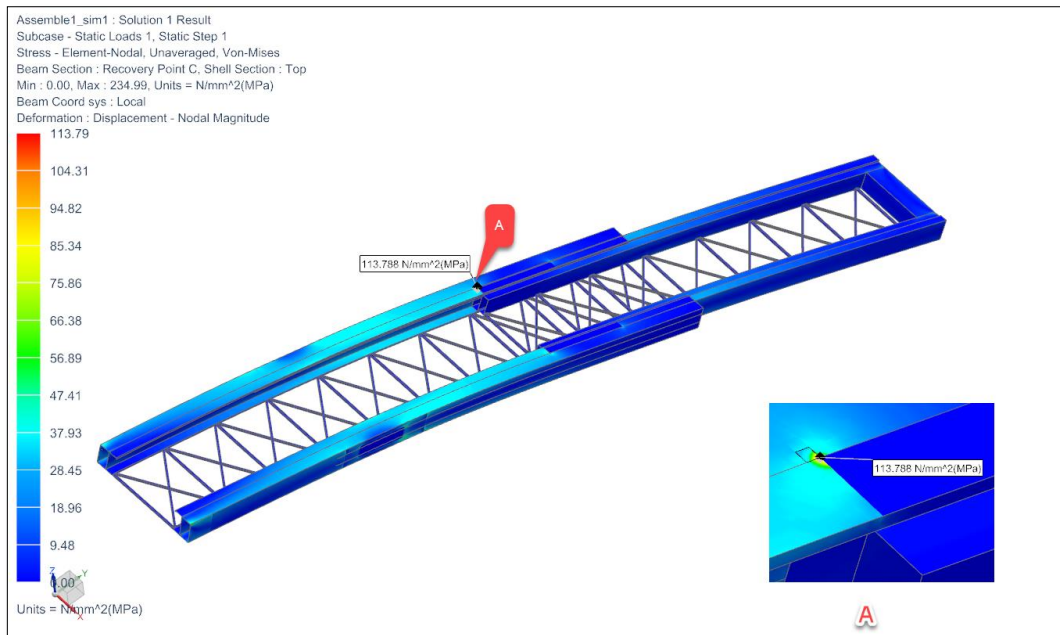


Fig. 9.8 Stress of aluminum parts of gangway under load case NO-PT-I

## Deflection of overall structure

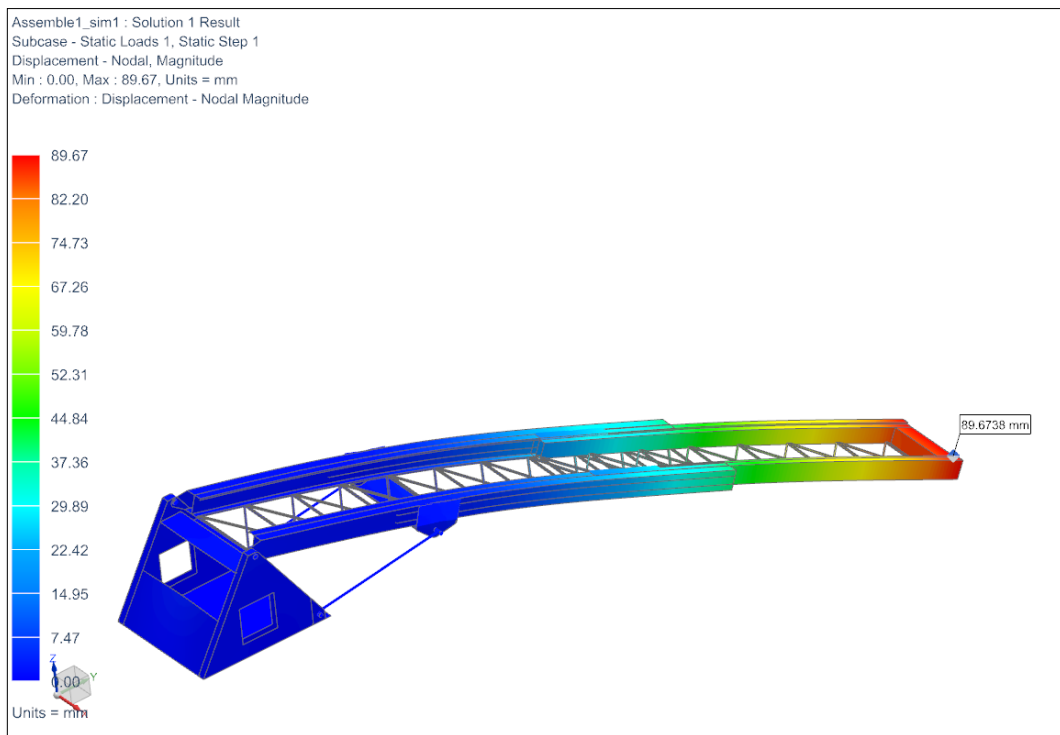


Fig. 9.9 Deflection of gangway under load case NO-PT-I

### Load case: EO

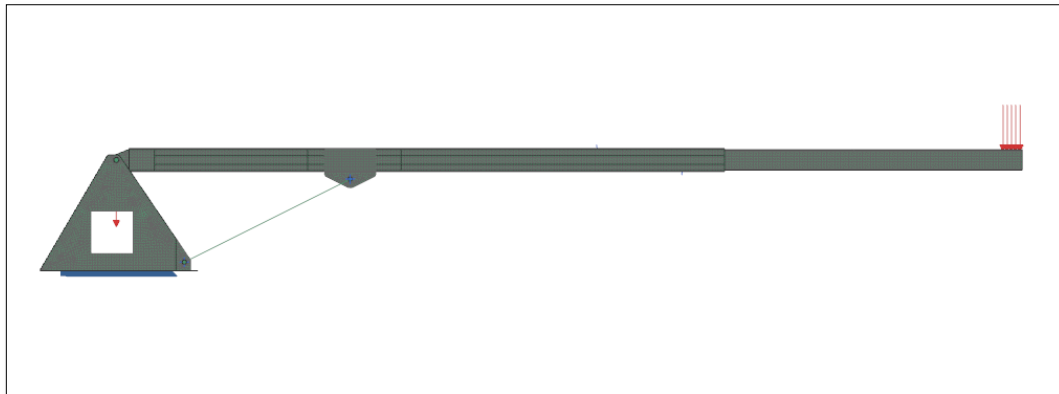


Fig. 9.10 Constraints and load set up for load case EO

### Stress for overall structure including steel and aluminum parts

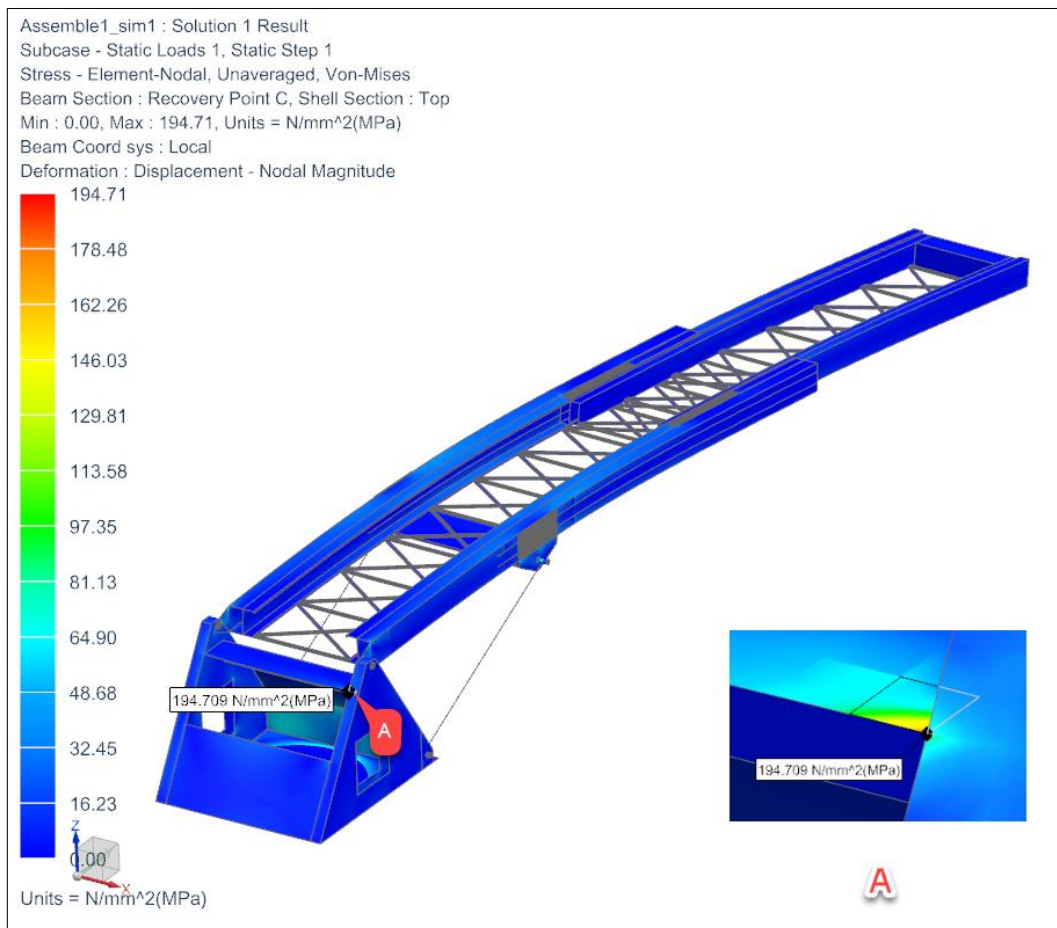


Fig. 9.11 Stress of overall structure of gantry under load case EO

## Stress for aluminum parts

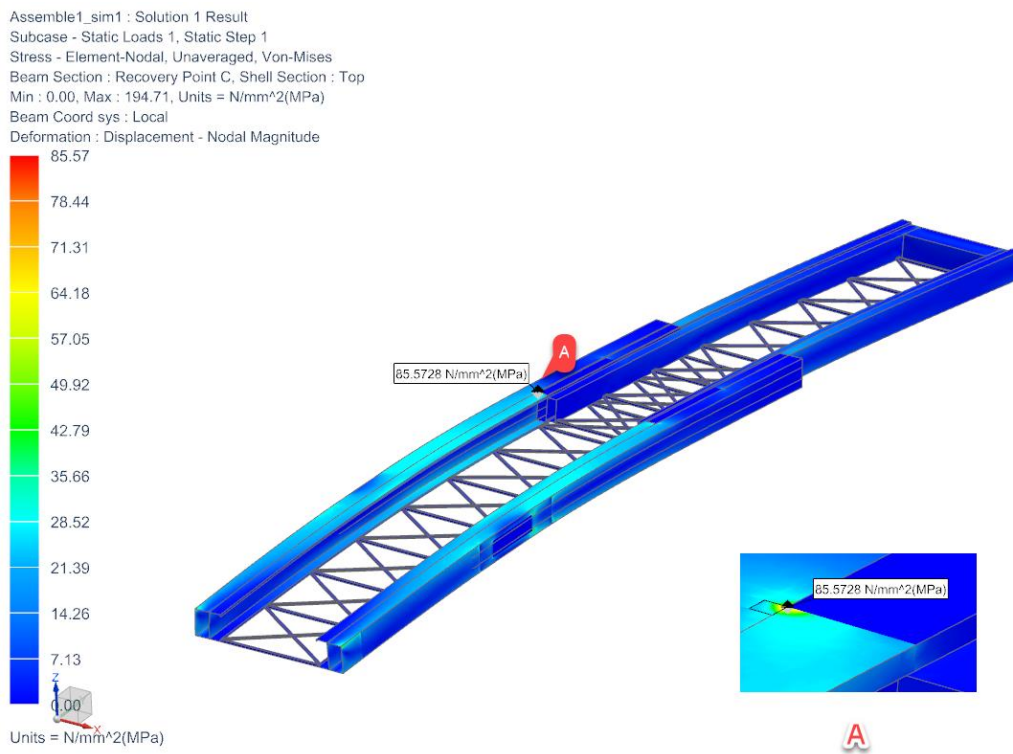


Fig. 9.12 Stress of aluminum parts of gangway under load case EO

## Deflection of overall structure

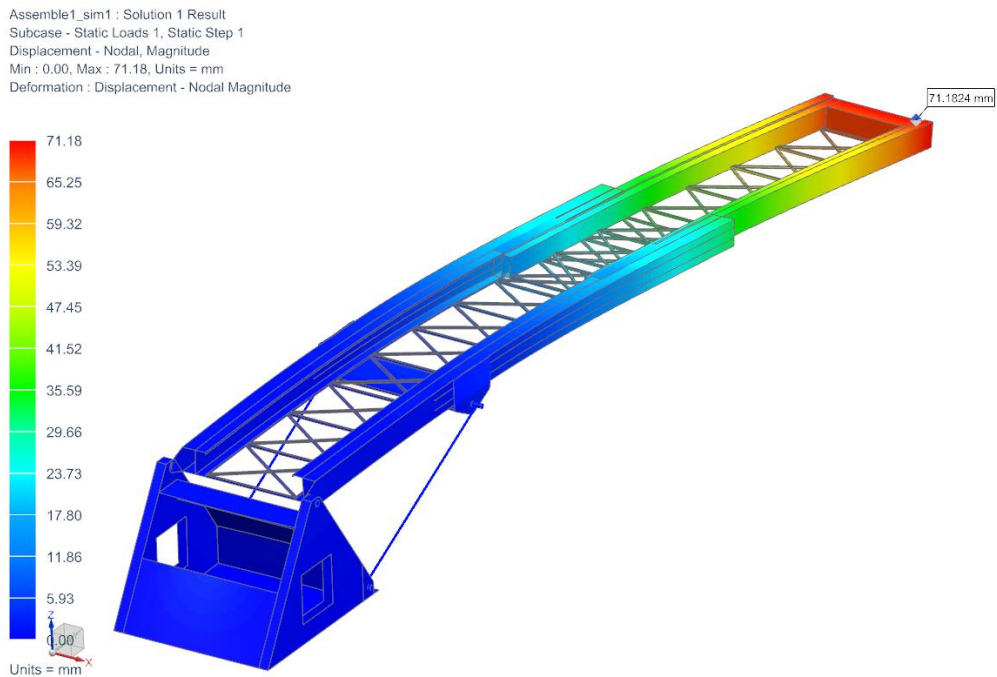


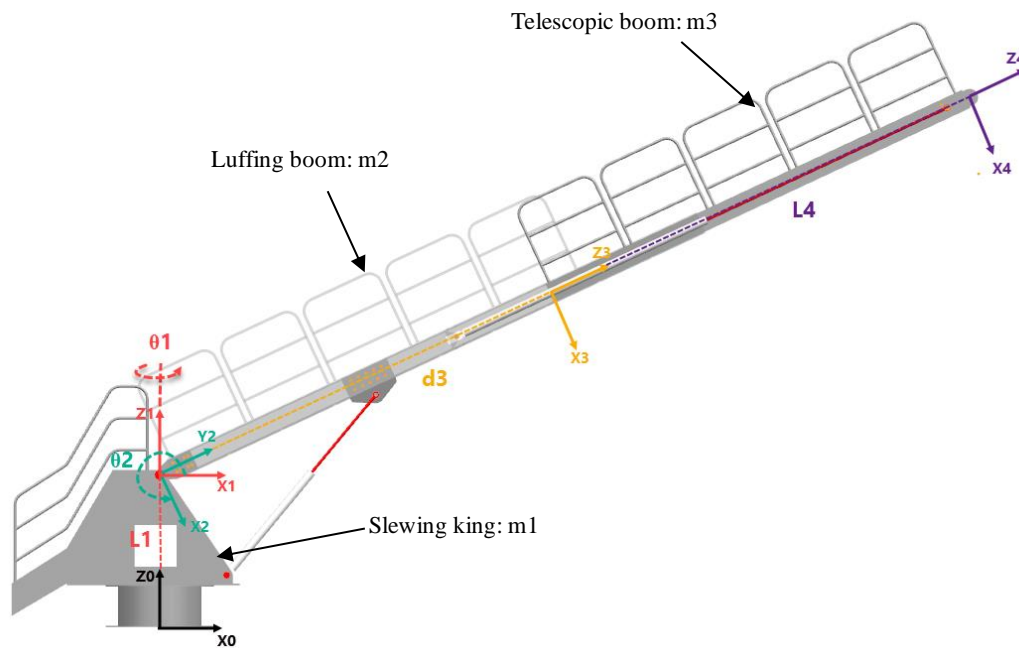
Fig. 9.13 Deflection of gangway under load case EO

#### **A.4 Result Discussions**

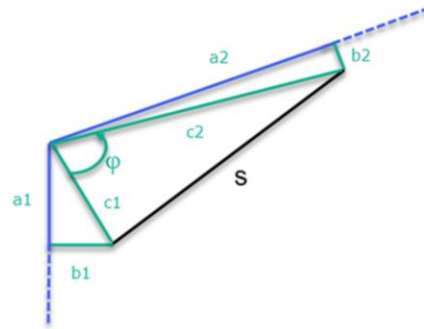
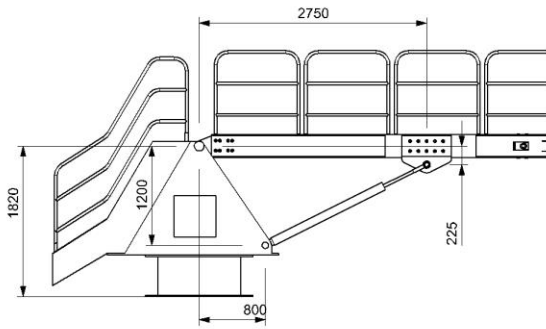
From above gangway design analysis, we can see that the designed gangway can meet the designed requirements very well in terms of strength and deflection. The stress concentration in our analysis is mainly due to sharp edge or because the use of RBE2 element, it will not affect the strength of the overall structure. Because the focus of this thesis is not about detail mechanical design of gangway, so only global strength analysis is carried out. So more local analyses about different joints should be carried out in the future in order to optimization the overall structure. And fatigue analysis and bucking analysis should be checked in the future as well.



## Appendix B Parameters of Gangway for Kinematic and Dynamic Calculation



Parameters	Value (Unit)
Minimum total length of gangway $L_{min}$	7.8 (m)
Length of $L1$	1.82 (m)
Length of telescopic boom $L4$	5.65 (m)
Mass of slewing king $m1$	864.5 (kg)
Mass of luffing boom $m2$	532.2 (kg)
Mass of telescopic boom $m3$	321.2 (kg)
COG of slewing king in frame {1}	[0; 0; -1.07] (m)
COG of luffing boom in frame {2}	[0; 3.48; 0](m)
COG of telescopic boom in frame{3}	[0; 0; 2.90](m)
Principal moments of inertia of slewing king in frame{1}	[421;331;524]( kgm <sup>2</sup> )
Principal moments of inertia of luffing boom in frame {2}	[2170;212;1973]( kgm <sup>2</sup> )
Principal moments of inertia of telescopic boom in frame {3}	[958;888;75](kgm <sup>2</sup> )

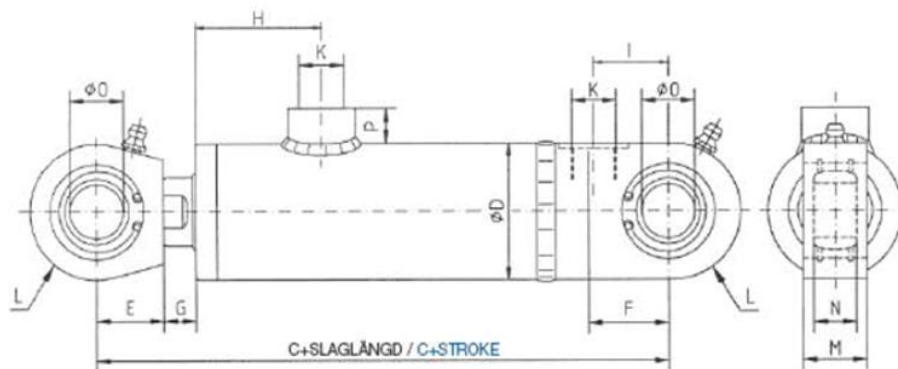


Luffing Cylinder Geometry Parameters	Value (Unit)
a1	1.2 (m)
b1	0.8(m)
a2	2.75(m)
b2	0.225(m)



## Appendix C Technical Sheets for Selected Hydraulic Components

### C.1 Selected Luffing Cylinder



Model-No.  
25ca-65/35-1/85  
Type  
Cylinder 25CA

Product Attribute	Value
Bore $\varnothing$	65
Rod $\varnothing$	35
Stroke	1
Position	0
Accessories	No accessories
Material	Chrome plated
Connection turned 90°	No

Part number	Description	Bore $\varnothing$	Rod $\varnothing$	C	D	E	F	G	H	I	K	L	M	N	O	P	Pusharea cm <sup>2</sup>	Pullarea cm <sup>2</sup>	Weight 0 stroke/100mm
25CA-40/25-***/85	Cylinder 25CA	40	25	184	50	25	30	12	47	28	G3/8"	25	24±0.5	16	20	13	12,6	7,6	2,2/0,9
25CA-50/30-***/85	Cylinder 25CA	50	30	205	60	35	35	14	50	29	G1/2"	30	30±0.5	16	20	18	19,6	12,6	3,7/1,2
25CA-50/35-***/85	Cylinder 25CA	50	35	205	60	35	35	14	50	29	G1/2"	30	30±0.5	16	20	18	19,6	10	3,7/1,4
25CA-65/35-***/85	Cylinder 25CA	65	35	214	75	35	40	15	54	32	G1/2"	35	30±0.5	20	25	18	33,1	23,6	5,6/1,6
25CA-65/40-***/85	Cylinder 25CA	65	40	214	75	35	40	15	54	32	G1/2"	35	30±0.5	20	25	18	33,1	20,6	5,6/1,8
25CA-80/40-***/85	Cylinder 25CA	80	40	244	92	50	45	15	56	35	G1/2"	42	35±0.5	22	30	18	50,2	37,7	9,6/2,2
25CA-80/50-***/85	Cylinder 25CA	80	50	244	92	50	45	15	56	35	G1/2"	42	35±0.5	22	30	18	50,2	30,6	9,6/2,7
25CA-100/50-***/85	Cylinder 25CA	100	50	270	115	60	50	18	61	37	G3/4"	52	40±0.5	28	40	20	78,5	58,9	15/3,5
25CA-100/60-***/85	Cylinder 25CA	100	60	270	115	60	50	18	61	37	G3/4"	52	40±0.5	28	40	20	78,5	50,3	15/4,2

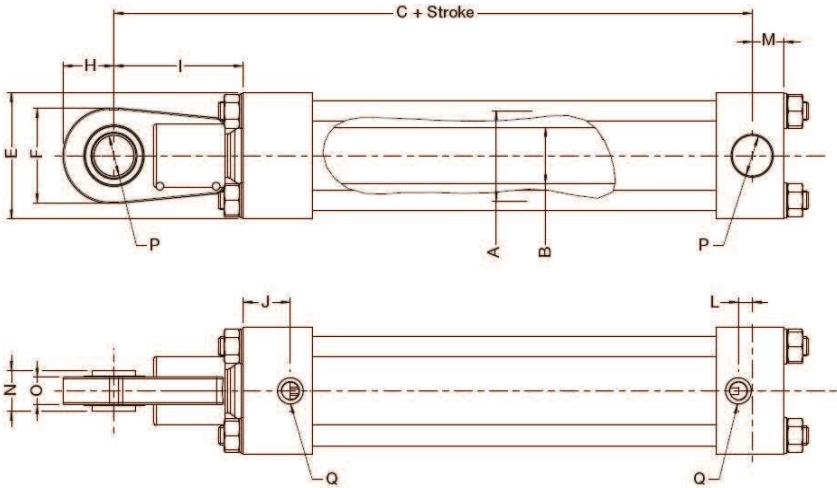
## C.2 Selected Telescopic Cylinder

# Product Specifications

Working pressure	380 bar (5500 psi)
Test pressure	570 bar (8250 psi)
Stroke length	standard – up to 3000 mm
Rated fatigue life	250,000 cycles at 380 bar, tested for 500,000 cycles at 380 bar
Maximum piston speed	0.3 m/s
Barrel material	carbon fibre reinforced composite
Piston material	aluminium
Piston rod material	hard chrome plated steel
Tie rod material	galvanised steel
Mountings	spherical bearings on piston rod, pivot bearing on base end cap, other mounting styles available to order
Sealing system	
– piston seal	thermoplastic polyester elastomer
– rod seal	polyurethane lip type
– wiper seal	polyester-based
– O-rings	polyurethane (PU)
Temperature range	-20 °C to +80 °C
Fluid medium	mineral hydraulic oil

For customised specifications, please contact [lightraulics@parker.com](mailto:lightraulics@parker.com) with details of your application.

# Specifying Your Cylinder



## Dimensions

A Bore Ø	B Rod Ø	C	E Ø	F	H	I	J	L	M	N	O	P Ø	Q (BSP)
80	36	362	120	94	50	120	25	9	43	40	33	40	G <sup>3</sup> / <sub>4</sub>
100	36 56	451 448	147	116	63	161 157	25 53	15	57	50	36	50	G <sup>3</sup> / <sub>4</sub>
125	56 70	493 501	176	130	70	188 189	45 64	16	65	60	46	60	G1
160	63 100	620 576	219	176	95	251 266	62 94	29	93	80	55	80	G1
180	90 125	663 646	248	210	115	273.5 283.5	84 113	35	107	90	60	90	G1
200	125	644	280	210	115	288	109	31	103	90	60	90	G1 <sup>1</sup> / <sub>4</sub>

## Performance

A Bore Ø	B Rod Ø	Rod type	Max. allowed force (kN)		Minimum stroke	Weight at minimum stroke <sup>2)</sup> (kg)	Additional weight per 100 mm stroke (kg)
			Compression <sup>1)</sup>	Tension			
80	36	solid	191	152	200	17	2
100	36	solid	267	260	200	27	2.7
	56	solid	298	205		33	3.8
	56	hollow	298	205		30	3.2
125	56	solid	437	373	250	51	4.7
	70	solid	466	320		58	5.8
	70	hollow	416	320		53	4.6
160	63	solid	555	646	300	99	6.3
	100	solid	764	466		118	10.0
	100	hollow	764	466		104	7.5
180	90	solid	967	725	300	153	10.0
	125	solid	967	501		178	14.6
	125	hollow	967	501		161	11.5
200	125	solid	1194	727	400	222	16.0
	125	hollow	1194	727		201	12.7

All dimensions are in millimeters unless otherwise stated. In line with our policy of continuous product improvement, specifications in this brochure are subject to change without notice. Please enquire for exact dimensions when placing order.

Please use the order code at the end of this brochure to enquire for a Lightraulics® T-Series Cylinder.

1) For maximum allowed compression force, the piston rod selection charts on the following page need to be considered in addition to the data given in the performance table above.

2) Further weight reduction possible by usage of customised rod eyes.



## C.3 Selected Pump

Catalogue HY11-3243/UK  
**Characteristics**

**Axial Piston Pump  
 Series PV**

### Technical data

Displacement [cm <sup>3</sup> /rev]	from 16 to 270
Operating pressures	
Outlet [bar]	nominal pressure $p_N$ 350
	max. pressure $p_{max}$ 420 <sup>1)</sup>
	drain port 2 <sup>2)</sup>
Inlet min. [bar]	0.8 (absolute)
max. [bar]	16
Minimum speed [min <sup>-1</sup> ]	300 min <sup>-1</sup>
Mounting interface	4-hole flange ISO 3019/2 optional ISO 3019/1, SAE
Installation	drain port as high as possible

<sup>1)</sup> max. 20% of working cycle

<sup>2)</sup> peak pressure only, special version up to 20 bar available (X-Modification X5877 on request)



Pump with Standard Pressure Comp.



Pump with Horse Power Comp.



Combination PV/PV



Combination PV/PGP

### Pump combinations

See pages 26–27

### Selection table

Model	Max. displacement [cm <sup>3</sup> /rev]	Output flow at 1500 min <sup>-1</sup> [l/min]	Input horse power at 1500 min <sup>-1</sup> and 350 bar [kW]	Max speed * [min <sup>-1</sup> ]	Moment of inertia [kgm <sup>2</sup> ]	Weight [kg]
PV016	16	24	15.5			
PV020	20	30	19.5	3000	0.0017	19
PV023	23	34.5	22.5			
PV032	32	48	31			
PV040	40	60	39	2800	0.0043	30
PV046	46	69	45			
PV063	63	94.5	61.5	2800		
PV080	80	120	78	2500	0.018	60
PV092	92	138	89.5	2300		
PV140	140	210	136	2400	0.030	90
PV180	180	270	175	2200		
PV270	270	405	263	1800	0.098	172

\* The maximum speed ratings are shown for an inlet pressure of 1 bar (absolute) and for a fluid viscosity of  $\nu = 30 \text{ mm}^2/\text{s}$ .

PI PVplus UK.PMD RH



## C.4 Selected Pressure Pipe and Return Pipe

PIPES & TUBES



### Seamless colddrawn stainless steel pipe – AISI 316 L

#### Pipe stainless steel ASTM A269/A213 – AISI 316 L

Part No	Size	ID Code	Working Pressure			Burst Pressure		Weight [kg/m]
			1. DNV [bar]	2. DNV [bar]	3. DIN [bar]	4. DNV [bar]		
6X1 AISI316L	6 x 1.0	3301061000	525	607	365	2120	0.07	
8X1 AISI316L	8 x 1.0	3301081000	379	436	283	1514	0.17	
8X1.5 AISI316L	8 x 1.5	3301081500	602	698	404	2446	0.24	
10X1 AISI316L	10 x 1.0	3301101000	297	340	231	1178	0.22	
10X1.5 AISI316L	10 x 1.5	3301101500	465	537	333	1871	0.31	
10X2 AISI316L*	10 x 2.0	3301102000	650	755	427	2650	0.40	
12X1 AISI316L	12 x 1.0	3301121000	244	279	195	964	0.27	
12X1.5 AISI316L	12 x 1.5	3301121500	379	436	283	1514	0.39	
12X2 AISI316L	12 x 2.0	3301122000	525	607	365	2120	0.49	
12X2.5 AISI316L*	12 x 2.5	3301122500	682	794	442	2789	0.59	
15X1.5 AISI316L	15 x 1.5	3301151500	297	340	231	1178	0.50	
16X1.5 AISI316L*	16 x 1.5	3301161500	277	317	218	1097	0.54	
16X2 AISI316L	16 x 2.0	3301162000	379	436	283	1514	0.69	
16X2.5 AISI316L	16 x 2.5	3301162500	487	563	345	1963	0.83	
16X3 AISI316L*	16 x 3.0	3301163000	602	698	404	2446	0.96	
18X1.5 AISI316L	18 x 1.5	3301181500	244	279	195	964	0.61	
18X2 AISI316L	18 x 2.0	3301182000	333	382	255	1325	0.79	
20X2 AISI316L	20 x 2.0	3301202000	297	340	231	1178	0.89	
20X2.5 AISI316L	20 x 2.5	3301202500	379	436	283	1514	1.08	
20X3 AISI316L	20 x 3.0	3301203000	465	537	333	1871	1.26	
22X1.5 AISI316L*	22 x 1.5	3301221500	197	225	162	776	0.76	
22X2 AISI316L	22 x 2.0	3301222000	268	307	212	1060	0.99	
25X1.5 AISI316L*	25 x 1.5	3301251500	172	196	143	677	0.87	
25X2 AISI316L	25 x 2.0	3301252000	233	267	188	922	1.13	
25X2.5 AISI316L	25 x 2.5	3301252500	297	340	231	1178	1.39	
25X3 AISI316L	25 x 3.0	3301253000	362	417	273	1445	1.63	
25X4 AISI316L	25 x 4.0	3301254000	501	579	352	2019	2.07	
28X2 AISI316L	28 x 2.0	3301282000	207	236	169	815	1.28	
28X2.5 AISI316L	28 x 2.5	3301282500	263	301	208	1039	1.57	
28X3 AISI316L*	28 x 3.0	3301283000	320	367	246	1272	1.85	
30X2 AISI316L*	30 x 2.0	3301302000	192	220	158	757	1.38	
30X2.5 AISI316L*	30 x 2.5	3301302500	244	279	195	964	1.70	
30X3 AISI316L	30 x 3.0	3301303000	297	340	231	1178	2.00	
30X4 AISI316L	30 x 4.0	3301304000	408	469	300	1631	2.56	
35X2 AISI316L	35 x 2.0	3301352000	164	187	137	642	1.63	
35X2.5 AISI316L	35 x 2.5	3301352500	201	236	169	815	2.00	
35X3 AISI316L	35 x 3.0	3301353000	251	288	201	994	2.37	
38X2.5 AISI316L*	38 x 2.5	3301382500	190	217	157	746	2.19	
38X3 AISI316L	38 x 3.0	3301383000	230	263	186	909	2.59	
38X4 AISI316L	38 x 4.0	3301384000	314	360	242	1247	3.35	
38X5 AISI316L	38 x 5.0	3301385000	402	462	296	1606	4.07	

Items with black letters: Recommended sizes. Normally stock items.  
\*) Items with grey letters: Non-standard sizes. Limited availability.

1. Bended pipe including manufacturing and corrosion tolerances.  
2. Straight pipe including manufacturing and corrosion tolerances.  
3. DIN 2413 III: Dynamic straight pipe including manufacturing tolerance.  
4. Based on Tensile value, wall thickness tolerance not included.

Continue next page

GS-FLANGE SYSTEM

PIPES & TUBES

CLAMPS

VALVES

TEST EQUIPMENT

BITTE TYPE FITTINGS

SAE J514 JIC

HOSES & COUPLINGS

QUICK DISCONNECT

SWIVELS

ADAPTORS

OTHER COMPONENTS

MACHINES

GENERAL INFORMATION

## Seamless colddrawn stainless steel pipe – AISI 316 L

## Pipe stainless steel ASTM A269/A213 – AISI 316 L

Part No	Size	ID Code	Working Pressure			Burst Pressure	Weight [kg/m]
			1. DNV [bar]	2. DNV [bar]	3. DIN [bar]	4. DNV [bar]	
42X2AISI316L	42 x 2.0	3301422000	135	154	115	530	1.97
42X2.5AISI316L	42 x 2.5	3301422500	171	195	142	671	2.43
<b>42X3AISI316L</b>	<b>42 x 3.0</b>	<b>3301423000</b>	<b>207</b>	<b>236</b>	<b>169</b>	<b>815</b>	<b>2.89</b>
<b>42X4AISI316L</b>	<b>42 x 4.0</b>	<b>3301424000</b>	<b>282</b>	<b>323</b>	<b>221</b>	<b>1116</b>	<b>3.75</b>
<b>50X3AISI316L</b>	<b>50 x 3.0</b>	<b>3301503000</b>	<b>172</b>	<b>196</b>	<b>143</b>	<b>677</b>	<b>3.48</b>
<b>50X5AISI316L</b>	<b>50 x 5.0</b>	<b>3301505000</b>	<b>297</b>	<b>340</b>	<b>231</b>	<b>1178</b>	<b>5.55</b>
50X6AISI316L	50 x 6.0	3301506000	362	417	273	1445	6.51
56X8.5AISI316L	56 x 8.5	3301568500	472	544	337	1897	9.96
<b>60X3AISI316L</b>	<b>60 x 3.0</b>	<b>3301603000</b>	<b>142</b>	<b>162</b>	<b>121</b>	<b>558</b>	<b>4.22</b>
<b>60X5AISI316L</b>	<b>60 x 5.0</b>	<b>3301605000</b>	<b>244</b>	<b>279</b>	<b>195</b>	<b>964</b>	<b>6.78</b>
60X6AISI316L	60 x 6.0	3301606000	297	340	231	1178	7.99
66X8.5AISI316L	66 x 8.5	3301668500	392	451	291	1567	12.05
80X10AISI316L	80 x 10.0	3301801000	379	436	283	1514	17.21
97X12AISI316L	97 x 12.0	3301971200	375	431	281	1496	25.50
115X4AISI316L	115 x 4.0	3301911540	98	111	85	382	10.95
115X15AISI316L	115 x 15.0	3301911515	398	458	294	1590	36.99
130X15AISI316L	130 x 15.0	3301913015	347	399	263	1383	42.54
140X4.5AISI316L	140 x 4.5	3301914045	90	102	79	352	15.04
150X15AISI316L	150 x 15.0	3301915015	297	340	231	1178	49.94
165X5AISI316L	165 x 5.0	3301916550	85	96	98	331	19.73

Items with black letters: Recommended sizes. Normally stock items.

\* Items with grey letters: Non-standard sizes. Limited availability.

1. Bended pipe including manufacturing and corrosion tolerances.

2. Straight pipe including manufacturing and corrosion tolerances.

3. DIN 2413 III: Dynamic straight pipe including manufacturing tolerance.

4. Based on Tensile value, wall thickness tolerance not included.

## **Appendix D Thesis based Paper**

In the following section, the paper written based on this thesis is presented.

Title: Parallel Force/Position Control of Motion Compensated Gangway in Offshore Operations

# Parallel Force/Position Control of Motion Compensated Gangway in Offshore Operations

Feilong Yu, Yingguang Chu\*, Houxiang Zhang, Vilmar Æsøy

Department of Ocean Operations and Civil Engineering

Norwegian University of Science and Technology

[feilon@stud.ntnu.no](mailto:feilon@stud.ntnu.no)

## Abstract

Ship-based motion compensated gangway systems are one of the most economical and effective access systems for the transportation of maintenance personnel, equipment, and spare parts to offshore wind turbines. During the transferring operation, the gangway passageway connecting the ship and the wind turbine is either landed on top of the wind turbine platform or pushed against to it via bumpers or similar clamping mechanisms. Considering the limited space and weight of wind turbine platforms, the latter is usually preferred. However, in either case, the contact force to the gangway is hard to control with pure active motion compensation. Consequently, the contact force may damage the wind turbine and the gangway, and affect the dynamic positioning of small weight-class vessels. Current applications usually include passive systems to provide the flexibility to the gangway movement, or with a free end at the gangway tip. This study introduces a parallel force/position control algorithm for the control of the contact force between the gangway tip and the platform during motion compensated operations. Model development of the dynamic systems including the hydraulic power systems and the multi-body dynamics of gangway are described. The proposed parallel position/force control algorithm is verified through simulations.

**Keywords:** Motion compensated gangway, Parallel position/ force control, Hydraulic power system, Multi-body dynamics, Bond graph

## 1 Introduction

Offshore wind turbines are increasingly developed as one of the renewable sources of energy. Compared to applications on land, offshore wind farms are generally more beneficial because of better wind conditions in the open sea; however, the installation and maintenance costs are higher. Operations in rough weather conditions encounter decreased accessibility to the wind turbines. Motion compensated gangway is believed to be one of the most economical and effective access solutions to enlarge the weather window for operations, thus reduce the operation downtime for offshore wind turbines. There are mainly two types of motion compensated gangway systems, which dominate the current market. Ampelmann's solution is to mount the transfer deck on top of a so-called Stewart platform which is a parallel mechanism and can provide motions in all six degrees of freedom using six hydraulic cylinders [1]. This solution requires relatively precise measurements of the ship motions. The performance of compensation relies on the Stewart platform. The other alternative solution, e.g., Uptime International AS, directly uses the luffing cylinders of the gangway and the telescope section driven by either hydraulic cylinders or winches [2]. This provides the counter motions of the ship to keep the gangway tip stable. During the transferring operation, the gangway passageway connecting the ship and the wind turbine is either landed on top of the wind turbine platform or pushed against to it via bumpers or similar clamping mechanisms.



Considering the limited space and weight of wind turbine platforms, the latter is usually preferred, as shown in Fig. 1. But inaccuracy of either the measured motions of the ship from sensors or the compensating motions of the gangway causes residual motions that hampers safe positioning of the operation. And in either case, the contact force between gangway tip and the wind turbine platform is hard to control with pure active motion compensation (AMC). Consequently, the uncontrollable contact force may damage the wind turbine and the gangway, and affect the dynamic positioning of the small weight-class vessels. As a result, it is usually applied to consider the compensation of the residual motions of the gangway, whether through passive control of actuators or feeding force control to the controller.

This study introduces a parallel force/position control algorithm for the control of the contact force between the gangway tip and the platform during motion compensated operations. Model development of the dynamic systems including the hydraulic power systems and the multi-body dynamics of gangway are described. The proposed parallel position/ force control algorithm is verified through simulations.



Fig. 1 Gangway transferring operation [3]

## 2 Related Work

AMC technology has been utilized in offshore industries for many years. The basic principle is that the actuators of the mechanism try to compensate the relative movements induced

by ship motions which can be obtained through the motion detection units, e.g. Inertial Measurement Unit (IMU) and Motion Reference Unit (MRU). Based on the input data, the control system calculates how the actuators have to react to the movements. For offshore gangway operations, the objective is to make the gangway tip move in the counter direction of ship motion through the hydraulic actuators, thus keep the gangway tip stable in the global frame. Similar control strategy for offshore crane has been described in [4].

Combining force and position control is not new in robotics [5]. One of the widely used control algorithm for both position and force trajectory is termed as admittance controller [6]. It uses a force compensator complies with the environmental interaction to react to the contact forces by modifying the reference motion trajectory. An example is to use the inner position control loop and outer force control loop to implement the force control on industrial manipulators to address friction in the joints and transmission system [7]. Related to marine applications, a parallel position and force controller is proposed for the control of the load through the wave zone in offshore crane operation in order to reduce the wire oscillations [8]. For AMC gangway, currently, the contact force between gangway tip and wind turbine platform is passively controlled by adjusting the pressure of the relief valve in the hydraulic circuits [2]. Depending on the performance of the hydraulic systems, this control method is more efficient in principle since the pressure relieve valve directly responds to the controlled force. However, the effectiveness of such controller is unknown when both position and force control are active. In this paper, we proposed a parallel position and force control strategy to control the contact force between gangway tip and wind turbine platform within the desired level during gangway transferring operation.

Model development of the gangway system for simulation is carried out using the bond graph

(BG) method and handled by a software tool 20-sim [9]. This includes the multi-body dynamics of the gangway, and the hydraulic power systems of its actuators. Modeling of the multi-body dynamics of manipulator using bond graph is discussed in [10]-[11]. The equations of motions are derived with the Lagrange's method, and rewritten into the Hamiltonian form for the implementation using a special type of bond graph called IC-field. Model implementation of the hydraulic components of an offshore crane system using the BG approach is presented in [12], where the main components such as pump, pressure compensate valve (PCV), directional control valve (DCV), counter balance valve (CBV), hydraulic cylinder and motor are described.

### 3 Model Development

The AMC gangway consists of a slewing unit mounted on the top of the pedestal, a luffing boom and a telescopic boom. The slewing unit is actuated by a hydraulic motor, and the luffing boom and telescopic boom are actuated by hydraulic cylinders. For simplification, the gangway body is assumed as rigid and the mass distribution of each part is symmetric with respect to the body-attached frame at the center of mass. The kinematic frames of gangway is shown in Fig. 2.

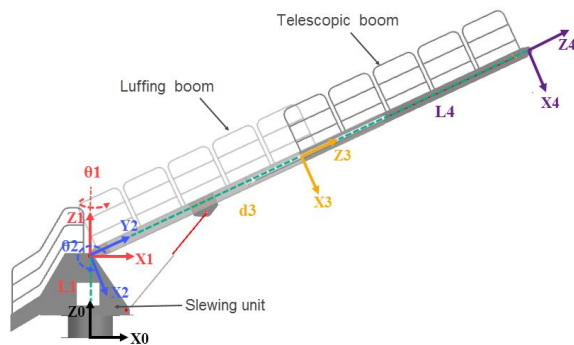


Fig. 2 Gangway configuration and coordinate system setup

### 3.1 Mechanical System Model

Based on Denavit-Hartenberg (D-H) method, the forward transformation matrix from the gangway foundation to the gangway tip can be derived as given by Eqn. (11) [13]. The gangway tip position in the Cartesian space expressed in frame {0} is given by Eqn. (2).

$$T_4^0 = \begin{bmatrix} c1c2 & -s1 & -c1s2 & -c1s2(d3 + L4) \\ s1c2 & c1 & -s1s2 & -s1s2(d3 + L4) \\ s2 & 0 & c2 & L1 + (d3 + L4)c2 \\ 0 & 0 & 0 & 1 \end{bmatrix} \quad (1)$$

$$P_{tip} = \begin{bmatrix} P_{tipx} \\ P_{tipty} \\ P_{tipz} \end{bmatrix} = \begin{bmatrix} -c1s2(d3 + L4) \\ -s1s2(d3 + L4) \\ L1 + (d3 + L4)c2 \end{bmatrix} \quad (2)$$

Where  $s_i = \sin\theta_i$ ,  $c_i = \cos\theta_i$  and  $i = 1, 2, 3$

The Jacobian matrix relating the gangway tip velocity to joint velocity is given by Eqn. (4)

$$v_{tip} = J_{tip}\dot{q} \quad (3)$$

$$J_{tip} = \begin{bmatrix} s1s2(d3 + L4) & -c1c2(d3 + L4) & -c1s2 \\ -c1s2(d3 + L4) & -s1c2(d3 + L4) & -s1s2 \\ 0 & -s2(d3 + L4) & c2 \end{bmatrix} \quad (4)$$

Where  $v_{tip}$  is the vector of gangway tip velocity in the Cartesian space expressed in frame {0}, and  $\dot{q}$  is the vector of joint velocity.

The Lagrange's equation of motion for describing the gangway dynamics are given by Eqn. (5)

$$\frac{d}{dt} \frac{\partial L}{\partial \dot{q}} - \frac{\partial L}{\partial q} = \tau \quad (5)$$

Where  $L$  is Lagrangian defined as the difference between kinetic energy and potential energy of gangway system,  $\tau$  is the vector of generalized external torque,  $q$  and  $\dot{q}$  denote the joint displacement and velocity.

The kinetic energy is expressed as in Eqn. (6)

$$T = \frac{1}{2} \dot{q}^T D(q) \dot{q} \quad (6)$$

Where  $D(q)$  is the inertia matrix of gangway given by Eqn. (7).

$$D(q) = \begin{bmatrix} d11 & d12 & d13 \\ d21 & d22 & d23 \\ d31 & d32 & d33 \end{bmatrix} \quad (7)$$

The non-zero components are written as below:

$$\begin{aligned} d11 &= I_{z1} + (I_{y2} + I_{z3})c2^2 + (I_{x2} + I_{x3})s2^2 \\ &\quad + (m2Y_{c2}^2 + m3(Z_{c3} + d3)^2)s2^2 \\ d22 &= I_{z2} + I_{y3} + m2Y_{c2}^2 + m3(Z_{c3} + d3)^2 \\ d33 &= m3 \end{aligned}$$

The following notations are used:

$I_{xi}, I_{yi}, I_{zi}$  represents the principal moments of inertia about x, y and z-axes of the body-attached frame at mass center of each link of gangway

$m_i$  represents the mass of the  $i$ th link of gangway

$X_{ci}, Y_{ci}, Z_{ci}$  represents the coordinate of center of mass of each link expressed in the body-attached frame

The partial derivative of potential energy of gangway with respect to joint displacement  $q$  are given in Eqn. (8).

$$g(q) = \begin{bmatrix} 0 \\ -(m2Y_{c2} + m3Z_{c3} + m3d3)gs2 \\ m3gs2 \end{bmatrix} \quad (8)$$

The state space model describing the basic dynamics of manipulator using the IC-field BG are written as in Eqn. (9) and (10).

$$\dot{q} = D(q)^{-1}p \quad (9)$$

$$\dot{p} = e'(p, q) + \tau \quad (10)$$

Where  $p$  is the vector generalized momentum,  $\tau$  is the vector generalized torque,  $e'(p, q)$  is the vector generalized effort.

The vector of the generalized effort  $e'(p, q)$  is defined as:

$$e'(p, q) = \frac{\partial L}{\partial q} = \frac{\partial T}{\partial q} - g(q) \quad (11)$$

where the first term can be derived from Eqn. (6) and (7) as below in Eqn. (12)

$$\frac{\partial T}{\partial q} = \begin{bmatrix} 0 & 0 & 0 \\ C_{21} \cdot \dot{\theta}_1 & 0 & 0 \\ C_{31} \cdot \dot{\theta}_1 & C_{32} \cdot \dot{\theta}_2 & 0 \end{bmatrix} \cdot \begin{bmatrix} \dot{\theta}_1 \\ \dot{\theta}_2 \\ \dot{d}_3 \end{bmatrix} \quad (12)$$

Where

$$\begin{aligned} C_{21} &= (m2Y_{c2}^2 + m3 * (Z_{c3} + d3)^2)s2c2 \\ &\quad + (I_{x2} + I_{x3} - I_{y2} - I_{z3})s2c2 \\ C_{31} &= m3(Z_{c3} + d3)s2^2 \\ C_{32} &= m3(Z_{c3} + d3) \end{aligned}$$

Then the BG representation of the gangway dynamics using the IC-field is shown Fig. 3 .

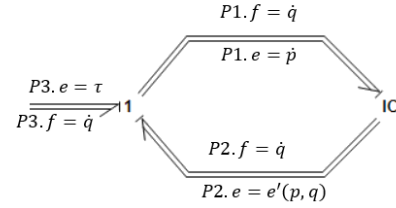


Fig. 3 IC-field representation of dynamics equation

Since the weight of actuators is so small compare to gangway body, so the dynamic effects of the actuators are neglected in our study. However, the driving forces of actuators are not the same as the generalized torques in the equations of motion. The torque of the slewing motor is easy to implement by applying a gear ratio  $n$ . The force of the telescopic boom is the same as the telescopic cylinder output force. The transformation for luffing cylinder can be obtained according to its geometry relation as shown in Fig. 4.

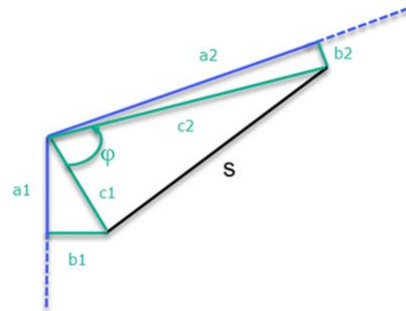


Fig. 4 Geometry relation of luffing cylinder

Hence, the transformation matrix for the actuators is presented.

$$T(\theta) = \begin{bmatrix} n & 0 & 0 \\ 0 & \frac{c1c2 \sin(\varphi)}{s} & 0 \\ 0 & s & 1 \end{bmatrix} \quad (13)$$

Where  $s = \sqrt{c1^2 + c2^2 - 2c1c2 \cos(\varphi)}$ ,  $c1 = \sqrt{a1^2 + b1^2}$ ,  $c2 = \sqrt{a2^2 + b2^2}$  and  $\varphi = \theta2 - \pi - \arctan\left(\frac{b1}{a1}\right) - \arctan\left(\frac{b2}{a2}\right)$

The relation of the generalized torques and the actuators is given

$$\tau = T(\theta)F \quad (14)$$

Where  $F$  represents the vector of the slewing motor torque and cylinder forces.

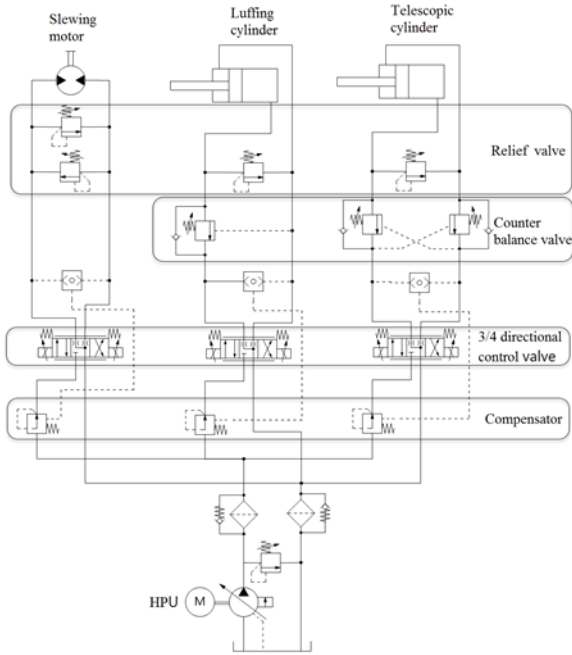


Fig. 5 The hydraulic diagram of the AMC gangway

### 3.2 Hydraulic System Modeling

The considered AMC gangway of the actuation system consists of three hydraulic circuits, i.e., for the slewing unit, the luffing boom and the telescopic boom respectively as shown in Fig. 5. The main components of the

hydraulic system includes the hydraulic power unit (HPU), pipelines, valves, cylinders and motor. Due to words limit of this paper, the model implementation using the BG method is not presented here, but can be found in the reference [9] and [12].

## 4 Control Strategy

The proposed parallel force and position controller is based on the inner position loop and outer force loop control, as shown in Fig. 6. The reference position trajectory is adjusted to achieve a desired force acting on the wind turbine platform.

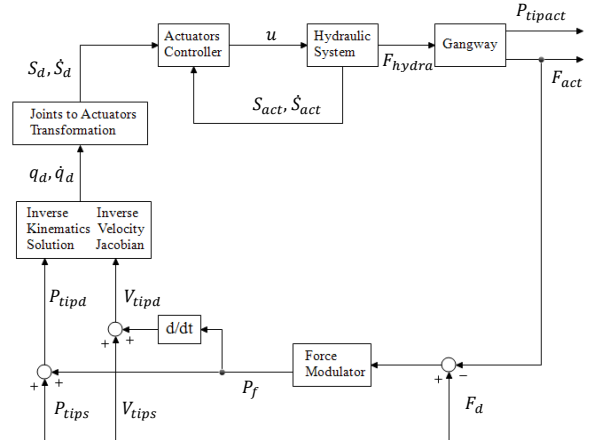


Fig. 6 The parallel position and force control diagram

In this controller, the gangway tip is commanded to follow a desired trajectory  $(P_{tipd}, V_{tipd})$  in frame  $\{0\}$  (or the global frame in practice). That is the sum of the gangway tip trajectory  $(P_{tips}, V_{tips})$  for compensating the ship motion and the trajectory offset  $(P_f, \frac{dP_f}{dt})$  needed to maintain the desired force  $F_d$ .

$$P_{tipd} = \begin{bmatrix} P_{tipXd} \\ P_{tipYd} \\ P_{tipZd} \end{bmatrix} = P_{tips} + P_f \quad (15)$$

$$V_{tipd} = V_{tips} + \frac{dP_f}{dt} \quad (16)$$

Considering the situation that the gangway tip is pushed against the wind turbine platform, the force control in X-direction  $P_f$  is written as:

$$P_f = \begin{bmatrix} X_f \\ 0 \\ 0 \end{bmatrix} \quad (17)$$

Where  $X_f$  is the position offset of gangway tip in the direction of X-axis of frame  $\{0\}$ .

The control algorithm of force modulator is given below.

$$X_f = \frac{F_d}{K_e} + K_f(F_d - F_{act}) + K_{fi} \int (F_d - F_{act}) dt \quad (18)$$

Where  $F_d$  and  $F_{act}$  is the desired force and actual force exerted on platform by gangway respectively,  $K_e$  is the approximate stiffness of the rubber bumper which is chosen to be  $10^6 N/m$ ,  $K_f$  and  $K_{fi}$  are the controller gains which will be tuned for during simulation.

The inverse kinematics and inverse velocity Jacobian for mapping the desired gangway tip trajectory to the desired joint trajectory are presented below by solving Eqn.2 and recalling Eqn. 4.

$$\begin{bmatrix} \theta_{1d} \\ \theta_{2d} \\ d_{3d} \end{bmatrix} = \begin{bmatrix} \arctan\left(\frac{P_{tipYd}}{P_{tipXd}}\right) \\ \arctan\left(\frac{P_{tipXd}}{\cos\theta_1(L1 - P_{tipZd})}\right) \\ \frac{P_{tipXd}}{-\cos(\theta_1) \cdot \sin(\theta_2)} - L4 \end{bmatrix} \quad (19)$$

$$\dot{q}_d = \begin{bmatrix} \dot{\theta}_{1d} \\ \dot{\theta}_{2d} \\ \dot{d}_{3d} \end{bmatrix} = (J_{tip})^{-1} \cdot V_{tipd} \quad (20)$$

The transformation from desired joint trajectory to the desired actuator trajectory can be derived based the geometry relation of actuators by recalling Eqn. (13).

$$S_d = \begin{bmatrix} S_{motord} \\ S_{luffd} \\ S_{teled} \end{bmatrix} = \begin{bmatrix} \theta_1 \cdot n \\ \sqrt{c1^2 + c2^2 - 2c1c2 \cos(\varphi)} \\ S_{shortest} + d3 + L4 - L_{min} \end{bmatrix} \quad (21)$$

$$\dot{S}_d = \begin{bmatrix} \dot{S}_{motord} \\ \dot{S}_{luffd} \\ \dot{S}_{teled} \end{bmatrix} = T(\theta) \cdot \dot{q}_d \quad (22)$$

Where  $S_{motord}$ ,  $S_{luffd}$  and  $S_{teled}$  are desired motor angle and cylinders' length,  $S_{shortest}$  is the shortest length of telescopic cylinder and  $L_{min}$  is the minimum total length of gangway,  $\dot{S}_d$  is the vector of desired actuator velocity.

The control of actuator motion is achieved by adjusting the flow to the actuator through the directional control valve. For simplification, we assume the response of DCV response fast enough and the valve dynamics such as the spool inertia effects and friction are neglected. A proportional-derivative (PD) controller with velocity feedforward is applied to the control signal of the DCV.

$$u = K_{ffc} \dot{S}_d + K_p(S_d - S_{act}) + K_d(\dot{S}_d - \dot{S}_{act}) \quad (23)$$

Where  $K_{ffc}$  is the gain of velocity feedforward and  $K_p$  and  $K_d$  the proportional gain for the PD controller,  $S_{act}$  is actual the motor angle or cylinder length.

To complete the model for simulation, the contact force is modelled as a spring mechanism.

$$F_{act} = \begin{cases} K_e \cdot \Delta X & \text{if } \Delta X > 0 \\ 0 & \text{else} \end{cases} \quad (25)$$

Where  $\Delta X$  is the distance between the wind turbine platform and gangway tip position in X-axis.

## 5 Simulation and Discussion

The ship motions in vertical (Z-axis) and horizontal (X-axis) are represented by regular sine wave models.

$$Z_{ship} = \sin\left(\frac{2\pi}{12} t\right) \quad (246)$$

$$X_{ship} = 0.5 \cdot \sin\left(\frac{2\pi}{12} t\right) \quad (257)$$

The initial coordinates of the gangway tip and platform in world frame and the desired contact force are given as below:

- Gangway tip :  $[9.30; 0; 1.82]m$
- Platform:  $[9.29; 0; 1.82]m$
- Desired contact force: 4000 N

In order to verify the effectiveness of the force controller, a comparison between the active motion controller (pure position controller) and the proposed parallel position and force controller is presented. Figure 7 shows the gangway tip position in X-axis, and Fig. 8 shows the Z-axis position.

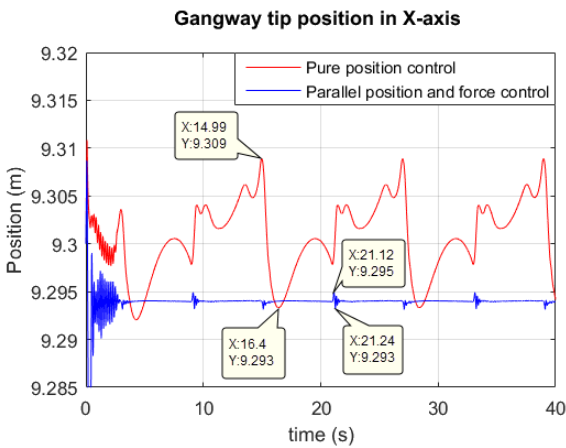


Fig. 7 Gangway tip position and Ship Motion in X-axis under two-control algorithms

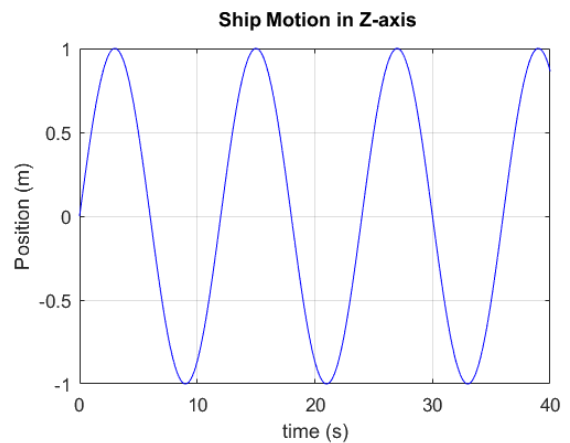
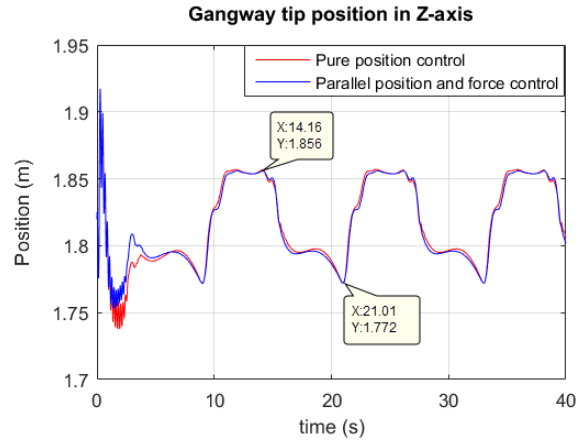
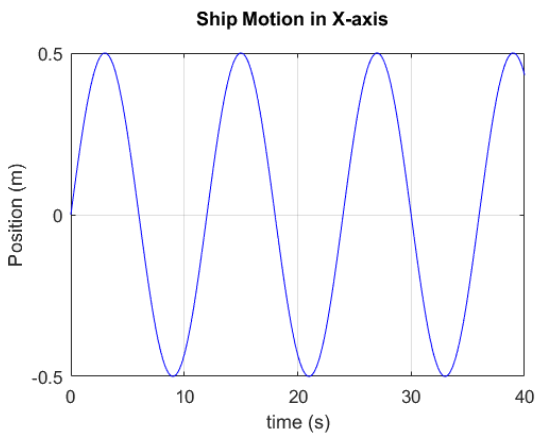


Fig. 8 Gangway tip position and Ship Motion in Z-axis under two-control algorithms

When the gangway is only under position controller, the position error from initial values are  $[-0.007, 0.009]$  m in X-axis and  $[-0.048, 0.036]$  m in Z-axis. Consequently, due to these small position errors, the contact force when the gangway is connected to the wind turbine varies between  $[3430, 18900]$  N in X-axis. In contrast, under parallel position and force controller, the gangway tip position is stabilized at around the desired value within  $[-0.001, 0.001]$  m in X-axis and  $[-0.048, 0.036]$  m in Z-axis. The contact force between the gangway tip and the platform is stabilized at  $[3418, 4932]$  N, as shown in Fig. 9.



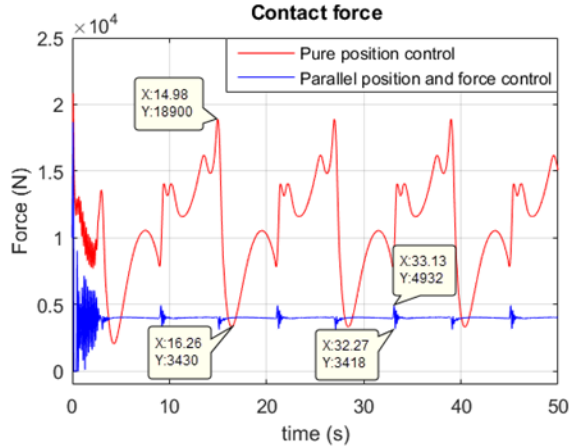


Fig. 9 The contact force in X-axis using the two control algorithms

These cyclic oscillations of gangway tip position and contact force in X-axis under parallel position and force control are mainly due to the DCV transition across the dead band and the fluid dynamics between the DCV and the cylinder. The pressure characteristics of the telescopic cylinder under both cases are shown in Fig. 10. As can be seen, the pressure change is much less using the parallel control algorithm.

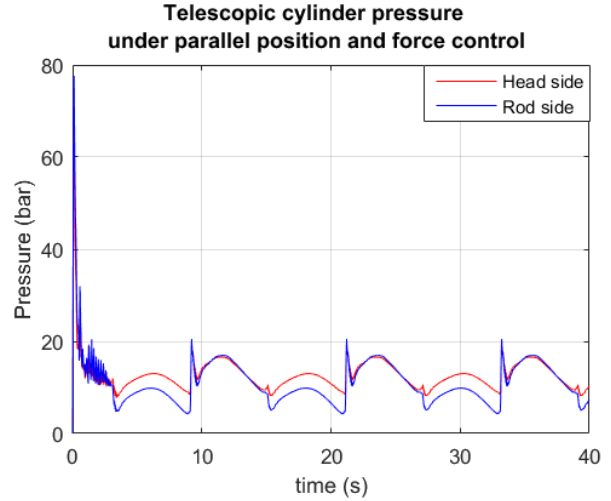
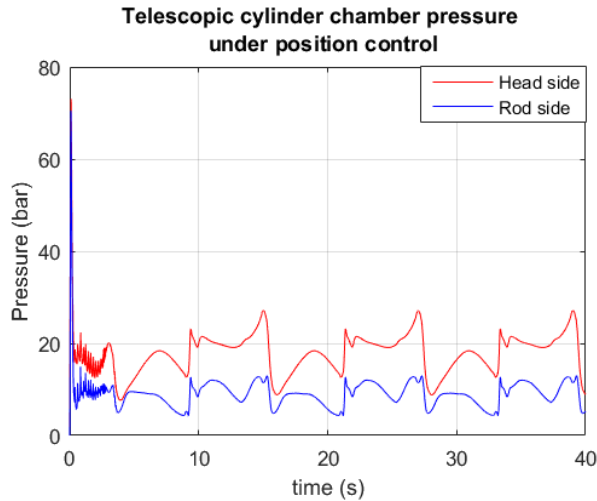


Fig. 10 Telescopic cylinder pressure under two control algorithms



## 6 Conclusion

This study introduced a parallel position/force control algorithm for the AMC gangway system during offshore wind turbine operations. Based on the proposed control algorithm, the contact force between the gangway tip and the wind turbine when connected is stabilized comparing to pure motion compensation. Modelling and simulation of the gangway dynamics were described and presented, including the kinematics, multi-body dynamics and hydraulic systems. An integrated model of the AMC gangway was implemented using the BG method. The equations of motion of the gangway were derived using the Lagrange's method and rewritten into the Hamiltonian form, which provides an elegant form for the representation using a special type BG called IC-field.

The simulation results validates the proposed control algorithm which will improve the operation efficiency and safety during gangway transfer applications. Depending on the applications, force control in the Z-axis can be implemented and expects similar results. The performance of the hydraulic systems is crucial to the effectiveness of the control algorithm. The hydraulic models implemented

in this study are simplified and idealized considering basically the power transformations from the hydraulic domain to the mechanical domain. This, however, is not the focus of this study. What's more, the design of the actuators, in particular, the telescope cylinders, is redundant due to the size of the boom.

## 7 References

- [1] D. J. C. SALZMANN, "Development of the Access System for Offshore Wind Turbines," PhD thesis, Delft University of Technology, 2010.
- [2] I. M. Salen, "Apparatus and method for providing active motion compensation control of an articulated gangway," ed: Google Patents, 2016.
- [3] Uptime International AS. Available online at: <http://www.uptime.no/wp-content/uploads/Uptime-234-AMC-gangway-768x512.jpg>
- [4] Y. Chu, F. Sanfilippo, V. Asoy, and H. Zhang, "An effective heave compensation and anti-sway control approach for offshore hydraulic crane operations," in *Mechatronics and Automation (ICMA), 2014 IEEE International Conference on*, 2014, pp. 1282-1287: IEEE.
- [5] S. Chiaverini and L. Sciavicco, "The parallel approach to force/position control of robotic manipulators," *IEEE Transactions on Robotics and Automation*, vol. 9, no. 4, pp. 361-373, 1993.
- [6] H. Seraji, "Adaptive admittance control: An approach to explicit force control in compliant motion," in *Robotics and Automation, 1994. Proceedings., 1994 IEEE International Conference on*, 1994, pp. 2705-2712: IEEE.
- [7] J. Maples and J. Becker, "Experiments in force control of robotic manipulators," in *Robotics and Automation. Proceedings. 1986 IEEE International Conference on*, 1986, vol. 3, pp. 695-702: IEEE.
- [8] B. Skaare and O. Egeland, "Parallel force/position crane control in marine operations," *IEEE Journal of Oceanic Engineering*, vol. 31, no. 3, pp. 599-613, 2006.
- [9] D. C. Karnopp, D. L. Margolis, and R. C. Rosenberg, *System Dynamics : Modeling, Simulation, and Control of Mechatronic Systems*, 5th ed. ed. (System Dynamics: Modeling, Simulation, and Control of Mechatronic Systems, Fifth Edition). Chichester: Wiley, 2012.
- [10] B. Rokseth, S. Skjong, and E. Pedersen, "Modeling of generic offshore vessel in crane operations with focus on strong rigid body connections," *IEEE Journal of Oceanic Engineering*, 2016.
- [11] Y. Chu and V. Æsøy, "A Multi-Body Dynamic Model Based on Bond Graph for Maritime Hydraulic Crane Operations," in *ASME 2015 34th International Conference on Ocean, Offshore and Arctic Engineering*, 2015, pp. V001T01A010-V001T01A010: American Society of Mechanical Engineers.
- [12] Y. Chu, V. Æsøy, H. Zhang, and O. Bunes, "Modelling And Simulation Of An Offshore Hydraulic Crane," in *ECMS*, 2014, pp. 87-93.
- [13] M. W. Spong, *Robot modeling and control*. Hoboken, N.J: Wiley, 2006.